2006

Commissioning Of A Dynamic Mechanical Analyzerfor The Characterization Of Low Temperature Nitife Shape Memory Alloys

Maruthi Diwakar Nandiraju
University of Central Florida

COMMISSIONING OF A DYNAMIC MECHANICAL ANALYZER FOR THE CHARACTERIZATION OF LOW TEMPERATURE NiTiFe SHAPE MEMORY ALLOYS

by

MARUTHI DIWAKAR NANDIRAJU
B.Tech. Indian Institute of Technology, Madras, 2004

A thesis submitted in partial fulfillment of the requirements
for the degree of Master of Science
in the Department of Mechanical, Materials and Aerospace Engineering
in the College of Engineering and Computer Science
at the University of Central Florida
Orlando, Florida

Fall Term
2006

ABSTRACT

NiTiFe shape memory alloys can undergo transformations between cubic, trigonal and monoclinic phases at low temperatures. The low hysteresis associated with the trigonal R-phase transformation make them candidates for actuator applications at low temperatures. However, the literature available on these alloys is limited and there is a need to establish processing-structure-property correlations. This study was undertaken with the objective of determining and understanding such correlations in a $Ni_{46.8}Ti_{50}Fe_{3.2}$ alloy.

First, a dynamic mechanical analyzer (DMA) was successfully commissioned to facilitate mechanical testing between -150 and 600ºC. The experiments performed over selected ranges of stress and temperature probed a range of deformation phenomena in these materials. In addition to conventional elastic and dislocation based plastic deformation, also probed were stress-induced formation of the R- and martensite (B19') phases, and twinning in the R- and martensite (B19') phases. Constrained recovery experiments, wherein phase transformations were thermally induced against external loads, were also performed to assess the performance of these alloys in actuator applications.

In addition to a DMA, a differential scanning calorimeter, liquid helium dilatometer and a transmission electron microscope were also used. The samples tested were subjected to different thermo-mechanical processing parameters (i.e., percentage of cold work, solutionizing, aging, and annealing time/temperature). Selected combinations of cold work and annealing temperature/times were found to result in narrower transformations (in temperature space), making such alloys of value in cyclic actuator applications.

Thus this work contributed to further understand the processing-structure-property relationship in NiTiFe alloys that exhibit the R-phase transformation and in lowering the operating temperature range of shape-memory alloys in order for them to be used in hydrogen related technologies. The immediate benefit to NASA Kennedy Space Center is the development of a shape-memory thermal conduction switch for application in cryogenic liquefaction, densification and zero boil-off systems. This is being extended to include the potential use of shape-memory alloy actuator elements for cryogenic seals, valves, fluid-line repair, self-healing gaskets, and even to ambient debris-less separation and latch/release mechanisms. The financial support of NASA through grant NAG3-2751 is gratefully acknowledged.

Dedicated
to
my Parents

ACKNOWLEDGMENTS

I would like to take this opportunity to express my gratitude to my advisor Dr. Raj Vaidyanathan, who is one of the best teachers I have met, for introducing me to this fascinating field of shape memory alloys and for all the support and guidance he gave through out my course of graduate study. I would like to thank Dr. Helge Heinrich and Dr. Samar Kalita for serving on my thesis committee and for their valuable suggestions.

Thanks to Dr. Kevin P. Menard from Perkin Elmer Inc. for all his help and advice during commissioning of the dynamic mechanical analyzer. I would also like to thank my friends and colleagues, Vinu B. Krishnan, R. Mahadevan Manjeri, Prakash Palanisamy and Shipeng Qiu for their constant cooperation in my project work, sharing their expertise in shape memory alloys and material characterization and also spending few lighter moments with me.

My sincere gratitude is expressed towards Ms. Karen Glidewell, Ms. Cynthia Harle, Ms. Kari Stiles and Ms. Waheeda Illasarie in ordering all the equipment required and in submitting all the paperwork.

Last but not the least, I would like to acknowledge all my wonderful friends, Haritha in particular, whose support and encouragement helped me in moving towards my goal.

Above all, I would like to thank my parents whose unfailing love, support and encouragement made me to achieve this.

TABLE OF CONTENTS

LIST OF FIGURES

LIST OF TABLES

LIST OF ACRONYMS/ABBREVIATIONS

A_f	Austenite finish
A_s	Austenite start
DMA	Dynamic Mechanical Analyzer
DSC	Differential Scanning Calorimeter
EDM	Electrical Discharge Machining
KSC	Kennedy Space Center
M_d	Martensite desist
M_f	Martensite finish
M_s	Martensite start
NASA	National Aeronautics and Space Administration
PMMA	Poly-methyl methacrylate
SIM	Stress Induced Martensite
SMA	Shape Memory Alloy
SME	Shape Memory Effect
TEM	Transmission Electron Microscopy

CHAPTER 1: INTRODUCTION

1.1 Motivation

Shape memory alloys (SMAs) are promising materials for (micro-) actuation in space applications among others, because of the large deformations and forces that can be achieved. SMA actuators are suitable for these applications since their large power density offers compact and lightweight solutions and their operation involves low accelerations and low voltage. These actuators have successfully been applied on spacecraft in release and unfolding mechanisms for solar panels, such as those of the Hubble Space Telescope as well as new micro satellites [Fragnito *et al.* 2002].

The behavior of these SMAs at various temperatures plays a substantial role in the operation of these actuators. The motivation for this project comes from the requirement for the selection of suitable alloys used in a cryogenic thermal conduction switch which could be utilized by NASA-Kennedy Space Center for future Mars missions. A switch of this kind, which use SMAs as the actuating elements, has been designed to regulate temperatures between liquid methane and liquid oxygen dewars. A prototype switch was developed by V. Krishnan in 2004 [Krishnan 2004] which used NiTi strips which were thermo-mechanically treated and was further developed by J. Lemanski in 2005 [Lemanski 2005] using a NiTiFe alloy operating in the low temperature range. The need to select a suitable NiTiFe alloy and to study the deformation behavior in the cryogenic range required the commissioning of a dynamic mechanical analyzer (DMA). The facility was used in characterizing the deformation behavior of the alloy at various

temperatures. For a switch actuator, to operate in a particular temperature range, reduced hysteresis is required, which is observed in an intermediate R-phase between austenite and martensite in NiTiFe. The effect of thermo-mechanical treatment on the properties of this phase has been studied as a part of this project.

Addition of Fe in the NiTi system effectively suppresses the M_s temperature [Matsumoto and Honma 1976] thus separating the R-phase transition from the subsequent martensitic transformation on the temperature scale. This allows the actuators to operate in cryogenic temperatures under certain conditions and a low hysteresis thermal actuator can be achieved by the suitable selection of the alloy and the appropriate heat treatment which introduces and stabilizes the intermediate R-phase.

1.2 Shape Memory Alloys

Shape Memory Alloys (SMAs) are novel materials which have a unique ability to return to a predetermined shape when heated. This phenomenon which is known as the Shape Memory Effect (SME) is a result of a thermo-elastic transformation as the material undergoes a solid to solid phase transformation from a low temperature martensite phase to high temperature austenite phase. If the shape memory alloy encounters any resistance during this transformation, it can generate extremely large forces. This phenomenon provides a unique mechanism for actuation. Even though numerous alloys were found to exhibit this effect, only alloys such as NiTi and copper based alloys such as copper-aluminum-gold and copper-zinc-aluminum are of importance because they recover considerable amount of strain (or exert significant force). Apart from the shape memory effect, shape memory alloys exhibit superelasticity which is

characterized by the accommodation of large amount of strains (up to 8 %) without any plastic deformation in the material. Buehler and his co workers discovered the shape memory effect in an equiatomic alloy of nickel and titanium [Buehler *et al.* 1967]. Further details regarding the shape memory effect and the superelastic behavior of shape memory alloys are discussed in the subsequent sections.

1.2.1 Temperature Induced Transformation

Shape memory alloys exhibit a phase transformation between two phases upon heating/cooling. Austenite is a "stronger" phase which exists at relatively high temperatures and martensite is a "weaker" phase which is easy to deform at low temperatures. These alloys may exhibit two kinds of shape memory behaviors. The two behaviors are one way and two way memory. The one way shape memory effect in NiTi is illustrated using Figure 1.1. When a parent austenite phase (Figure 1.1a) which has a cubic structure above A_f (austenite finish temperature) is cooled below M_f (martensite finish temperature), the monoclinic structure dominates. In this stage there is not much macroscopic deformation in the material since the transformation occurs in a self accommodating manner. In the martensitic phase, if an external stress is applied then the strain in the material is accommodated by detwinning of lattice planes into selected variants of martensite (Figure 1.1c). When this phase is heated back above A_f it recovers all the strain and reverts back to the austenitic phase (Figure 1.1d). The strain is completely recoverable because this is accommodated by twinning unlike slip which is a permanent and destructive deformation of the lattice.

The two way shape memory effect has macroscopic movement both during heating and cooling. In this case, the material remembers its low temperature shape (deformed shape) in addition to the high temperature shape. This two way shape memory effect is achieved by "biasing" or "training" the SMA specimen, where it is cycled several times between its low temperature shape and high temperature shape [Saburi 1998].

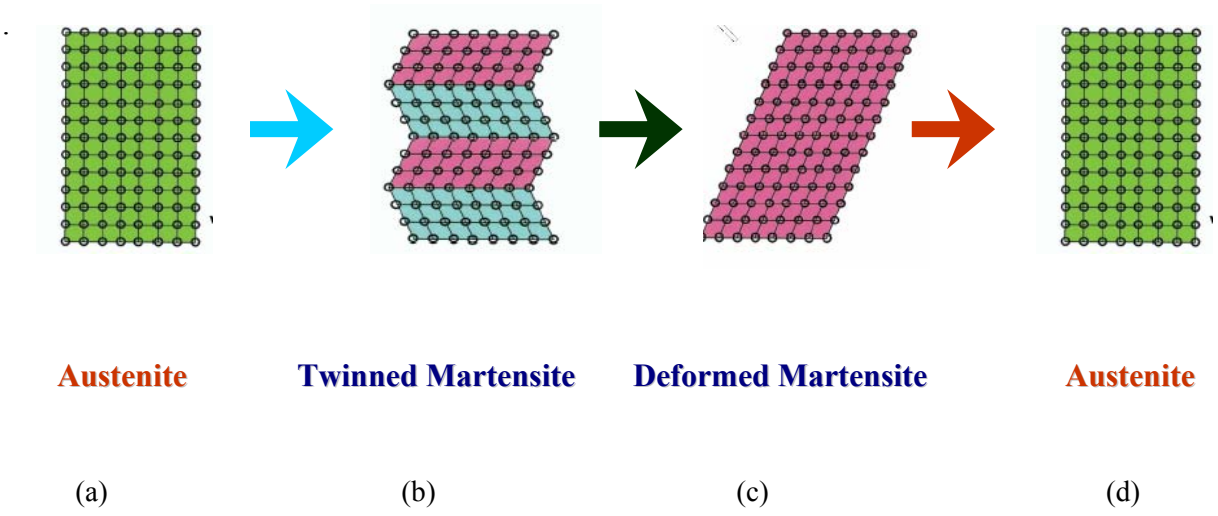

Figure 1.1: Mechanism of one way shape memory effect

(a) parent austenite phase (b) twinned martensite after cooling to lower temperatures (c) detwinned martensite after deformation (d) recovery back to austenite phase after heating above A_f

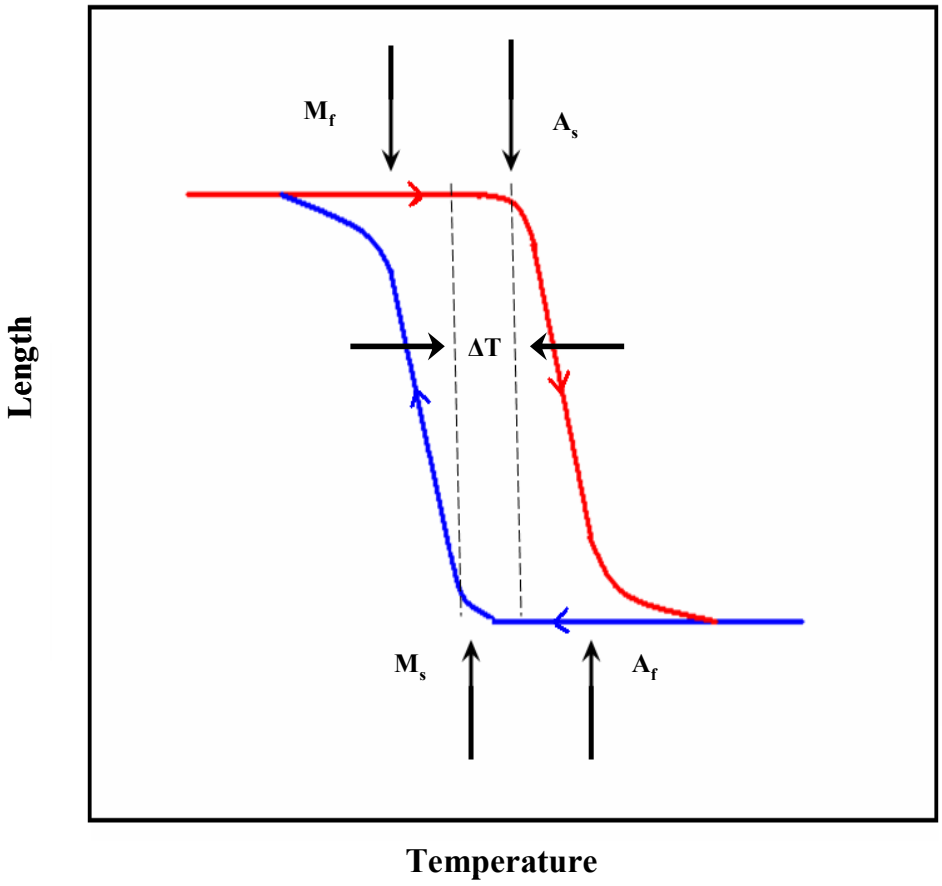

Figure 1.2: Transformation temperatures during the shape memory effect

The range of transition for the martensite to austenite transformation, which takes place upon heating, is slightly higher than that for the reverse transformation upon cooling. The difference between the transition temperatures upon heating and cooling is called hysteresis. This difference is typically 20 – 60 °C [Buehler *et al*. 1967, Funakubo 1987] in the case of a martensitic transformation in NiTi alloys. Generally, the hysteresis is measured as the difference between the M_s (martensite start temperature) and A_s (austenite start temperature) temperatures during the transformations. Figure 1.2 shows a typical hysteresis curve for a shape memory alloy

indicating the fraction of phase transforming from austenite to martensite completely as you decrease the temperature and vice versa while heating.

1.2.2 Stress Induced Transformation / Pseudoelasticity

A unique property exhibited by shape memory alloys which involves a phase transformation due to stress is known as superelasticity or pseudoelasticity. Application of an external stress causes martensite to form at temperatures higher than M_s. The macroscopic deformation is accommodated by the formation of martensite. When the stress is removed, the martensite transforms back into austenite and the specimen returns back to its original shape. There is a temperature above which inducing martensite with stress is no longer possible known as M_d. Thus, superelasticity appears in a temperature range from near A_f and upto M_d. Figure 1.3 shows the change in crystal structure from cubic to monoclinic with the application of stress and reverting back to austenite with the removal of stress.

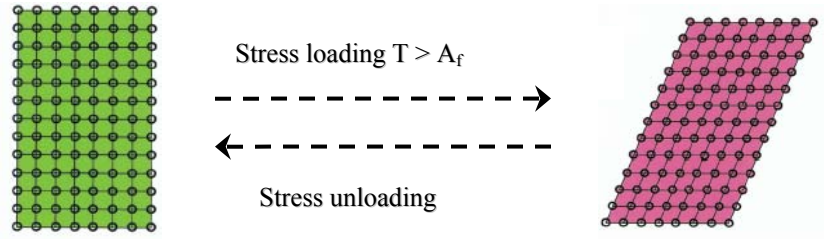

Figure 1.3: Superelasticity: (a) austenite (b) martensite

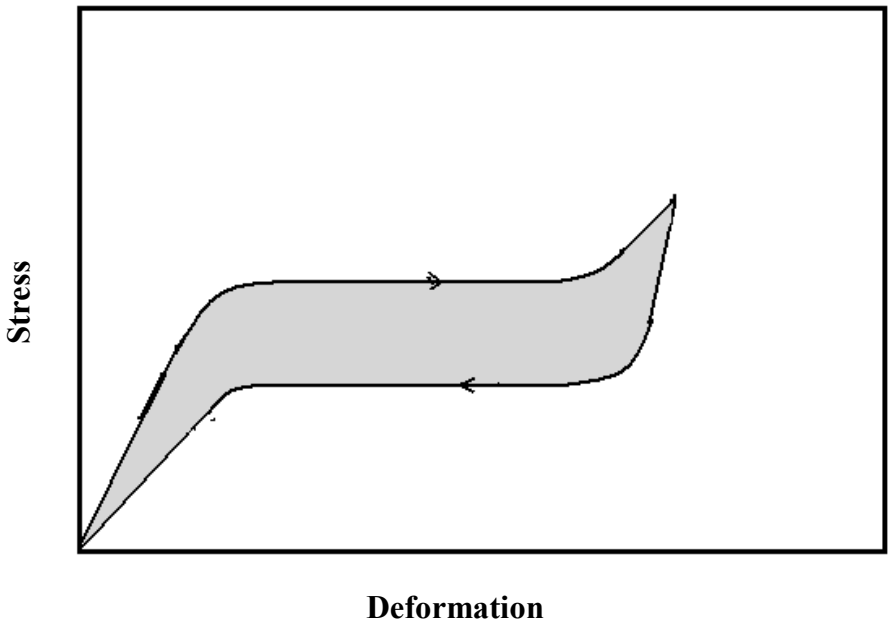

Figure 1.4: Stress-strain curve showing superelastic behavior

A typical stress strain curve showing superelastic behavior of a shape memory alloy is shown in Figure 1.4 where upon removal of stress the material reverts back to austenite recovering the entire strain. Due to the amount of strain it can recover due to the loading and unloading of stress, this particular phenomenon is widely used in cell phone antennae, cardio vascular stents, eye glass frames, orthodontic wires and a variety of medical applications.

1.2.3 Constrained Recovery

The property of a shape memory alloy generating recovery stresses when impeded during heating from martensite to austenite is known as constrained recovery. The generation of the recovery stresses starts from macroscopic deformation in the martensitic state. During subsequent heating, free recovery occurs till a temperature T_c. The recovery of the remaining deformation, characterized by the contact strain is impeded by an external mechanical obstacle.

From the temperature T_c, recovery stresses are generated at a nearly constant stress rate $d\sigma/dT$. This particular shape memory property can be used in many successful applications e.g., well-known tube couplings, actuators etc.

1.3 Applications of Shape Memory Alloys

Shape memory alloys have many unique properties which lend themselves to a variety of applications. Apart from the large amount of recoverable strains (8 %) in these alloys, if a shape memory alloy is constrained to physically prevent the SME from occurring, then stresses up to 700 MPa can be generated [Melton 1998]. An enormous number of applications have been suggested using this range of deliverable properties available to the designer. In many of the practical applications of shape memory alloys, they are used in such a way that they yield an abrupt shape change at a specific temperature during thermal cycling under load.

In general, the first successful application of these shape memory alloys was made by Raychem Corp. in the case of fasteners and tube couplings. The classical advantages of the cryogenic NiTi couplings for the aircraft hydraulic tubes are:

1. Light weight - some alloys can be specifically processed in order to increase the recovery strength significantly [Proft *et al*. 1990].
2. Easy, craft insensitive installation even in difficult to access areas.
3. Proven reliability – shape memory alloy couplings have an excellent track record.

Due to their property to recover to their original shape after sensing a temperature these materials are used in actuator applications. A shape memory alloy actuator is a type of thermal actuator which is capable of converting thermal energy to mechanical energy. It utilizes the

shape memory effect to generate motion and force. The ability of these alloys to recover large strains against significant force make them an appealing choice for actuator elements. Shape memory alloy actuators have an advantage because they are easier to design and have an additional advantage of the shape memory alloy element behaving both as a sensor and as an actuator. The shape memory alloy element can be heated by means of exposure to a temperature change or by means of electrical resistance heating which allows a window for design and flexibility in application.

NiTi is used as a biomaterial due to its excellent corrosion resistance, biocompatibility and strength. The first efforts to exploit the potential of NiTi as an implant material for bio medical applications were made by Johnson and Alicandri in 1968 [Castleman *et al.* 1976]. The potential use of NiTi in various medical applications was first reported in the 1970s [Cutright *et al.* 1973, Simon *et al.* 1977].

Superelastic properties of shape memory alloys can be used in many of the medical applications such as in dentistry as a dental arch wire [Ohura *et al.* 1984, Sachdeva *et al*. 1989]. In addition to these properties NiTi alloys can exhibit a high mechanical damping capacity due to the easy movement of twin boundaries [Lin *et al*. 1993, Lin *et al*. 1995] and excellent wear/erosion resistance resulting from their rapid work hardening and pseudoelastic properties [Clayton *et al*. 1993, Richman *et al.* 1992].

Many of the shape memory alloys cannot be used at temperatures higher than 100 °C due to the limitation of the martensitic temperatures. To extend their industrial applications, shape memory alloys which can exhibit the shape memory effect at higher temperatures are in high demand. Ti-Ni-X (X=Au, Pd, Zr) ternary alloys have been developed as potential high temperature shape memory alloys [Wu *et al*. 1987, Enami *et al*. 1987]. Among the several types

of high performance materials, NiTi films are excellent candidates in fabricating micro-actuators. Hence, efforts have been made to fabricate NiTi films using many different coating techniques [Walker *et al*. 1990, Busch *et al*. 1991]. An emerging field for shape memory alloys in biomedical applications is stents. Stents are intravascular scaffolding devices as shown in Figure 1.5 that have been used significantly during the last decade and the main advantage of using NiTi alloys instead of stainless steel is that those stents can be self expandable (when removed from the catheter) due to the superelastic effect or just by the shape memory effect during adaptation to the body temperature.

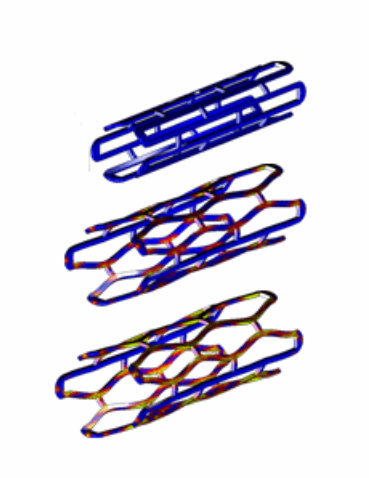

Figure 1.5: Applications of shape memory alloys in the form of stents

[www.mscsoftware.com]

Due to the toxic nature of Ni, the main interest in the medical field is in Ni free shape memory alloys [Kim *et al*. 2006]. Superelasticity has been observed in Ti-Nb alloys at room temperature although the recovery strain is small due to the low critical stress for slip deformation [Kim *et al*. 2004].

1.4 Dynamic Mechanical Analysis

Dynamic Mechanical Analysis (DMA) can be simply described as *applying an oscillatory force to a sample material and analyzing the material's response to that force*. From this, one can calculate properties like the tendency to flow (called viscosity) from the phase lag and the stiffness from the sample recovery. These properties are often described as the ability to lose energy as heat (damping) and the ability to recover from deformation (elasticity). Dynamic mechanical analysis (DMA) or dynamic mechanical thermal analysis (DMTA) is a technique used to study and characterize materials in different temperature ranges. It is most useful for observing the viscoelastic nature of polymers. An oscillating force is applied to a sample of material and the resulting displacement of the sample is measured. From this, the stiffness of the sample can be determined, and the sample modulus can be calculated. By measuring the time lag in the displacement compared to the applied force it is possible to determine the damping properties of the material. DMA can also resolve beta transitions in many materials that the DSC technique is not sensitive enough to pick up.

The aforementioned phenomenon is used in the characterization of shape memory alloys since these materials vary properties with temperature. Unlike the dynamic mode utilized for polymers, a static mode (quasi static loading) is applied to study the deformation behaviors in various phases of these materials. The factors which can be varied at the same time such as temperature, load and displacement make this technique powerful in characterizing materials.

CHAPTER 2: LITERATURE REVIEW

Shape memory materials have attracted considerable attention in recent years in a variety of industrial and medical applications. Due to their ability to perform sensing and actuating functions [Grummon *et al*. 1997], these materials are also termed as "smart materials". The subsequent sections in this chapter give a brief overview on the aspects of NiTi alloys, properties of the R-phase and NiTiFe alloys.

2.1 NiTi Shape Memory Alloys

Among the numerous alloys available as shape memory materials, NiTi based alloys are commonly used because of their excellent mechanical properties, corrosion resistance and biocompatibility. The hysteresis in the equiatomic NiTi alloys is around 40 °C [Saburi 1998]. In order to develop a suitable material for switch actuators, it should possess low hysteresis which is acquired by addition of Fe to the NiTi system due to the characteristic R-Phase transformation.

2.1.1 Phase Transformations in NiTi Alloys

As presented earlier, a near equiatomic NiTi alloy undergoes a transformation from a parent phase (β) with a B2 structure to the phase with a monoclinic B19' structure, or with a two-step transformation from the β to a trigonal phase (so called R-phase) and then to the B19' phase. These transformation behaviors and the mechanical properties in NiTi alloys can be affected by many factors such as the addition of ternary alloying elements, cold working, thermal cycling

and aging of Ni-rich alloys. Depending on various conditions, the phase transformation can take various paths such as B2 ⟶ B19', B2 ⟶ R ⟶ B19', B2 ⟶ B19 ⟶ B19', B2 ⟶ R ⟶ B19 ⟶ B19' [Beyer 1995].

2.1.1.1 R-phase in NiTi Alloys

The R-phase transformation in shape memory NiTi alloys has been studied intensively for nearly three decades owing to its characteristic crystal structure (trigonal) and the so-called precursor phenomena as well as excellent shape memory properties.

Due to its low hysteresis value which is in the range of 2 K when compared to that of 10 K or more for martensitic transformation this particular phenomena is used in designing certain actuators. The maximum recoverable strain obtained in this transformation is around 1 % and is small when compared to that of the martensitic transformation which is around 8 % [Miyazaki and Otsuka 1984].

The R-phase transformation which is formed in NiTi alloys appears under certain conditions prior to the transformation to B19' phase. This transformation is characterized by a sharp increase of electrical resistivity with extremely small temperature hysteresis (1-2 K) and the appearance of sharp super lattice reflections in diffraction patterns along the <110> and <111> directions of the parent phase in reciprocal space. The understanding of the crystal structure and the phenomena was controversial for many years. This phenomena was interpreted in various ways such as a order-disorder transition [Wang *et al*. 1965] and after extensive work by Sandrock *et al*. [1971] it was considered to be a precursor phenomena due to displacement waves, which is necessary to create the subsequent B19' martensitic structure. However, after

subsequent studies they have established that this transformation is a martensitic transformation from B2 to R phase due to the following reasons. R-phase martensite plates are clearly observed in electron microscopy [Hwang *et al.* 1983]. The shape memory and superelasticity effects which are characteristic of a thermoelastic transformation are also observed associated with this phenomenon. Both the B2 to R and the B2 to B19' transformations compete with each other; if the R-phase appears first, the successive transformation occurs in a sequence of

B2 $\longrightarrow$ R $\longrightarrow$ B19' and if the B19' transformation occurs first then the R phase transformation is suppressed.

2.1.1.2 Structure of R-Phase

The R-phase has a trigonal structure which is described by a hexagonal lattice for convenience. Although the R-phase is reported to be tetragonal, it is recognized as a rhombohedral distortion and it can be described by stretching the cubic parent lattice along the <111> diagonal direction, i.e., the corner angle α which is 90° in the B2 parent phase deviates from 90° with decreasing temperature [Salamon *et al*. 1985] as shown in Figure 2.1.

The space group of the R-phase is currently in debate, but initially it was reported by Goo and Sinclair to be P31m. Later, Hara *et al*. [1997] studied the structure of the R-phase by utilizing various techniques such as convergent beam electron diffraction, and found it to be P3. However, Sitepu [2003] carried out synchrotron radiation experiments and claimed to find agreement with the $P\bar{3}$ space group rather than P3. Recent studies conducted by Allafi *et al*. [2006] using electron diffraction and neutron diffraction studies on a $Ni_{50.8}Ti_{49.2}$ alloy at room

temperature using different models tested with all possible symmetries using the Rietveld refinements showed that the symmetry favored is $P\bar{3}$.

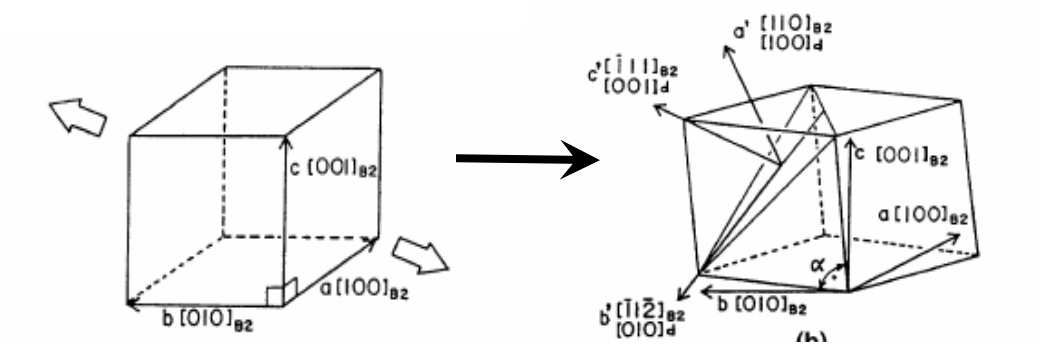

Figure 2.1: Lattice change from B2 to R-phase. The axes a', b', c' represent the principal axes in that lattice deformation [Otsuka and Ren 2005]

2.1.2 Effect of Ternary Alloying in NiTi alloys

It has been observed that the shape recovery temperature is highest at the stoichiometric composition (50 at% Ti- 50at% Ni) in the binary Ni-Ti system. Addition of the ternary alloying elements affects the transformation temperatures and thus the shape recovery temperatures of Ni-Ti alloys [Saburi 1998]. Substitution of vanadium, chromium, manganese or aluminum for titanium lowers the transformation temperatures. Substitution of cobalt or iron for nickel also lowers the martensitic transformation temperature ranges of B2 to R and the R to B19' effectively.

Addition of Fe is of interest in many of the actuator applications because it allows for the observation of the R-phase which in turn has very low hysteresis and high fatigue life when

compared to martensite. Composition dependence of the atom locations of the third elements in Ni-Ti-X shape memory alloys (X=Cr, Mn, Fe, Co, Cu) was investigated by electron channeling microanalysis [Nakata *et al*. 1991] and it was found that the added third elements occupied different atom sites depending upon the kind of third elements. In case of $Ti_{50-x}Ni_{50}X_x$ alloys, Mn and Cu mainly occupied the Ti atom while Fe and Co occupied the Ni site and Cr occupied both sites with equal probability.

Some ternary alloying additions, even at very small levels (for example, Fe or Co substituted for Ni, and Al, Mn, V, or Cr substituted for Ti), will severely depress the transformation temperatures of NiTi alloys but still result in a monoclinic martensite phase after transformation of the matrix [Bozzolo *et al*. 2005].

2.1.3 Effect of Thermo-Mechanical Treatment in NiTi alloys

Thermo-mechanical treatment plays an important role in the mechanical properties of NiTi alloys and assists in the introduction and the stability of the R-phase. Thermo mechanical treatments on NiTi alloys include combination of solutionizing, aging, cold working followed by annealing and thermal cycling [Miyazaki and Otsuka 1986]. Ni- rich NiTi alloys are of importance because they are susceptible to thermo-mechanical treatments. Aging in Ni rich alloys have been studied by Allafi *et al*. [2002] wherein they observed the transformation of B2 to B19' from a single step to a multi-step process and the formation of the R phase with aging in NiTi alloys is due to the formation of Ni_4Ti_3 precipitates and due to the difference between the nucleation barriers for R-phase (small) and B19' (large).

2.1.4 Effect of Cold Rolling and Annealing in NiTi Alloys

Cold rolling and annealing have significant effects on the mechanical behavior and the superelastic properties in NiTi alloys. The superelastic properties increase when a NiTi alloy is cold rolled to certain extent and annealed at relatively low temperatures not allowing the matrix to undergo recrystallization. Superelasticity is not observed in the solution treated condition because slip is easily introduced [Otsuka and Ren 2005]. The material undergoes a smooth martensitic transformation when annealed at a lower temperature not allowing the lattice to recrystallize but still holds high strength due to rearranged dislocations. Best superelasticity and shape memory characteristics were obtained when a Ti-49.8Ni alloy was annealed at 673 K after cold working [Miyazaki *et al.* 1982].

The R-phase transformation which is formed in near equiatomic NiTi alloys can become a two stage transformation depending upon the cold working and the annealing temperatures [Chrobak *et al*. 2005]. This group investigated the affect of annealing at higher temperatures compared to similar studies made on these alloys that were annealed at lower temperatures while varying the annealing time [Chrobak *et al.* 2003]. The DSC graphs (Figure 2.2) and the resistivity measurements show that the transformation occurred in two steps and this was explained on the basis of the dislocation density where regions of lower density transformed to R-phase first at a higher temperature and regions of higher dislocation density transform to R-phase at a lower temperature and vice versa for the B19' transformation.

Thus, it was concluded that the course of transformation is dependent on the mutual interaction of the inhomogenities and the internal stresses introduced by the cold rolling process.

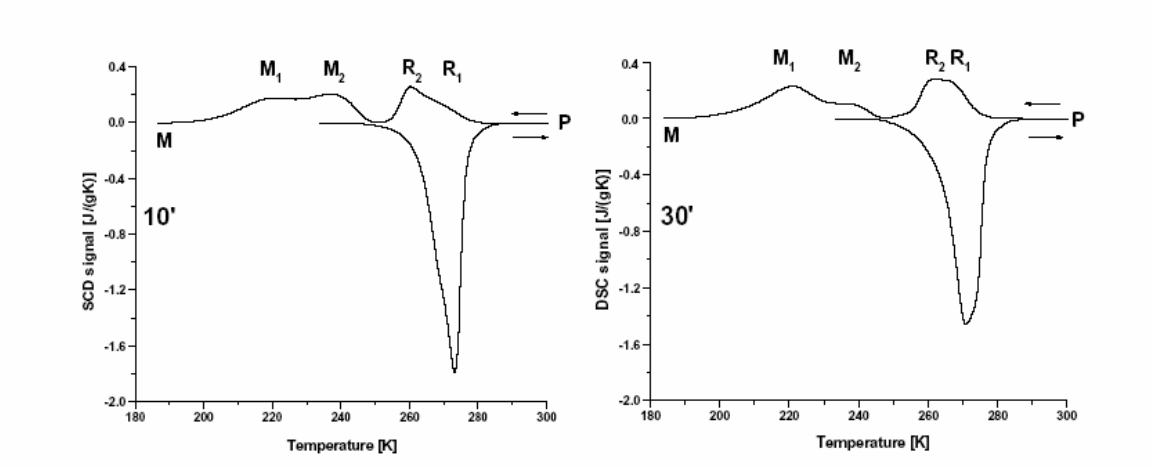

Figure 2.2: DSC for 15 % cold rolled samples and annealed at 773 K for (a) 10 minutes and (b) 30 minutes [Chrobak *et al.* 2005]

The effect of cold working and annealing temperature on the development of transformation and plastic strain in shape memory alloys with one way shape memory was studied by Miller *et al.* [2001]. Fully annealed shape memory alloy specimens of identical composition were cold rolled to reduce the specimen width 10, 20, 30 and 40 % of the initial wire diameter and then annealed at 300, 400 and 500 °C for 15 minutes. It was observed that the maximum transformation strain was independent of the cold work percentage and annealing temperature, and as the cold work was increased for similar annealing temperatures, it raised the stress level for the onset of plastic strain and decreased the additional plastic strain development.

(a)

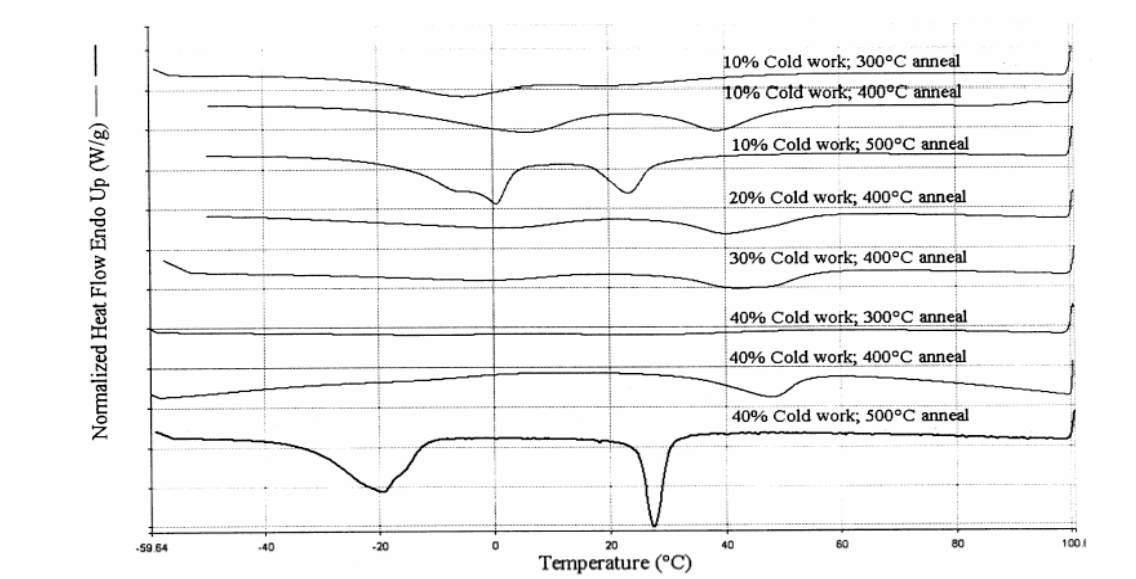

(b)

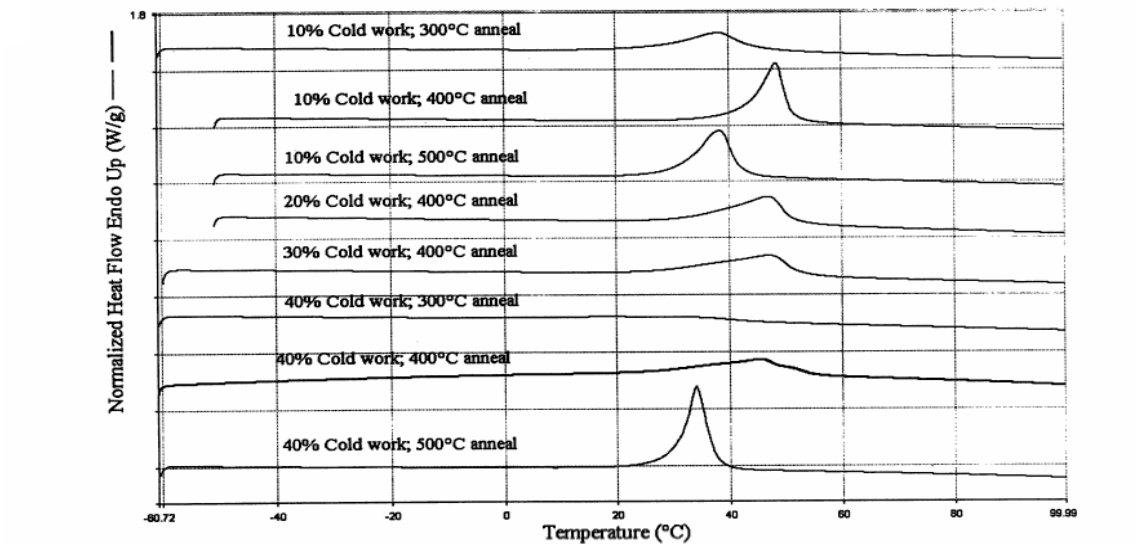

Figure 2.3: (a) DSC cooling curves showing the variation of transformation temperatures for various levels of cold work and heat treatment during the austenite to martensitic transformation. (b) DSC heating curves of the martensitic to austenitic transformation [Miller *et al*. 2001]

As the annealing temperature was decreased for similar cold work percentages, the stress level for the onset of plastic strain increased. DSC curves from these experiments shown in

Figure 2.3 concluded that the latent heat of transformation decreases with decreasing annealing temperatures and increasing amount of cold work.

This was explained by the dislocations associated with high levels of plastic deformation generating an internal stress state which restricted martensite from transforming to austenite. This martensite phase remained 'pinned' in the microstructure until the dislocations were removed through an annealing process. Therefore, the generation of the 'pinned' martensitic microstructure reduced the latent heat of transformation because of less material undergoing the transformation.

2.2 NiTiFe Shape Memory Alloys

A typical NiTi alloy undergoes a direct B2 to B19' transformation - however, the addition of Fe introduces an intermediate phase and makes it a two stage transformation B2 to R to B19' [Otsuka and Ren 2005]. The addition of Fe results in a gradual decrease in the transformation temperature of the R-phase but excessive amounts have a significant effect on the martensitic transformation in such a way that the transformation is completely suppressed until 4 K [Canales 1995]. Thus due to these characteristics, NiTiFe alloys are suitable for actuator design which can use the R-phase transformation at cryogenic temperatures.

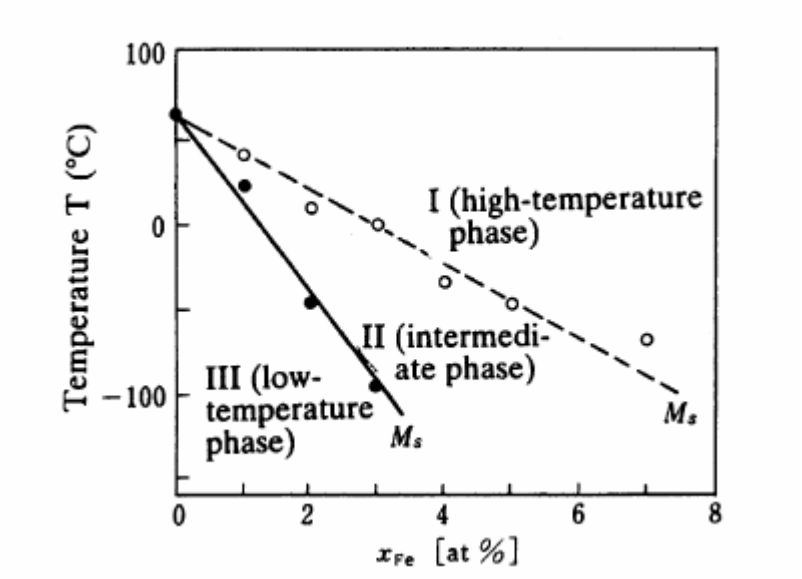

Figure 2.4: Effect of Fe addition on the martensitic transformation temperature

[Otsuka and Ren 2005]

2.2.1 Martensitic Transformations in NiTiFe Alloys

Addition of 2 at% Fe separates the R-phase transformation from the martensitic transformation by 60 °C [Xu 2000]. Substitution of 3 at% Fe for nickel in NiTi lowers the martensitic transformation by more than 100 °C [Hwang *et al*. 1983]. In the studies conducted by Hwang *et al*. [1982] on the $Ti_{50}Ni_{47}Fe_3$ alloy the martensite start temperature was estimated to be about -98 °C. The formation of martensite was observed using electron microscopy where lenticular shape martensite plates were seen to abruptly grow. However, the 1/3 rd super lattice reflections which were characteristic of the R-phase in NiTi alloys were not found in this transformation. They confirmed the crystal structure of the martensite to be monoclinic from the diffraction patterns obtained. As mentioned before, addition of Fe reduces the M_s to a great extent and in some cases it completely suppresses the martensitic transformation such as in

$Ti_{50}Ni_{45}Fe_5$ [Canales 1995]. The study done on this alloy did not show any martensitic transformation as low as 4 K.

2.3 Mechanical Behavior of Shape Memory Alloys

A characteristic stress strain curve of a shape memory alloy tested between the temperatures M_s and M_d is schematically shown in Figure 2.5. Characteristic features of this curve are described as follows [Hosoda 1998]:

1. The first yield like behavior occurs when stress induced martensite transformation forms.
2. After completion of martensite formation, a plateau appears by reorientation of martensite variants.
3. The second yield like behavior occurs when plastic deformation of the martensite phase takes place.

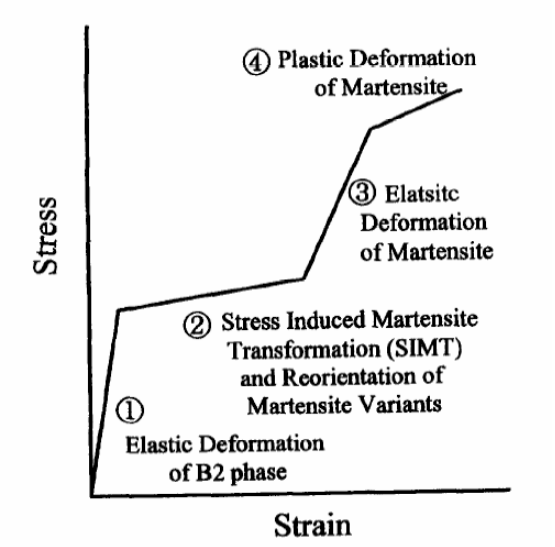

Figure 2.5: A stress strain curve for a shape memory alloy between M_s and M_d temperatures [Hosoda 1998]

2.3.1 Deformation in NiTi Alloys

The deformation behavior of NiTi alloys of various temperature ranges is significant from an application point of view such as actuators. Many materials exhibiting the shape memory effect when subjected to stress, results in the formation of specific variants of the martensite. Consequently, the martensitic start temperature increases as the externally applied stress increases. However, in some cases an anomalous behavior of M_s decreasing as the external applied stress increases is observed in the B2 to R transition of a Ti-51 at % Ni alloy which includes the aligned particles of Ti_3Ni_4 precipitates formed by aging under an applied stress [Fukuda *et al*. 1997]. Detailed studies of the deformation behaviors associated with the R-phase and the martensitic transformation were carried out over a wide temperature range in NiTi alloys subjected to various heat treatments [Miyazaki and Otsuka 1986]. It was observed that aging after solution treatment and annealing at temperatures below the recrystallization temperature immediately after cold work showed the R-phase over a wide temperature range in the electron microscopy observations and in tensile tests. Deformation behavior associated with the R-phase and the martensitic transformations were classified depending on the deformation modes and the shapes of stress-strain curves.

Investigations have been made in NiTi alloys and the stress-strain curves show that they consist of three stages similar to FCC and HCP single crystals [Rozner and Wasilweski 1966] and [Cross *et al*. 1969]. However, these groups did not study the unloading portions and did not clarify the nature of these stages.

2.3.2 Deformation in NiTiFe Alloys

When an external stress is applied to a specimen kept slightly above $M_{s,}$ stress induced martensitic transformation occurs. The study conducted by Fukuda *et al*. [1997] demonstrated that the stress induced R to B2 transformation occurs and the explanation is given thermodynamically. Different tensile tests were conducted on a $Ti_{50}Ni_{48.5}Fe_{1.5}$ alloy at various temperatures (one completely in R-phase, second a mixture of R phase and B2 and the third completely in B2 phase). They observed that the residual strain decreased with the increase in temperature as the phase transformation from R phase to B2 occurs. The stress strain graphs at various temperatures are shown in Figure 2.6.

.

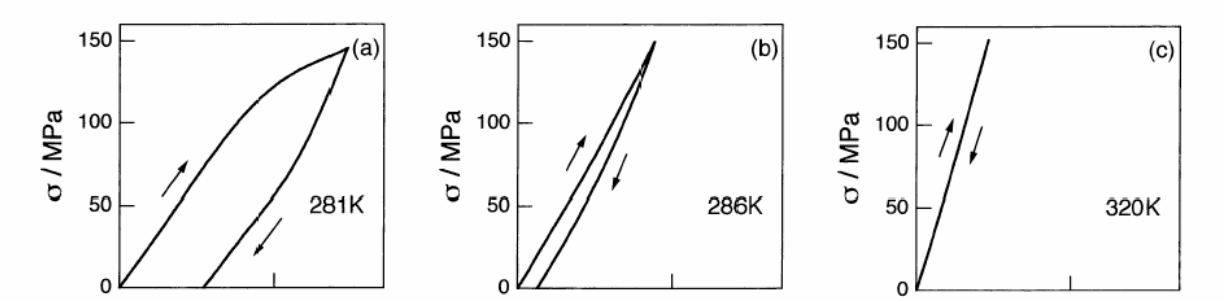

Figure 2.6: Stress-strain graphs of a $Ti_{50}Ni_{48.5}Fe_{1.5}$ alloy at various temperatures

[Fukuda *et al*. 1997]

Deformation of a $Ti_{50}Ni_{48}Fe_2$ alloy tested at -70 °C and ambient temperatures was studied by Xu *et al*. [2000] and they observed that a maximum shape recovery strain of 5.6 % was obtained in this alloy when deformed at -70 °C (the starting stage of this alloy at that temperature is martensite). Deformation behavior of a $Ti_{50}Ni_{47}Fe_3$ alloy which shows a premartensitic transformation was studied in a wide temperature range from M_s to above T_R [Miyazaki and Otsuka 1984]. Stress-strain curves were divided into six regimes and found that two stage yielding was observed in the curves between temperatures M_f and T_X where the later represents the temperature at which the critical stress needed to induce the R-phase equals the stress required to induce the martensitic transformation. The first stage is confirmed to be associated with the R-phase transition and the second with the martensitic transformation.

2.3.3 Twinning in the R-Phase

As described in the previous Section 2.1.1.2, the structure of the R-phase is trigonal by which it is easy to describe it with hexagonal indices. Since the c-axis of the R-phase corresponds to the $<111>_p$ of the parent phase, there can be four lattice correspondence variants as shown in the Table 2.1. Twinning in the R-phase was studied by Miyazaki and Wayman [1988] and Fukuda *et al*. [1992]. They found that there are two types of twins $\{11\bar{2}1\}_R$ and $\{11\bar{2}\,\bar{2}\}_R$ which correspond to $\{100\}_p$ and $\{011\}_p$ of the parent lattice respectively. The values of s (twinning shear) is the same since they are conjugate twins to each other.

Table 2.1: Lattice correspondences between the B2 and R-phases

Variant	$[100]_R$	$[010]_R$	$[001]_R$	$(0001)_R$
1	$[1\bar{2}1\}_p$	$[11\bar{2}]$	$[111]$	$(111)_p$
2	$[211]_p$	$[\bar{1}1\bar{2}]_p$	$[\bar{1}11]_p$	$(\bar{1}11)_p$
3	$[121]_p$	$[112]_p$	$[\bar{1}\bar{1}1]_p$	$(\bar{1}\bar{1}1)_p$
4	$[211]$	$[11\bar{2}]$	$[1\bar{1}1]_p$	$(1\bar{1}1)_p$

[Fukuda et al. 1992]

2.3.4 Thermo-Mechanical Treatment on NiTiFe Alloys

Among the mechanical properties that are influenced by cold working and annealing, yield strength and ductility are significantly affected. Cold working introduces a combination of dislocations and twins into the structure. The grains which are formed in annealed samples are found to grow at the twins. Thus, the sub-grains which are formed in a heavily cold worked material are small and refined, which gives the combined properties of strength and ductility. Studies by Moberly *et al*. [1990] with different combinations of cold work and annealing temperatures on several $Ti_{50}Ni_{47}Fe_3$ samples show that unlike NiTi alloys, cold working does not cause the formation of stress induced martensite in NiTiFe alloys. It has been observed that the R to martensite transformation temperatures decreased with increasing the cold working percentage. In the NiTiFe alloys observed, the maximum two way shape memory effect was observed in the 5-10 % reduced samples [Wang *et al*. 2005].

2.3.5 Thermodynamics of Stress Induced Transformations

An approximation of the effect of stress on the martensite transformation can be obtained from the Clausius-Clapeyron equation [Warlimon *et al*. 1974, Miura *et al*. 1976]. It is given by $\frac{d\sigma}{dT} = \frac{\rho.\Delta H}{\Delta\varepsilon.To}$ where dσ/dT is the temperature coefficient of the critical stress for the transformation in the temperature range M_s but below M_d, Δε is the amount of strain due to the transformation, measured from the length of the initial plateau on the stress strain curve, ρ is the density of the alloy, ΔH the heat of transformation at the temperature T_o where the two phases are in chemical equilibrium. This relationship was used to determine the equivalence between stress and temperature involved in the phase transformations were calculated by using $\Delta\sigma_{trans}/\Delta T$ in case of polycrystalline NiTi tested in tension. Normally this value ranges between 3.3 to 13 MPa/K for the B2 to B19' transformation [Leo *et al*. 1993, Kato *et al*. 1994, Miyazaki and Otsuka 1986]. Compressive mechanical properties and the affect of TiC particles in a NiTi matrix were studied and this formulation was used in compression by Fukami-Ushiro *et al*. [1996].

CHAPTER 3: COMMISSIONING OF A DYNAMIC MECHANICAL ANALYZER

This chapter briefly describes the principle of the dynamic mechanical analyzer (DMA), its components and the operation procedure involved in conducting various experiments in the DMA. The author acknowledges Mike Brookhart for his extended help in writing the manual for the DMA.

3.1 Introduction to the Dynamic Mechanical Analyzer

Dynamic mechanical analyzer is an instrument based on the aforementioned principle of dynamic mechanical analysis.

Factors that can be varied in this instrument are:

1. Load - the maximum load that can be obtained on this instrument is 10 N for static loading and 10 ± 8 N for dynamic loading.
2. Displacement
3. Temperature – the temperature can be varied from -150 °C to 600 °C
4. Loading rate

3.2 Dynamic Mechanical Analyzer Components

DMA consists of an electromagnetic force motor which generates the force and the displacement in the material is recorded by a linear variable displacement transducer (LVDT).

The components of the DMA include the following as shown in Figure 3.1.

Figure 3.1: Dynamic Mechanical Analyzer

1. Measurement unit for sample setting and measurements
2. DMA Base unit (module)
3. Cooling control unit
4. Liquid nitrogen cooling container (including cooling lines, valves, etc.)

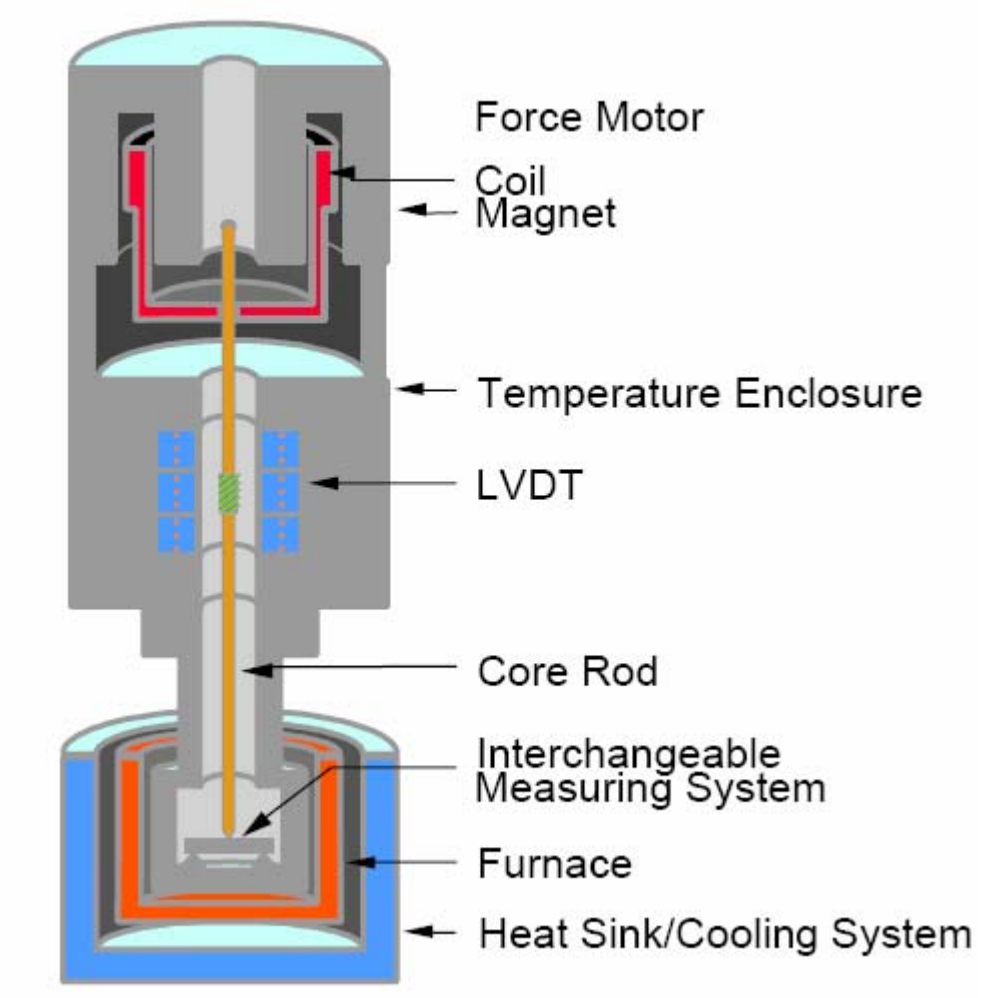

Figure 3.2: Schematic of the internal components in the measuring unit [Perkin Elmer Inc.]

The internal components of the DMA are shown in the schematic presented in Figure 3.2.

The assembled DMA module can be used as a thermal analysis system by connecting it with the pyris station (as shown in Figure 3.3). Option such as the automatic cooling system is also attached to the station to upgrade the functions of the station.

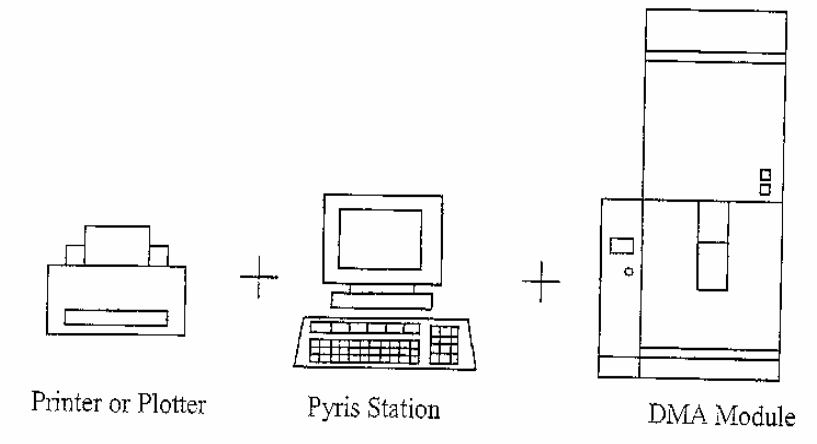

Figure 3.3: Standard DMA system configuration

3.2.1 Automatic Gas Cooling Unit

Operation Principle:

The analysis module simultaneously controls the temperature of the furnace according to the temperature program and sends appropriate control signals to the cooling controller, in accordance with the temperature program. The cooling controller in turn regulates the power to the heater inside the liquid nitrogen tank according to the cooling control signals it receives. The heater inside the liquid nitrogen tank evaporates an amount of liquid nitrogen proportional to the power it receives, with the evaporated liquid nitrogen leaving the tank as cooling gas. The cooling gas flows into the furnace through the cooling gas supply pipe and cools the furnace. The schematic of the automatic gas cooling unit is shown in Figure 3.4.

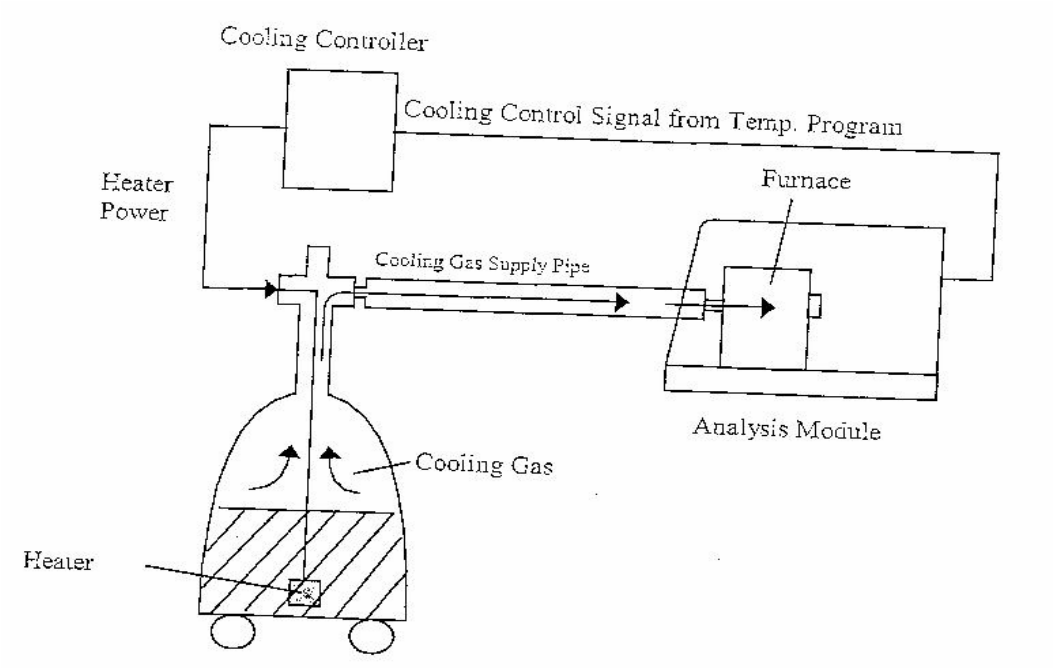

Figure 3.4: Automatic gas cooling unit

3.2.2 Cooling Controller

The cooling controller supplies power to the liquid nitrogen heater according to cooling control signals from the analysis module. The front panel of the cooling controller is shown in Figure 3.5.

3.2.2.1 Powering on the Cooling Controller and the Pyris Station

POWER ON

On the DMA base and cooling controller units there is a power switch located on the front left of the units.

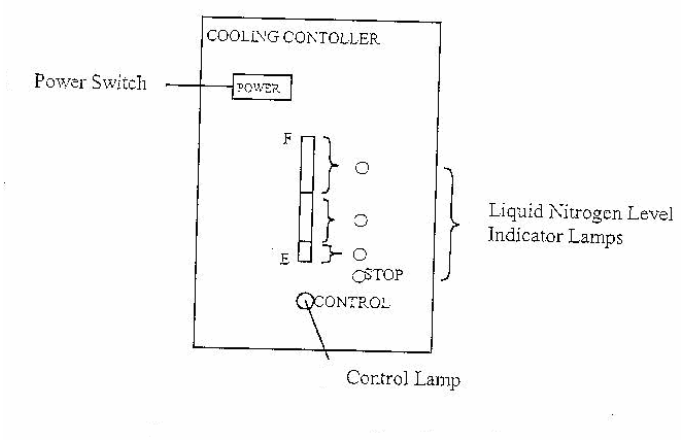

Figure 3.5: Front panel of the cooling controller

The cooling control unit can be turned on by pressing the power button on the cooling control unit.

1. First the DMA base unit should be switched on by pressing the power button on the base unit
2. Then the Pyris station (main computer) should be switched on using the power button on the CPU of the computer and the power button on the monitor (same practice as an ordinary office computer)

POWER OFF

1. Turning off the cooling controller with analysis module
   - The DMA base unit and the cooling controller are automatically shut down when the analysis software is exited on the Pyris station (main computer).
2. In the event that the machines do not automatically shut down
   - Behind each unit there is a small black button that will shut down each unit individually. THIS IS NOT THE PREFERRED METHOD OF SHUT DOWN for DMA base and cooling controller units. (Refer to step 1 for preferred shutdown method of both units).

3. The Pyris station is shut down by using the shut down command located under the start icon located on the desktop of the computer screen (same practice as shutting down an ordinary office computer).

3.2.3 Measurement Unit

The Measurement unit is the component which consists of the fixture for holding the sample, furnace, the electro magnetic motor and the LVDT. There are different fixtures that can be attached to this measurement unit depending on the kind of experiment that needs to be done. They are tension, compression and the bending fixtures.

3.2.3.1 Powering on the Measurement Unit

CAUTION:

1. Never move the liquid nitrogen tank or cooling gas supply pipe during or immediately after measurements which can damage the pipe.
2. Be sure to remove the dew and moisture from the furnace area and siphon after usage. Corrosion will occur if the moisture is not removed
3. Be sure to turn off the power supply when the instrument is not in use.

The power should be switched on from the measurement unit only after powering on the cooling controller (especially when desired to do experiments at lower temperatures which require the cooling controller).

3.2.4 Furnace

The furnace is used to heat the sample chamber and in turn the sample to higher temperatures or to heat back to room temperature after the experiment is conducted.

The furnace in the DMA is shown in Figure 3.6.

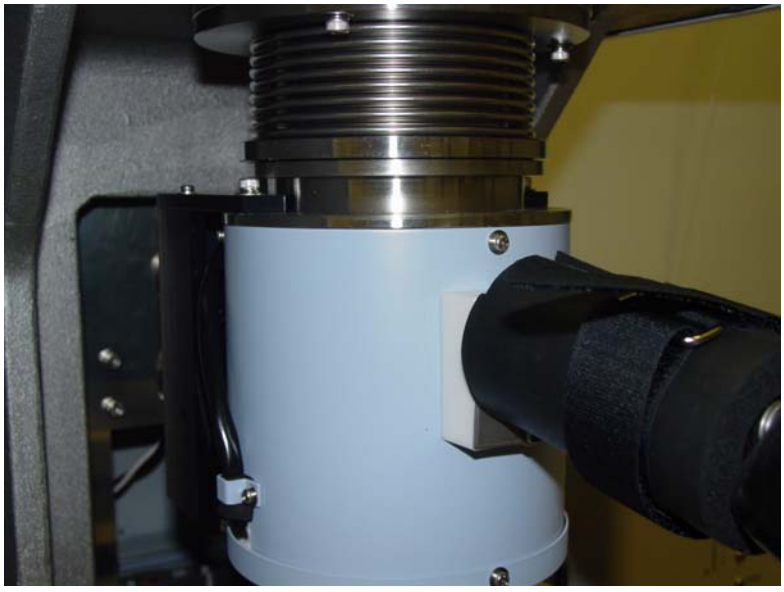

Figure 3.6: Furnace in the measurement unit

3.2.4.1 Movement of the Furnace

CAUTION

Check to ensure there are no obstructions blocking the movement of the furnace.

The furnace is moved by the following steps

1. With the DMA base unit powered on, use both hands to press and hold the two white buttons located on the front middle face of the DMA base unit

NOTE: The furnace will only move when both the furnace move switch on the right and the furnace control switch on the left are pushed simultaneously. If only one button is pressed the furnace will not move.

2. The furnace moves in a predetermined motion
    a. straight down below the material holding device
    b. straight back under the material holding device
3. Once the furnace has cleared and is behind the material holding device the buttons may be released

3.2.5 Loading the Test Sample

1. Remove the cooling gas diverting shield
    - Loosen the (4) allen head screws with the appropriate size allen head wrench located on the material holding device. Loosening these screws will allow the flat metal clamp plates to move.
2. Place the sample between the top metal plates using forceps to hold the material sample and slightly tighten.
    a) If needed adjust the sample so that it hangs vertically ensuring that it is as straight as possible. Use the vertical bars on the material holding device as guides and a pair of forceps for holding the material straight
    b) Tighten the top plates
3. Before tightening the bottom plates
    a) Recheck the test sample for vertical straightness

b) The sample may need to be held in this position while tightening the bottom plate screws

3.2.6 Fixtures

As mentioned above the DMA consists of three fixtures: tension, compression and 3-point bending etc. The tension fixture when fixed to the measurement unit is shown in Figure 3.7.

3.2.6.1 Tension to 3-Point Bending

1. Loosen the screws attached to the fixture and insert the chuck which corresponds to the tension Mode and remove the entire fixture as a whole.
2. When you remove the tension fixture **NORMALLY** the probe is in the zero position.

If you would like to insert the 3-Point bending fixture:

3. Go to module / motor control (on the main computer) and enter -16 mm
4. Click move
5. The zero position for 3-Point bending is at -16 mm.
6. Once the probe reaches -16 mm attach the bending fixture
7. Then tighten all the nuts and then remove the chuck from the fixture

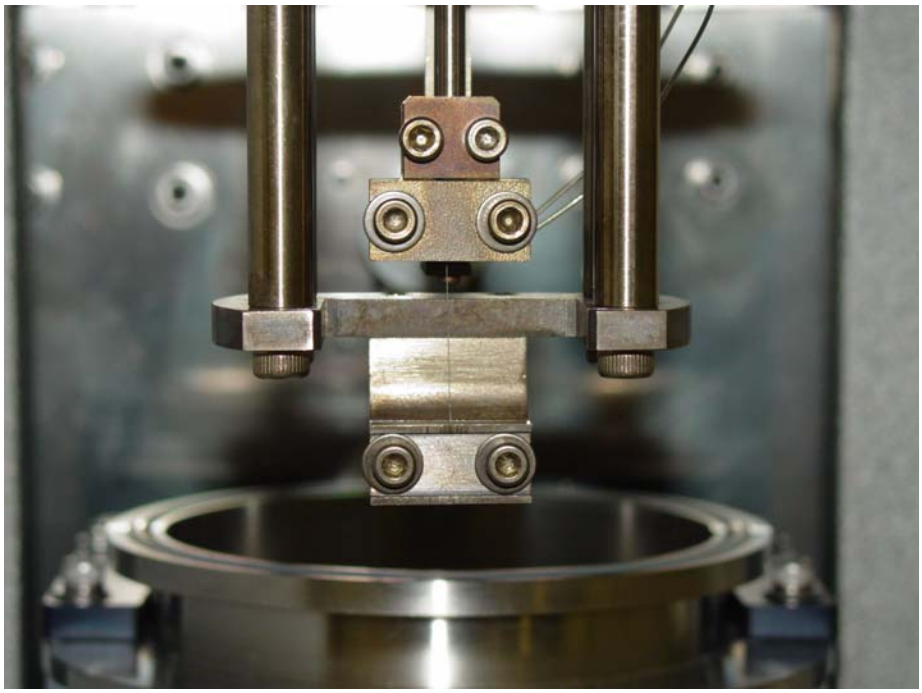

Figure 3.7: Tension fixture in the DMA

8. An auto adjustment is required after fixtures are changed (this will adjust the probe to compensate for the different fixture weights)
9. Now the unit is ready to perform the experiment in the bending mode.

3.2.6.2 3-Point Bending to Tension

1. Loosen the screws attached to the fixture and insert the chuck which corresponds to the tension mode and remove the entire fixture as a whole.
2. When you remove the bending fixture normally the zero position is at -16 mm
    a. Go to module /motor Control
    b. Enter 0 mm
    c. Click move

The zero position of the tension fixture is at 0 mm

3. Once the probe reaches 0 mm

    a. Attach the tension fixture

4. Then tighten all the nuts and then remove the chuck from the fixture

5. An auto adjustment is required after the fixtures are changed

    (this will adjust the probe to compensate for the different fixture weight)

6. Now the unit is ready to perform the experiment in the tension mode.

3.2.6.3 Introducing the Compression Fixture

For inserting the compression fixture, retain everything in tension mode and insert the compression plates in between the tension fixture (check the manual page I-2 to verify probe side compression plate and clamp side compression plate). After inserting the compression plates click auto adjustment so that the probe gets adjusted automatically.

3.3 Operation Procedure for Experimentation

3.3.1 Measurement Principle

In the dynamic viscoelasticity mode, a signal is sent to the force generator from the AC function generator and the DC function generator to generate an AC force and a DC force. These forces are transferred to the sample through the probe as a stress, and the differential transformer detects the strain in the sample. Through the determination of the amplitude and phase of the AC

component of the stress and strain signal, the dynamic viscoelasticity of the sample can be determined. The DC force cannot be used for bend or shear measurements.

There are different modes of deformation in which the measurements can be done such as bending, single cantilever, tension (standard) , 3point – bending , shear , compression and film shear (optional sample attachments).

3.3.2 Starting the Measurement Procedure

1. Ensure the measurement module base unit is connected to the main computer before the main computer is turned on
2. Switch on the main computer
3. Choose the Pyris icon on desktop of the main computer
4. Log in to the Pyris account

3.3.2.1 Gas Flow Adjustment

NOTE: The gas flow must be kept **ON** during the entire experiment including the cooling control unit. Once the experiment is completed the gas flow and the cooling unit may be turned off.

1. Before starting any kind of experiment open the gas flow from the cylinder
2. Adjust the gas flow to the desired setting of 50 psi +/- 2 psi (the flow can rest between 40 psi and 60 psi if needed but the desired is stated above)

3.3.2.2 Powering the Cooling Controller and the Base Unit

1. First switch on the power button on the cooling controller
2. Next turn the power button on the base unit (the LCD screen on the front left of the base unit will display options when powered)
3. Go to the main computer (Pyris station)
4. Find the icon labeled **MUSE** jobs on the desk top, **double click** the icon to open the program
5. Once the program is open, **double click** the **measure icon**
6. Now go to **File** and then cascade to **Open Communication port**
7. When **COM1** is displayed **click** OK
8. Now, the **MUSE Measurement** window shows **Linking** ……
9. Check that the same message is displayed on the LCD of the base unit
10. The computer asks for initialization, before initialization check the following:
    a. First the furnace needs to be moved away from the "material holding device", the furnace encapsulates the material holding device.
    b. If a test sample is already in place remove by the following steps
        i. Loosen the (4) allen head screws with an appropriate size allen head wrench located on the material holding device. Loosening these screws will allow the flat metal clamp plates to move.
        ii. Once the metal plates are loose the sample material will come out easily
        iii. After the sample has been removed, retighten the plate screws before initialization can begin
    c. Once there is no test material in the material holding device

i. Click OK in the initialization window by removing the option of the move target
ii. This initialization is performed to detect the origin point
iii. Ensure that the probe is free of samples and they are not in a “chucking state”

11. Measurement Window will show **Ready**
12. Once the window displays ready, it is time to write the program for the experiment

3.3.3 Running the Experiment

There are different kinds of experimental parameters which can be considered while conducting an experiment on the DMA. First we have to decide whether we would like to conduct an experiment in the dynamic loading mode or the static loading mode. Apart from these two modes the three important variables which one can vary are stress, strain and temperature. According to the machine they are load, displacement or deformation and temperature.

3.3.3.1 Setting the Experiment Parameters

In order to conduct an experiment in SS mode known as stress-strain control mode (this mode is generally used for metals) follow the steps listed below.

1. One can manipulate three main factors which are load, displacement and the temperature.
2. Choose which factor (load, displacement or temperature) is to be kept constant so that a variation is obtained of the other two with respect to each other. For example: temperature is held constant, load vs. displacement which can be converted to stress vs. strain at that particular temperature.

3. Conducting an experiment

   a. Go to condition editor (main computer)

   b. Enter the sample details in the sample condition tabs provided

      - Examples: sample name, shape, dimensions, operator name, comments etc. (Note: The comments given here in this tab will appear in the final result when you analyze it by standard analysis).

4. Give a suitable data file name so that you can retrieve the data later.

5. Go to method tab and select *SS Control* in the *DMS Measurement Mode*

NOTE: If conducting an experiment in the SS mode then it is a static loading mode. Other modes in the DMS Measurement mode like tension, compression, 3-point bending etc are selected only when we do dynamic loading.

3.3.3.2 Writing the Temperature and SS program

Both the temperature program and the SS program should be manipulated according to the requirements of the experiment.

1. Time is taken as an important factor to manipulate these two programs.
2. In the temperature program select ramp and then *Normal temperature control* in the *Temperature control mode*.
3. In the ramp the program looks like:

No.	End step	Start (cel)	Limit (cel)	Rate (cel/min)	Hold (min)	Sampling

4. Always start the program at 20 °C (room temperature)

5. Go to the required temperature and hold there for few minutes so that the sample temperature and the program temperature become equalized
6. Then give a next step if you would like to stay at that temperature for some amount of time.
7. If you go to the SS program tab you would have two SS control modes-one is *F control composite* (F = force control mode) and the other one is *L control composite* (L = displacement control mode).

   The SS program values look like the following:

   No. End step Start (mN) Limit (mN) Rate (mN/min) Hold (min)

Below is an example program for an easier understanding of the program writing procedure.

3.3.3.3 Example Program

We would like to conduct an experiment in F control mode (load control) for a sample and get the stress vs. strain variation at -80 °C. The loading rate is around 10 mN/min till 1000 mN while loading and while unloading it is 15 mN/min.

Writing the Program:

Now, to write the temperature program we desire the material to be taken to -80 °C and held there for a sufficient amount of time and then the loading and unloading take place at that particular temperature.

First step of the temperature program is:

No	Start (cel)	Limit (cel)	Rate	Hold	
1	20	-80	10	20	1

In this step you are taking the sample from 20 to -80 °C and then holding there at 20 min. total time required for this step is 30 min. (100/10 = 10 + 20 min holding time)

Now, during the second step of the temperature program we give a hold for some time which is decided by the time taken by the SS program in loading and unloading the sample.

SS Program looks like:

No.	End step	Start (mN)	Limit (mN)	Rate (mN/min)	Hold (min)
1		5	5	0	30
2		5	1000	10	2
3	√	1000	5	15	1

The first step is holding at load of 5 mN for 30 minutes so that the sample reaches -80 °C by that time (from the temperature program). Both the second step and the third step involve loading and unloading of the sample. Total time for step 2 and step 3 in the SS program is: 1000-5/10= 99.5 + 1000-5/15=66.33, total time = 155.83 minutes.

Now we know the time (minutes) to hold the sample at -80 °C.

Now the temperature program looks like:

No	End step	Start (cel)	Limit (cel)	Rate (cel/min)	Hold (min)	Sampling
1		20	-80	10	20	1
2		-80	-80	0	156	1
3	√	-80	20	15	2	1

- If you click the end step as three, the temperature program has three steps and in the third step it comes back to 20 °C at a heating rate of 15 °C/minute.
- Thus from the above example we determine to write both the SS program and the temperature program by manipulating the time which is required. By this process we can vary what we wish such as to take the stress to a limited value, hold at that stress for a long time and then vary the temperature in that hold time .
- The above example deals with F control mode where one controls the force. We can do displacement control by selecting the L control composite in the SS program and the only difference in the L control mode is we should know the maximum limit of the displacement to which the material should deform at a particular rate.

Once you finish writing the temperature program and the SS program you can verify the SS graph and the temperature graph in the figure which is given at the top of the condition editor.

- After entering all the values the experiment is ready
- Click OK in the condition editor such that all the information is saved. If you click cancel the information will not be saved.

Load the sample following the instructions in Section 3.2.5.

3.3.4 Starting the Experiment

1. Before starting the experiment ensure the following steps
    a. Sample is firmly chucked
    b. Furnace is pulled up and material holding device is encapsulated

c. The cooling gas pipe from the liquid nitrogen dewar is attached to the module (furnace)

d. Level of the liquid nitrogen in the dewar is above half.

2. Go to the main computer

3. Click the play button on the program screen to start the experiment.

Once the experiment has started

a. Go to view / real time which will allow viewing of real time experiment in a graph format

b. Or view / profile which gives the profile version of the ongoing experiment

c. If general profile is chosen then the ongoing experiment will be shown as it proceeds with time.

In the profile version, graphs are plotted between TMA (μm) and time and load vs. time. It is possible to change the X axis to temperature by right clicking / select axis signal and changing it to temperature.

4. At any point of time during the experiment it is possible to change the future program settings.

a. go to Condition editor

b. make the required changes with in the program and click OK to save the changes

3.3.5 Ending the Experiment

1. Once the program has run its course it will end automatically. The LCD screen (of the DMA base unit) displays **Ready** indicating that the experiment is completed.

2. If the experiment needs to be stopped at any point during the procedure, click the stop button on the muse window.

CAUTION: In any case where the final temperature of the experiment is very high or very low, do not touch the furnace or the sample directly with bare hands.

ALLOW MATERIALS/EQUIPMENT TO RETURN TO ROOM TEMPERATURE BEFORE HANDLING by clicking the button that has an arrow pointing upwards.

3.3.6 Analyzing the Results

1. Once the experiment is complete
    a. Go to the muse job gallery window
    b. Click standard analysis
2. Go to file

    Open the data file which you have named for this particular experiment.

3. Normally if you do the experiment in SS control mode, the standard analysis window will show the variation of TMA (μm) and load (mN) with temperature and time.
4. To get the data stored into an excel file
    a. Go to file
    b. Click output to excel
5. Once you get all the required data in excel one has load values which when divided by the cross section area of the sample gives the stress and the TMA values which will correspond to the displacement and when divided by the original length of the sample gives the strain.

6. Thus you can plot stress vs. strain at a particular temperature or strain vs. temperature at a constant stress (generally very low stress) which would give the phase transformation temperatures. The point where there is a steep slope change in the strain vs. temperature graph corresponds to the phase transformation.

3.4 Constrained Recovery Testing

Constrained recovery is a characteristic property of a shape memory alloy used in actuator applications. It includes applications in which the memory element is prevented from changing its shape and thereby generating stresses up to 800 MPa.

In this process the element is strained and at one stress level. The stress remains constant and then the temperature is varied such that the strain is recovered back in that heating process. We can do the above constrained recovery process in the DMA as follows. An example is given in such a way that the process of constrained recovery is explained.

We would like to conduct an experiment wherein the shape memory element is loaded up to 50 MPa at –30 °C and then heated back to a temperature of 100 °C at that constant stress of 50 MPa and observe the amount of strain recovery.

Experiment Parameters:

1. Follow the steps mentioned earlier (refer Section 3.3.3.1) and enter all the details such as sample length, sample shape, data file and operator etc.
2. Make sure that the system is initialized and put the sample in with the tension setting in place.

Writing the program contains two steps**:**

1. Writing the SS program
2. Writing the temperature program

Go to the condition editor and in the method tab check whether the DMS measurement mode is in SS control and the temperature control mode as Normal Temp. Control (no need to change any of the values in the DMS frequency and Measurement start tabs).

Writing the Temperature Program:

In this example we would like to take the sample to -30 °C and then increase the stress to a value of 50 MPa. The first step of the temperature program looks like:

End step	*Start (cel)*	*Limit (cel)*	*Rate (cel/min)*	*Hold (min)*	*Sampling*
	20	*-30*	*4*	*21*	*1*

In this step, the sample temperature is taken to -30 °C at the rate 4 °C/min and held there for 21 minutes. Now we would like to stay at -30 °C so that we can increase the stress up till 50 MPa (which is accounted in the 21 minute wait time after reaching -30 °C). Now we would like to heat up the sample up till -100 °C at the rate of 5 °C/min

End step	*Start (cel)*	*Limit (cel)*	*Rate (cel/min)*	*Hold (min)*	*Sampling*
	-30	*100*	*3*	*5*	*1*

Thus in this step the sample has been heated to 100 °C

Writing the SS Program:

We would like to give an initial force to the sample so that the sample is chucked between the grips. So an initial stress of 5 MPa is given and this is reached by slowly increasing the stress at a constant rate.

First step of the SS program looks like:

End step	*Start (mN)*	*Limit (mN)*	*Rate (mN/min)*	*Hold (min)*
	0	113	20	14

In this step the stress is taken to a minimal value of 5 MPa (to straighten the sample) and then held at that stress for 14 min so that the temperature reaches -30 °C

Now we increase the stress to a value of 50 MPa at a constant rate of 113 mN/min which is equivalent to 5 MPa/min and there is a long wait time of about 60 min so that the temperature is reached from -30 °C to 100 °C at a constant stress of 50 MPa.

Second step looks like:

End step	*Start (mN)*	*Limit (mN)*	*Rate (mN/min)*	*Hold (min)*
	113	1150	113	60

Thus, finally we obtain that the sample has been heated from -30 °C to 100 °C at a constant stress of 50 MPa.

Analyzing the results:

1. Go to standard analysis software and click open the appropriate data file.
2. Open the file and click output to excel.
3. Once you obtain all the data in an excel file, copy and paste all the temperature, TMA and the load data and convert the corresponding data to stress and strain by dividing the entire load column by area and the TMA column by the length of the sample.
4. Once you obtain the stress, strain and the temperature. Plot the data between the strain (Y axis) and the temperature on the X axis starting from the data point where the stress has remained at a constant value of 50 MPa.
5. Thus you get a variation of strain with temperature and we can calculate the amount of strain recovery when you heat it in that temperature range.

Thus a constrained recovery experiment is conducted in the DMA using the above factors.

CHAPTER 4: THERMO-MECHANICAL TREATMENT OF NiTiFe

As discussed in Chapter Two, the thermo-mechanical treatment of NiTiFe alloys is expected to enhance the properties of these alloys with the introduction of the R-phase. This chapter gives an overview of the thermo-mechanical treatments employed on NiTiFe alloys to enhance the properties of these materials. A $Ni_{46.8}Ti_{50}Fe_{3.2}$ shape memory alloy was used to conduct the following study. A billet of this particular alloy was purchased from Special Metals Corporation, New Hartford, NY which was vacuum induction melted and vacuum arc re melted after which it was cold drawn by 20 %.

4.1 Solutionizing and Aging of NiTiFe

Rectangular samples were cut from the billet mentioned above, measuring 3 mm x 3 mm x 25 mm for testing in a liquid helium dilatometer and differential scanning calorimeter (DSC). These samples were solutionized at 850 °C for 1 hr using an IVI corporation Mark-14 vertical vacuum quench furnace facility [Singh 2004] and subsequently oil quenched. The samples were inserted in a ceramic sleeve and introduced into the furnace after which a vacuum of 10^{-6} torr was created and power to the heating element was supplied. Heating at the rate of 2 °C for every 5-10 seconds was followed. After reaching the desired temperature and holding for the required time of 1 hr the power supply to the heater was turned off and the samples were quenched into the oil using a quench shaft.

After solutionizing all the samples at the same temperature, two samples were aged at 450 °C and 650 °C for 30 minutes and subsequently furnace cooled. The heat treatment setup utilized in the above processes is shown in Figure 4.1.

Figure 4.1: IVI Corporation Mark-14 vertical vacuum quench facility

4.2 Cold Rolling and Annealing

Cold rolling and annealing of the samples were done on the same alloy of NiTiFe which were taken from the billet mentioned in section 4.1.

4.2.1 Sample Preparation

Rectangular strips of various thicknesses (as mentioned in Table 4.1) and with similar widths of 13.4 mm were cut from the billet of composition $Ni_{46.8}Ti_{50}Fe_{3.2}$ using electrode discharge machining (EDM). Two samples per thickness category of thickness were taken and were solutionized at 900 °C for 24 hr. The solutionizing process was done using the heat treatment setup described in section 4.2.3.1.

4.2.2 Rolling

NiTiFe samples of different thicknesses were cold rolled using the cold rolling facility and reduction in thicknesses by 5, 10, 20, 30, 40, 60, 70, 75 percentages were successfully achieved. The values of the thicknesses before and after rolling are given in Table 4.1.

The cold rolling mill used in the process is shown in Figure 4.2. The length of the samples considerably increased after the cold rolling but the width of the samples almost remained constant. Cold rolling was limited to 75 % due to the cracks observed in the sample above 75 % of thickness reduction. The samples which were cold rolled to 70 % and 75 % are shown in Figure 4.3 before and after rolling and a rule is shown indicating the considerable increase in length of the sample with rolling.

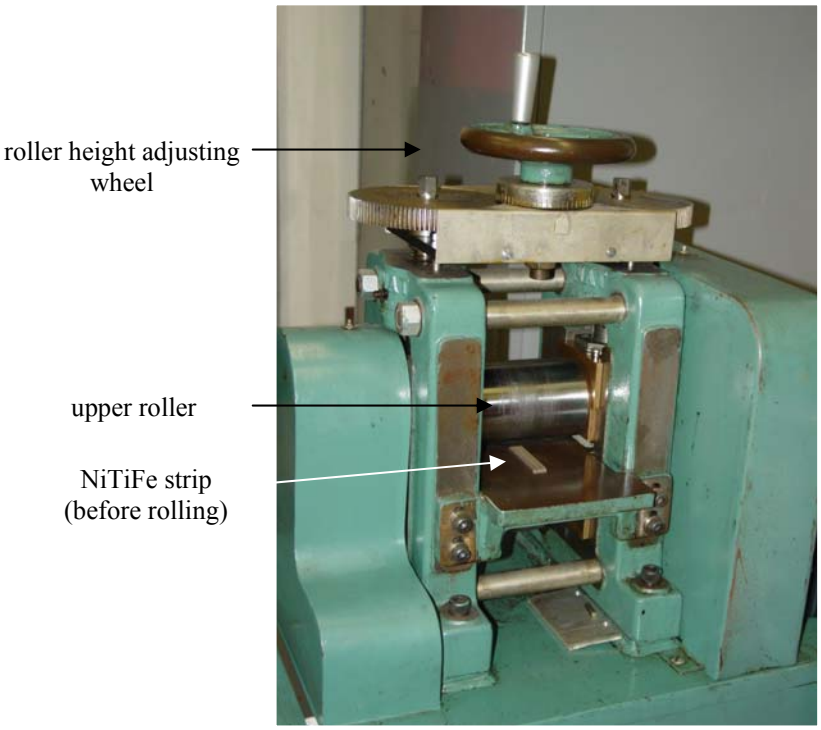

Figure 4.2: Cold rolling mill

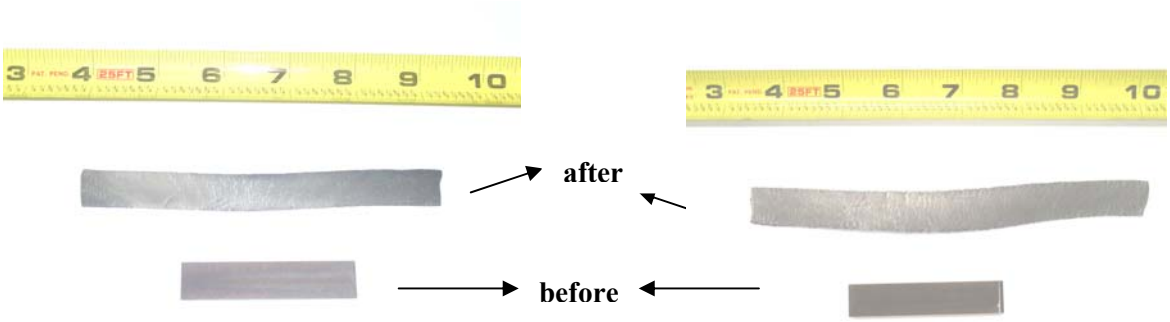

Figure 4.3: NiTiFe alloy before and after cold working

(a) 70 % (b) 75 %

Table 4.1: Cold rolling dimensions

Initial thickness(mm)	Final thickness (mm)	Percentage reduction (%)
0.31	0.29	5
0.35	0.30	10
0.38	0.31	20
0.45	0.32	30
0.45	0.26	40
1.2	0.46	60
1.2	0.34	70
2.99	0.70	75

4.2.3 Annealing

The samples which were cold rolled were annealed at 400 °C, 500 °C and 600 °C for 30 minutes using a muffle furnace after encapsulating the samples in vacuum using the setup described below in section 4.2.3.1.

4.2.3.1 Encapsulation Setup

A glass manifold consisting of 5 ports was attached to the chamber of the IVI arc melting furnace. Tygon tubing (R 3603) which is capable of holding high vacuum was used for this purpose. Small pieces of the tygon tubing were cut and attached to the ports of the manifold.

The samples which were required to be heat treated were put into the quartz tubes and the tubes were necked as shown in Figure 4.4 (a). The formed necks are shown in Figure 4.4 (b). Then, these tubes were inserted into the tygon tubes which were connected to the manifold. After all the tubes were connected to the ports of the manifold, argon gas was allowed to pass for 3 minutes to displace the oxygen present in these tubes. The ports which were not connected to the quartz tubes were closed before passing the argon gas. Once the argon gas flow was closed, vacuum was created in the chamber and the manifold, which in turn create vacuum in the quartz tubes.

Once the vacuum was created in the tubes, they were sealed using an oxy-acetylene torch at the necked portions resulting in the tubes holding a vacuum with the samples present in them. Vacuum of 10^{-6} torr was easily achieved with this setup. The setup with the quartz tubes connected to the manifold is shown in the Figure 4.4 (c). The process of final sealing is shown in Figure 4.4 (d).

Once this setup was designed, all the heat treatments were conducted by this procedure of encapsulating the samples and heat treating them inside the muffle furnace as shown in Figure 4.4 (e). The samples which were heat treated were taken out of the encapsulated tubes for further testing by breaking the tubes.

(a)

(b)

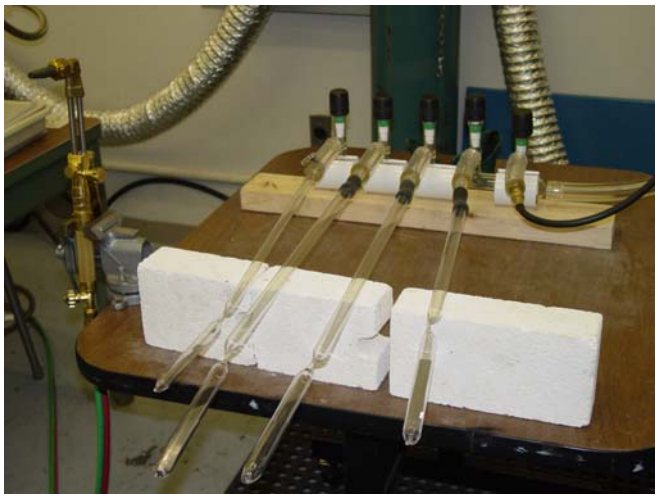

(c)

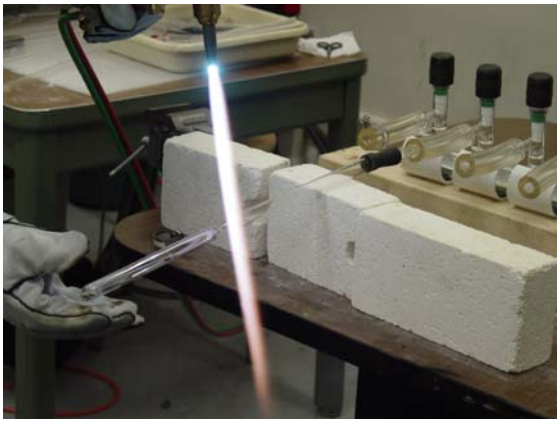

(d)

(e)

Figure 4.4: Encapsulation process shown in various steps

CHAPTER 5: CHARACTERIZATION OF NiTiFe

Characterization of NiTiFe requires the ability to detect the phase transformations in the cryogenic range. The R-phase transformation of these alloys occurs in the liquid nitrogen range but the martensitic transformation occurs at very low temperatures. Hence in order to determine the deformation behavior of these phases at various temperatures a dynamic mechanical analyzer (DMA) was commissioned as mentioned in Chapter Three. To determine the transformation characteristics, a differential scanning calorimeter (DSC) and a liquid helium dilatometer (to temperatures as low as 9 K) were used. This chapter gives a brief description of the testing done using these different characterization techniques.

5.1 Dynamic Mechanical Analysis

Since NiTiFe alloys are considered for use as actuator elements, the study of the deformation behavior in different phases of these alloys and the corresponding mechanical properties play a very significant role in the operation range of cryogenic actuators, for which a dynamic mechanical analyzer was used. The dimensions of the wires tested in the DMA varied from experiment to experiment and are given along with the results section of those experiments. Thin wires were selected for the experiments due to the limitation of the DMA (maximum force of 10 N). To achieve high stresses in the samples lower cross section areas were desired which was possible by selecting thin wires.

These thin wires were cut by EDM and were tested in the DMA within different temperature and stress ranges. The experiments involving the stress-strain response at a

particular temperature were conducted according to the procedure mentioned in section 3.3. In case of constrained recovery experiments, the procedure followed was similar to that mentioned in section 3.4.

The mechanical characterization was done in the DMA after obtaining the transformation temperatures from the DSC, so that the initial phase in which the sample was tested is known before hand and the deformation behavior in the respective phase can thus be studied.

5.2 Differential Scanning Calorimetry

The Differential scanning calorimeter (DSC) was used to measure the phase transformation temperatures in NiTiFe. The principle involved in this is, it measures heat flow vs. temperature for a sample which enables it to detect any phase changes in the sample which register as endothermic or exothermic peaks. The DSC used for characterizing the NiTiFe alloys is a Perkin-Elmer Diamond DSC, which has an operating range from -160 °C to 730 °C.

The procedure by which these samples were tested can be briefly outlined as follows. The sample is crimped into a small aluminum sample pan which is subsequently placed into the sample holder, and an empty pan of similar size is placed into the reference holder. The DSC measures the amount of heat required to raise the temperature of the sample and the reference at the same heating rate. At any stage, if there is a phase transformation, additional heat is required or released depending on the phase transformation in order to accommodate the latent heat requirements of the sample. The difference in heat flow between the sample and the reference (which does not undergo any phase transformation) registers on the heat flow vs. temperature

curve as an endothermic or an exothermic peak since the samples required more amount of heat to maintain that particular temperature as the reference.

In case of NiTiFe alloys, when the sample undergoes a solid to solid phase transformation from austenite to R-phase and vice versa, these get registered as exothermic and endothermic peaks, respectively. The temperatures at which these peaks occur on the curves make it easy to determine the phase transformation temperatures and the hysteresis values in the case of shape memory alloys.

Although the martensitic transformation is not found in the range of the DSC, the R-phase transition occurred well with in the limits and the effect of thermo-mechanical treatment on these transformation temperatures were studied with the DSC, and the results obtained with the analysis is discussed in detail in Chapter Six. The samples used in this testing were cut using a low speed diamond saw and the shapes of the samples were suitable to fit into the aluminum pans which were inserted into the respective holders.

5.3 Dilatometry

Apart from the DSC, a liquid helium dilatometer was also used to characterize the phase transformation temperatures in NiTiFe. Since the martensitic transformation temperatures in NiTiFe are low and below the DSC range, a dilatometer which can go down to 9 K was utilized. A dilatometer measures the contraction and the expansion of a sample corresponding to the change in temperature. A LVDT is used to detect the changes in length of the sample through the movement of the push rods wherein both the reference and the samples are connected to the push rods as shown in Figure 5.1. The reference is a material which has a known expansion or contraction rate (generally copper). The expansion or contraction in the sample is registered as specimen expansion vs. temperature.

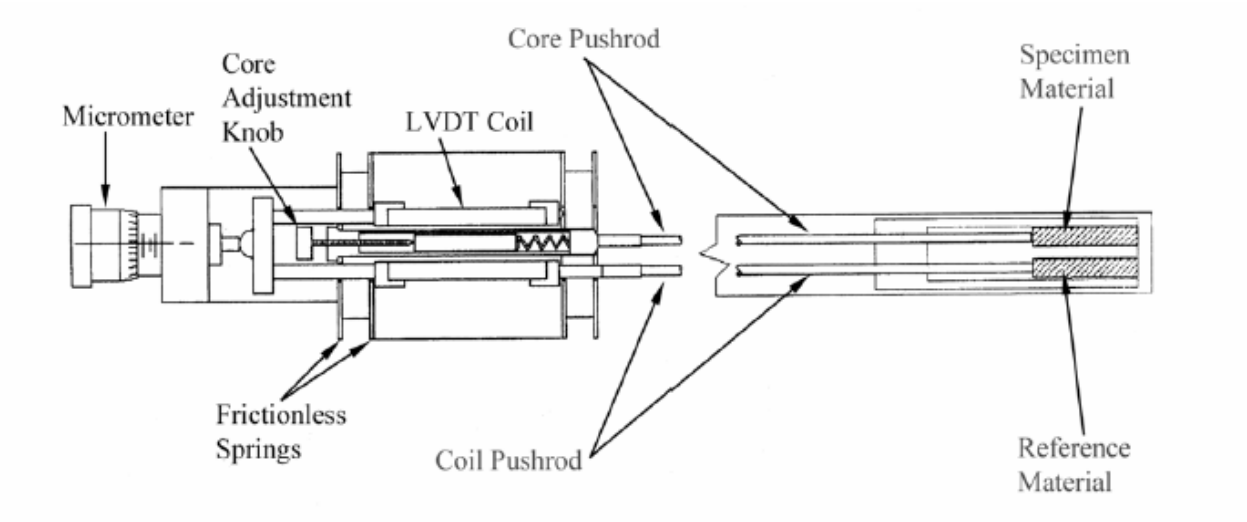

Figure 5.1: Differential sensor reference and specimen setup [Theta Industries Inc.]

In case of NiTiFe, a phase transformation is recorded as a non linear region in the expansion vs. temperature plot [Lemanski 2005]. This slope change in the graph occurs as the sample undergoes a change in crystal structure for, e.g., a body centered cubic to a trigonal structure.

5.3.1 Sample Preparation

The samples used for testing in the liquid helium dilatometer were cut by electrode discharge machining to measure 3 mm x 3 mm x 25 mm and the effect of different thermo-mechanical treatments on these alloys were studied.

5.3.2 Low Temperature Testing

The liquid helium dilatometer was commissioned by J. Lemanski [2005] such that the temperature can go as low as 20 K. In the process of characterization of NiTiFe the operating range was lowered and the sample temperature was able to go as low as 9 K. The procedure in which this was achieved is described briefly below.

The reference which was made of copper had data -253 °C (20 K) after which the experiment would get terminated automatically due to the lack of the reference data. Therefore, the data of the copper reference was extrapolated till -264 °C (9 K) and new software consisting of this data was installed in the instrument which allowed the sample temperature to go down till 9 K enhancing the temperature range of the instrument.

Thus, dilatometry was also employed to characterize NiTiFe and the results obtained from these experiments are discussed in the next chapter.

CHAPTER 6: RESULTS AND DISCUSSION

Thermo-mechanical treatments were conducted on a NiTiFe alloy of atomic composition $Ni_{46.8}Ti_{50}Fe_{3.2}$ using DMA, DSC and dilatometry. This chapter presents the results obtained from the DMA testing at various combinations of stress and temperatures. It also includes the results obtained from the DSC and dilatometry.

6.1 Aging of NiTiFe

Samples of $Ni_{46.8}Ti_{50}Fe_{3.2}$ were subjected to various heat treatments and tested in the Perkin-Elmer DSC. The samples for DSC were taken from the rectangular strips which were cut by electrode discharge machining from the original billet of $Ni_{46.8}Ti_{50}Fe_{3.2.}$ All the samples were tested in the DSC using the same temperature program, i.e., cooling between 0 °C and -60 °C and heating from -60 °C to 0 °C at the rate of 20 °C per minute. The results obtained are shown in Figure 6.1. The sample designations with different heat treatments are given below. These designations are used in subsequent sections.

A - As received

B - Solutionized at 850 °C for 1 hr and vacuum cooled

C - Solutionized at 850 °C for 24 hr and vacuum cooled

D - Solutionized at 850 °C/vacuum cooled and subsequently aged at 650 °C for 30 min

E - Solutionized at 850 °C/vacuum cooled and subsequently aged at 450 °C for 30 min

6.1.1 Differential Scanning Calorimeter Testing

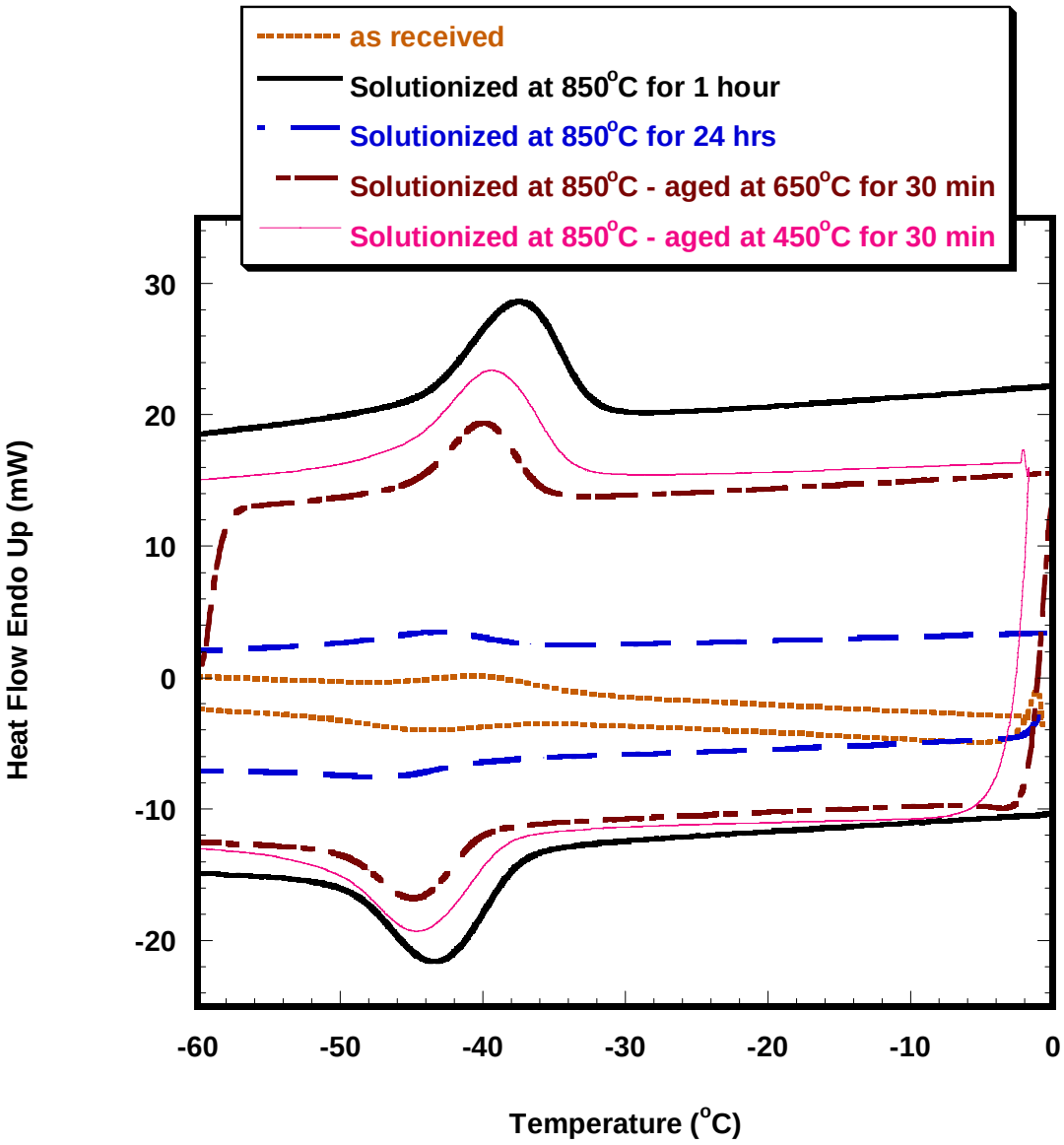

Figure 6.1: DSC curves from the sample with different heat treatments

The DSC results from the above curves are summarized in table 6.1.

Table 6.1: Results from the DSC curves in Figure 6.1

Category	R_s (°C)	R_f (°C)	A_s (°C)	A_f (°C)	Enthalpy of transformation (J/g)		Hysteresis (°C)
					Cooling	Heating	
A	-36.5	-52.6	-47.3	-33.9	-2.43	2.73	4.4
B	-39.8	-50.9	-45.4	-35.3	-2.87	2.99	5.2
C	-36.1	-53.5	-48.1	-31.0	1.70	1.70	5.3
D	-33.9	-49.6	-44.2	-31.1	-2.11	2.22	4.7
E	-39.4	-52.3	-46.8	-35.7	-3.33	3.04	4.8

It was observed that the transformation temperatures for both the R-phase to austenitic and the reverse transformation did not change significantly after the aging treatments. Since this is a titanium rich alloy, the possible explanation for the no change in transformation temperatures is the reduced amount of precipitates which is substantiated microscopically as observed in the TEM micrograph at room temperature in Figure 6.2. These precipitates act as nucleation sites for the R-phase to form earlier, than at expected temperatures which are absent in these cases. The dilatometric curves of these samples are given in the subsequent section.

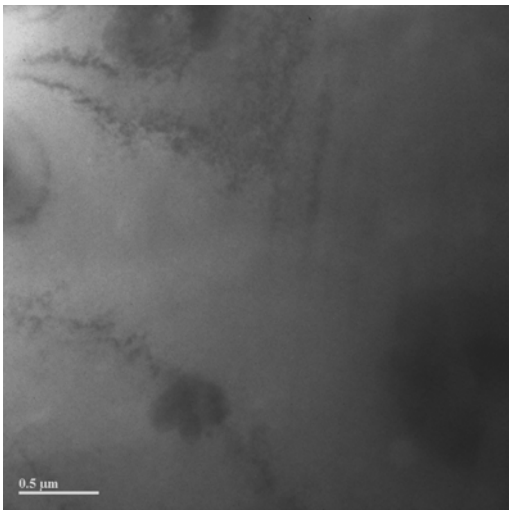

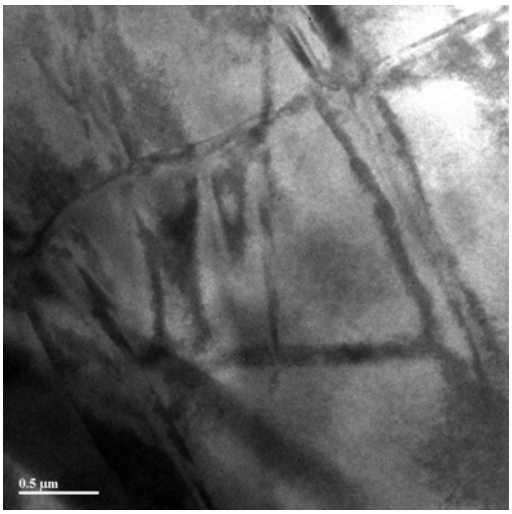

(a) (b)

Figure 6.2: TEM micrograph of sample solutionized at 850 °C and (a) aged at 650 °C for 30 minutes (b) aged at 450 °C for 30 minutes

6.1.2 Dilatometry

To verify and correlate the transformation temperatures obtained from DSC testing, B, D and E samples of NiTiFe (see section 6.1 for notation) were tested using a liquid helium dilatometer to temperatures as low as 9 K (-264 °C).

The temperature program utilized was to cool from room temperature to -264 °C and heat back from -264 °C to room temperature at the rate of 3 °C per minute. Figures 6.3, 6.4, 6.5 show the specimen expansion vs. temperature curves for the B, D and E samples, respectively.

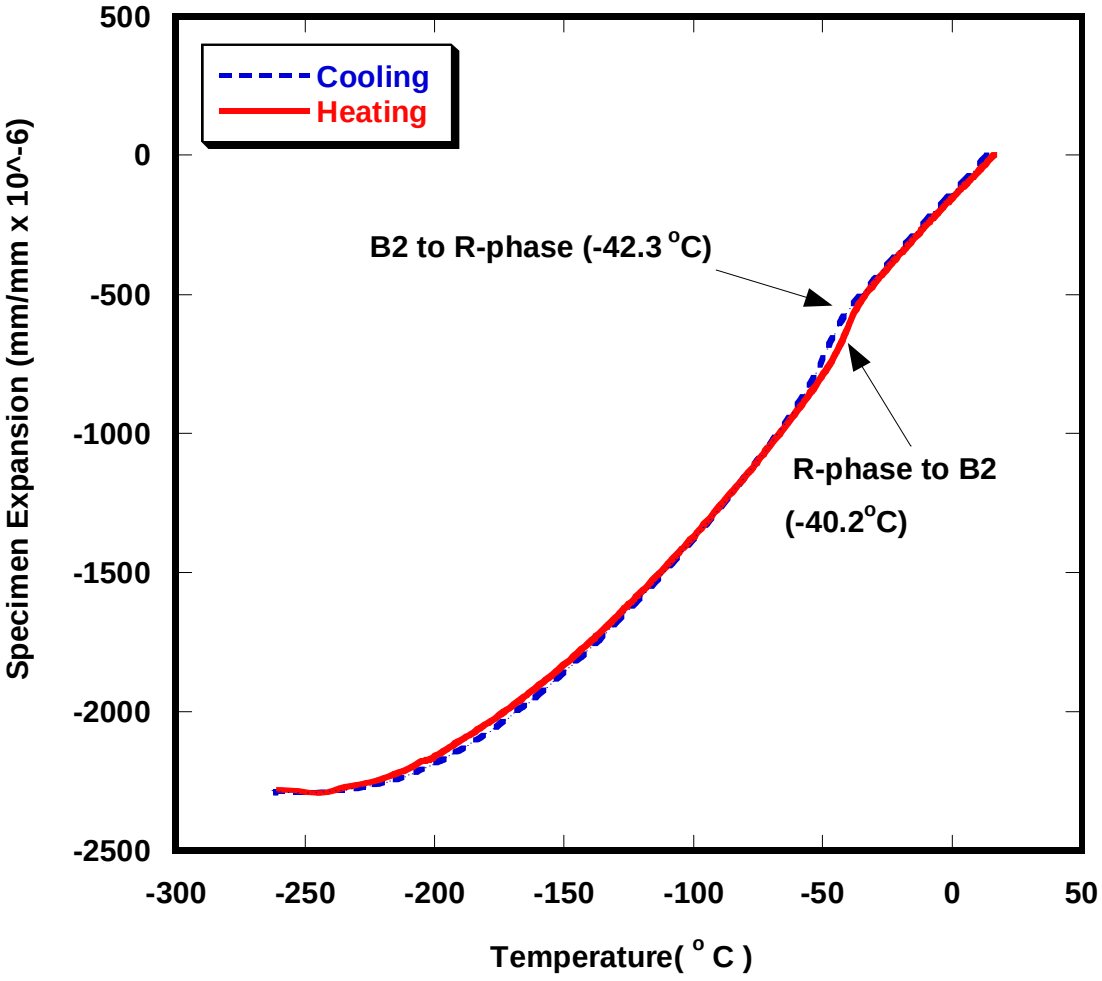

Figure 6.3: Specimen expansion vs. temperature for the sample solutionized at 850 °C for 1 hour and vacuum cooled

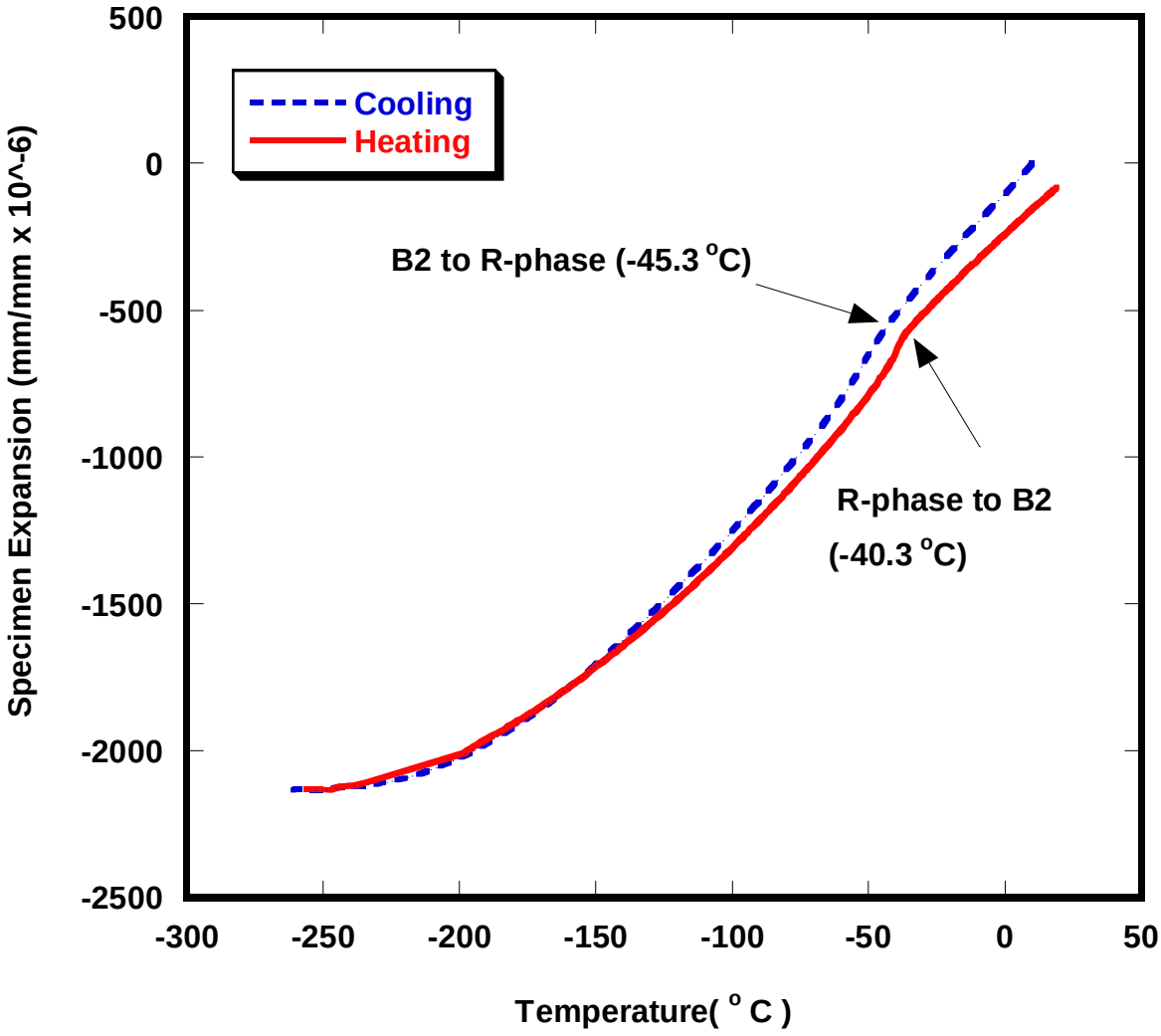

Figure 6.4: Specimen expansion vs. temperature for the sample solutionized at 850 °C for 1 hour and aged at 650 °C for 30 minutes

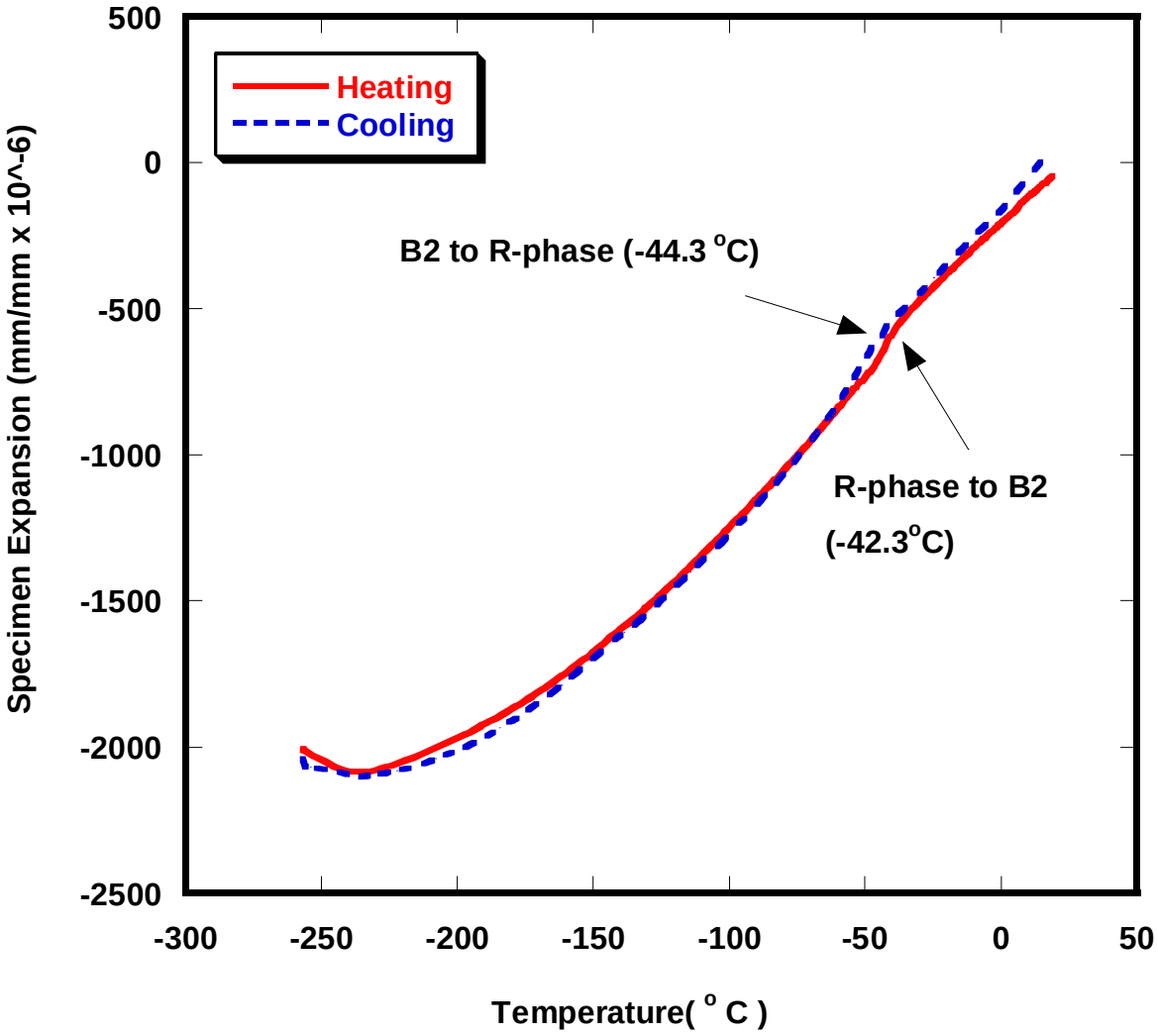

Figure 6.5: Specimen expansion vs. temperature for the sample solutionized at 850 °C for 1 hour and aged at 450 °C for 30 minutes

The transformation temperatures for the R-phase transformation (the temperature at which the change in slope is observed) were correlated using both DSC and dilatometry techniques and were found to be similar for different heat treatments indicating the consistency of the R-phase transformation and the techniques. However, there was no martensitic transformation found in any of the heat treated samples even though the sample was cooled to 9 K (-264 °C).

6.2 Cold Rolling and Annealing

Eight samples of type C (see section 6.1) were taken and subjected to 5, 10, 20, 30, 40, 60, 70, and 75 % of thickness reduction (for dimensions see table 4.1). After the cold rolling procedure, all these samples were annealed at 400 °C for 30 minutes using the heat treatment setup described in section 4.2.3.1 and were tested using the DSC. It was observed that none of the samples except the 70 % reduced sample showed any R-phase transformation as shown in Figure 6.6. The possible explanation for this behavior could be the low annealing temperature because the dislocations associated with the high levels of plastic deformation generate an internal stress state which may restrict the R-phase transformation to austenite and this can be removed by annealing at high temperatures. Similar kind of experiments were done on NiTiHf system where in they observed that for low amount of cold works and low annealing temperatures the R-phase was not found and this was explained based on the merging of the A to R and R to M transformations [Zhang et al 1997].

Hence, the next step employed was to anneal these samples at higher temperatures. All the samples were encapsulated and annealed at 600 °C for 30 minutes using the heat treatment setup described in section 4.2.3.1 and were subsequently tested in the DSC. The results showed that the samples which were cold rolled to higher percentages such as 60%, 70% and 75% exhibited the R-phase transformation and it increased as the cold work percentage increased. Figure 6.7 shows the DSC curves of the different cold worked samples annealed at 600 °C which are compared to the as received and the solutionized samples.

6.2.1 Differential Scanning Calorimeter Testing

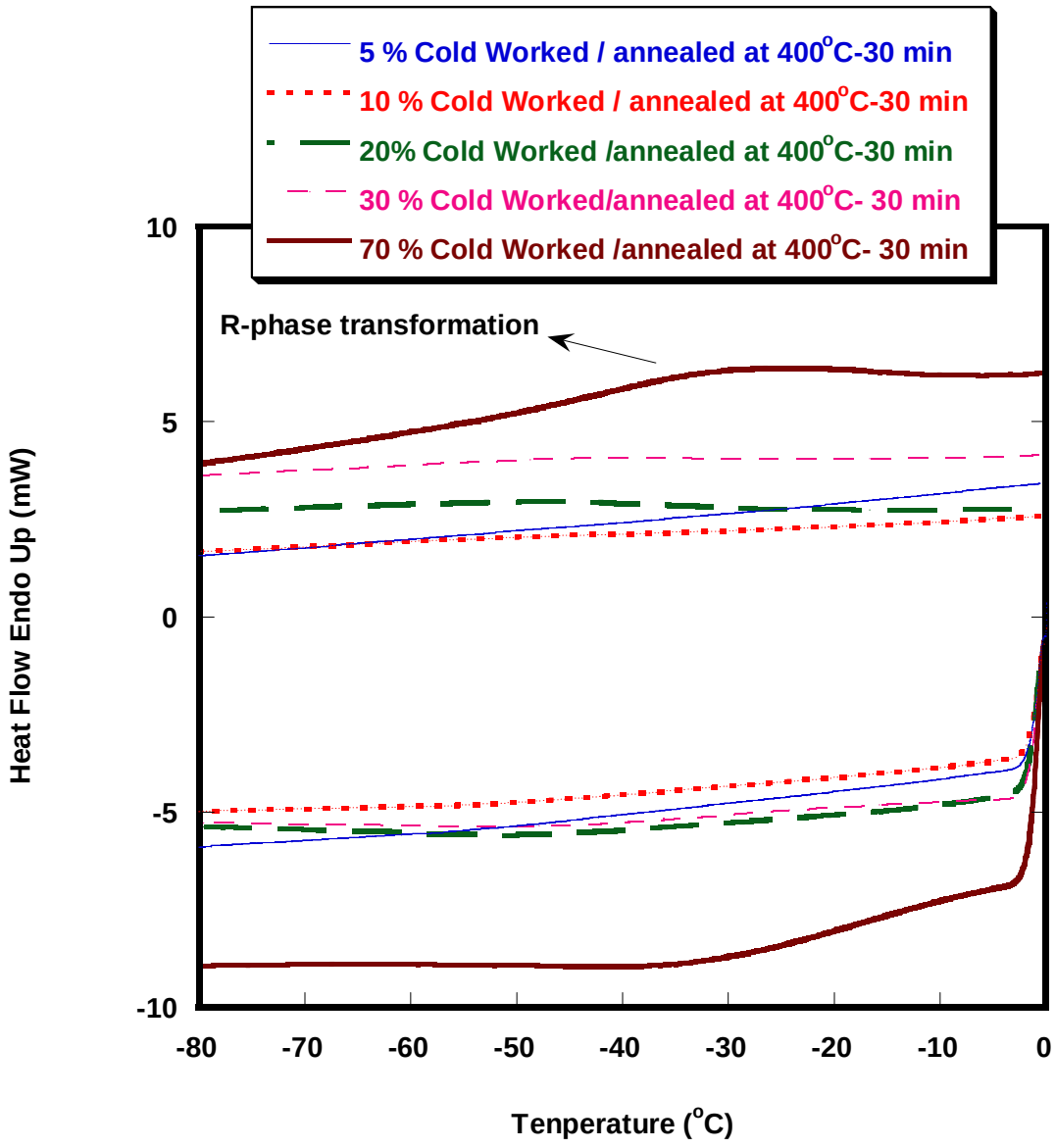

Figure 6.6: DSC curves for different levels of cold deformation (5 %, 10 %, 20 %, 30 % and 70 %) followed by annealing at 400 °C for 30 minutes

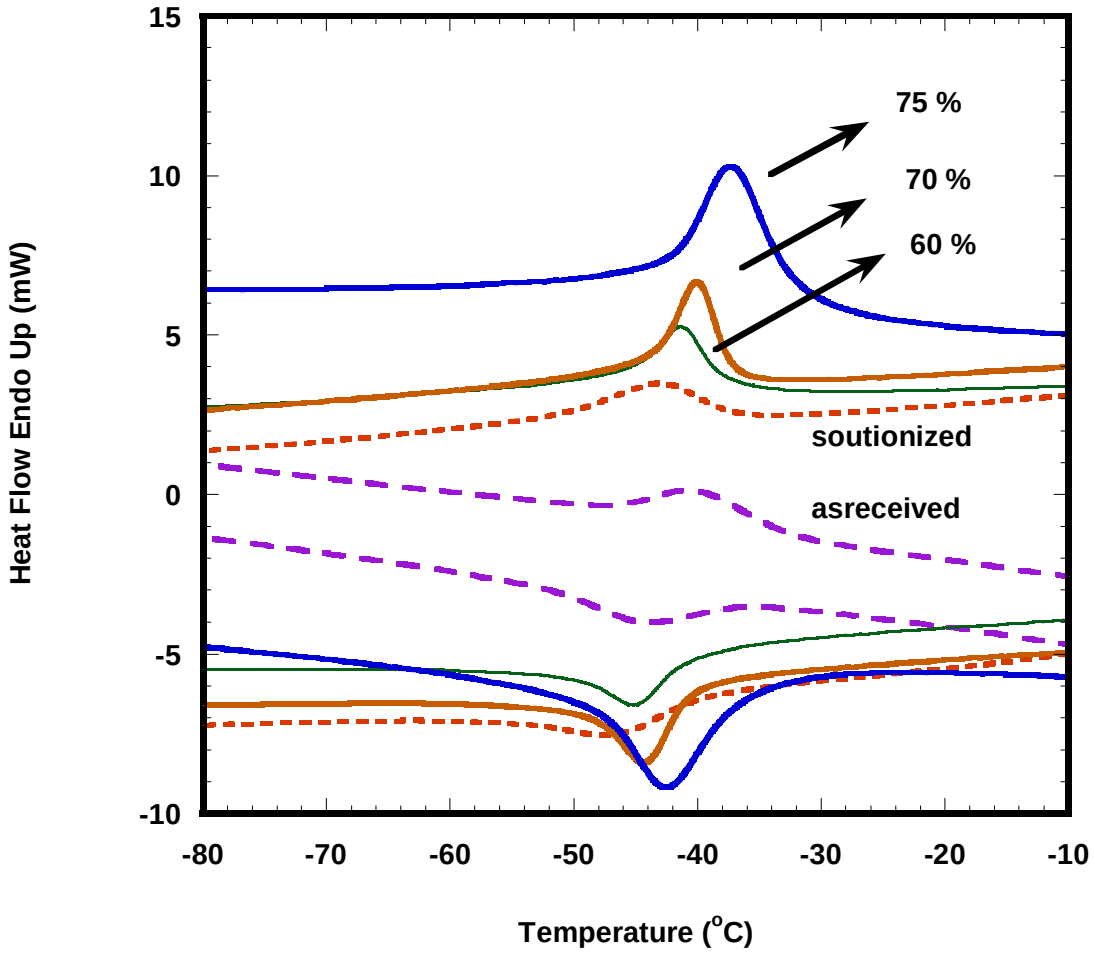

Figure 6.7: DSC curves for different levels of cold deformation percentages (60 %, 70 % and 75 %) followed by annealing at 600 °C for 30 minutes. The as received and solutionized samples are also shown.

The results from the above are summarized in Table 6.2.

Table 6.2: Results of DSC curves from Figure 6.7

Cold work (%)	R_s (°C)	R_f (°C)	A_s (°C)	A_f (°C)	Hysteresis (°C)	Enthalpy of transformation ΔH (J/g)	
						Cooling	Heating
60	-40.5	-51.4	-46.2	-37.8	3.7	-1.18	1.13
70	-40.5	-49.2	-43.9	-37.1	4.2	-1.82	1.82
75	-36.1	-48.8	-42.7	-32.0	5.2	-1.96	1.93

With an increase in cold working percentage it was observed that the peaks became sharper for the R-phase transformation indicating it to occur over a narrow temperature range from austenite which is ideal for actuator applications.

Similarly, to observe the effect of annealing temperatures, the 70 % cold worked sample was selected and subjected to annealing temperatures of 400 °C, 500 °C and 600 °C for 30 minutes. The samples were subsequently tested in the DSC and the results obtained are shown in Figure 6.8.

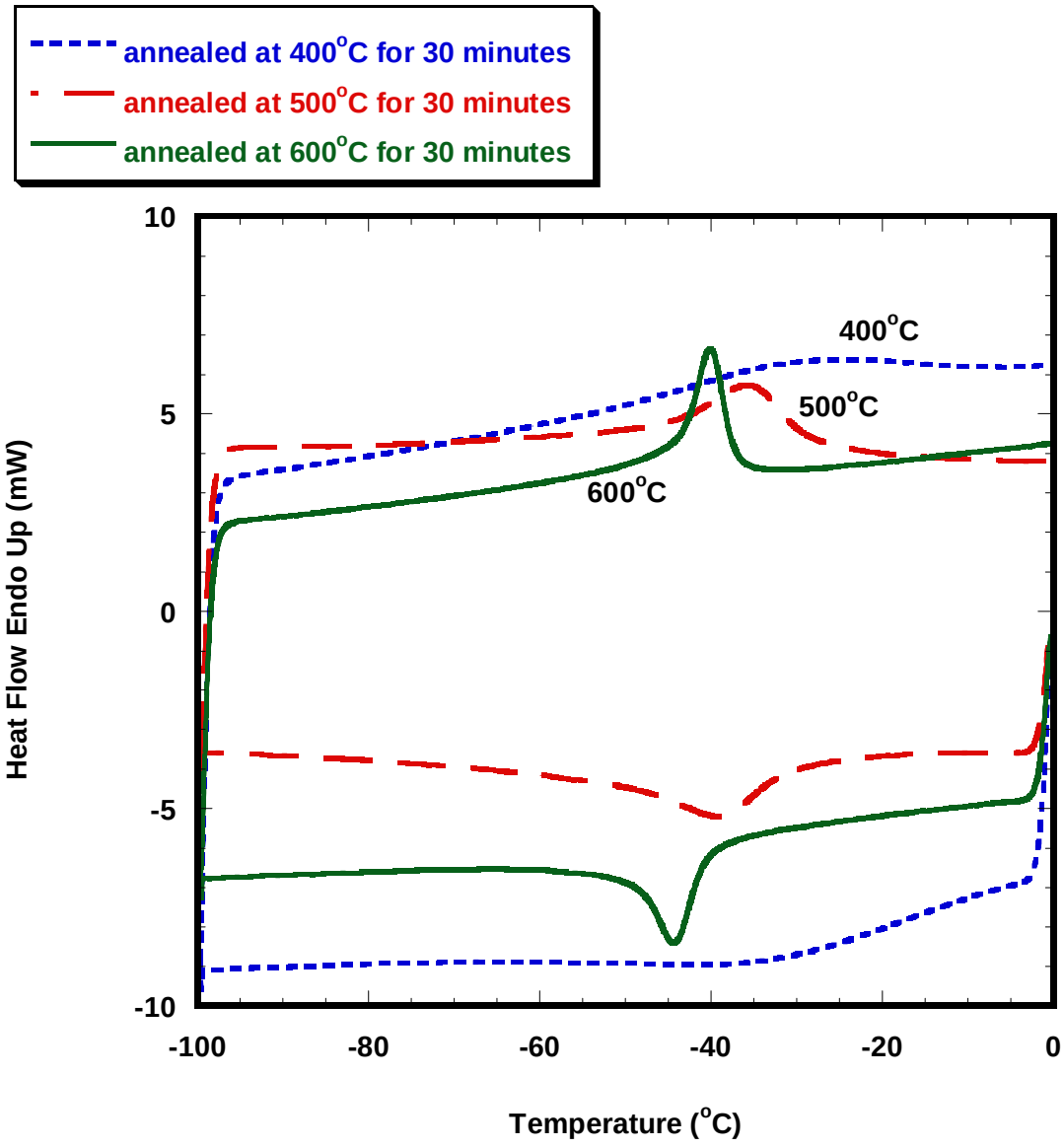

Figure 6.8: DSC curves of the 70 % cold worked sample annealed at 400 °C, 500 °C and 600 °C for 30 minutes

The results from the above are summarized in Table 6.3.

Table 6.3: Results of DSC curves shown in Figure 6.8

Annealing temperature (°C)	R_s (°C)	R_f (°C)	A_s (°C)	A_f (°C)	Hysteresis (°C)	Enthalpy of transformation ΔH (J/g)	
						Cooling	Heating
400	-12.1	-55.8	-51.9	-16.5	1.3	-0.95	1.3
500	-30.5	-47.5	-46.6	-28.1	3.4	-1.38	1.55
600	-40.0	-49.2	-40.0	-37.1	-4.2	-1.82	1.82

Cold work introduces dislocations and causes dislocation entanglement. Annealing of a cold worked structure rearranges and removes dislocations (decrease in internal stress). In the above case, when the sample is cold worked to 70 %, dislocations are introduced into the material. Annealing this at 400°C will remove few dislocations but due to the presence of dislocations which were not removed at that low annealing temperature, the R-phase is hindered and thus the R-phase transformation from austenite is not observed very clearly. However, with the increase in the annealing temperature dislocations are removed in the material but they should not be completely eliminated because these dislocations act as nucleation sites for the formation of R-phase. Thus, there should be an optimum number of dislocations inside the material which would not inhibit the formation of R-phase but inturn favors the nucleation of the R-phase.

6.3 Dynamic Mechanical Analyzer Testing

To determine the thermo-mechanical behavior of NiTiFe at various temperatures and stress, testing was done in the DMA and this section provides the results obtained from the DMA.

6.3.1 Commissioning of the Dynamic Mechanical Analyzer

To determine whether the DMA was successfully commissioned and to verify the standard sample, a superelastic NiTi wire and PMMA (poly methyl methacrylate) were tested in the DMA and their behavior was verified at various temperatures. The NiTi wire selected for this testing had a diameter of 0.17 mm. The testing procedure outlined in section 3.3 to obtain the stress vs. strain graphs was followed.

6.3.1.1 NiTi Testing

Superelastic NiTi wire with a gauge length of 20 mm was tested at room temperature at a loading rate of 10 MPa/min for which the stress strain response is shown in the Figure 6.9. The modulus determined from the slope of the stress strain graph was 64 GPa which is comparable to the value reported in the literature which is around 70 GPa [Vaidyanathan *et al*. 1999]. Similarly the sample was tested with a gauge length of 25 mm and the modulus determined to be 65 GPa. The stress strain response is shown in Figure 6.10. Thus the superelastic NiTi sample showed

consistent results with different gauge lengths. It was also found that the stress-strain response did not change with varying the loading rates at 5, 10, 20, 25 MPa/min.

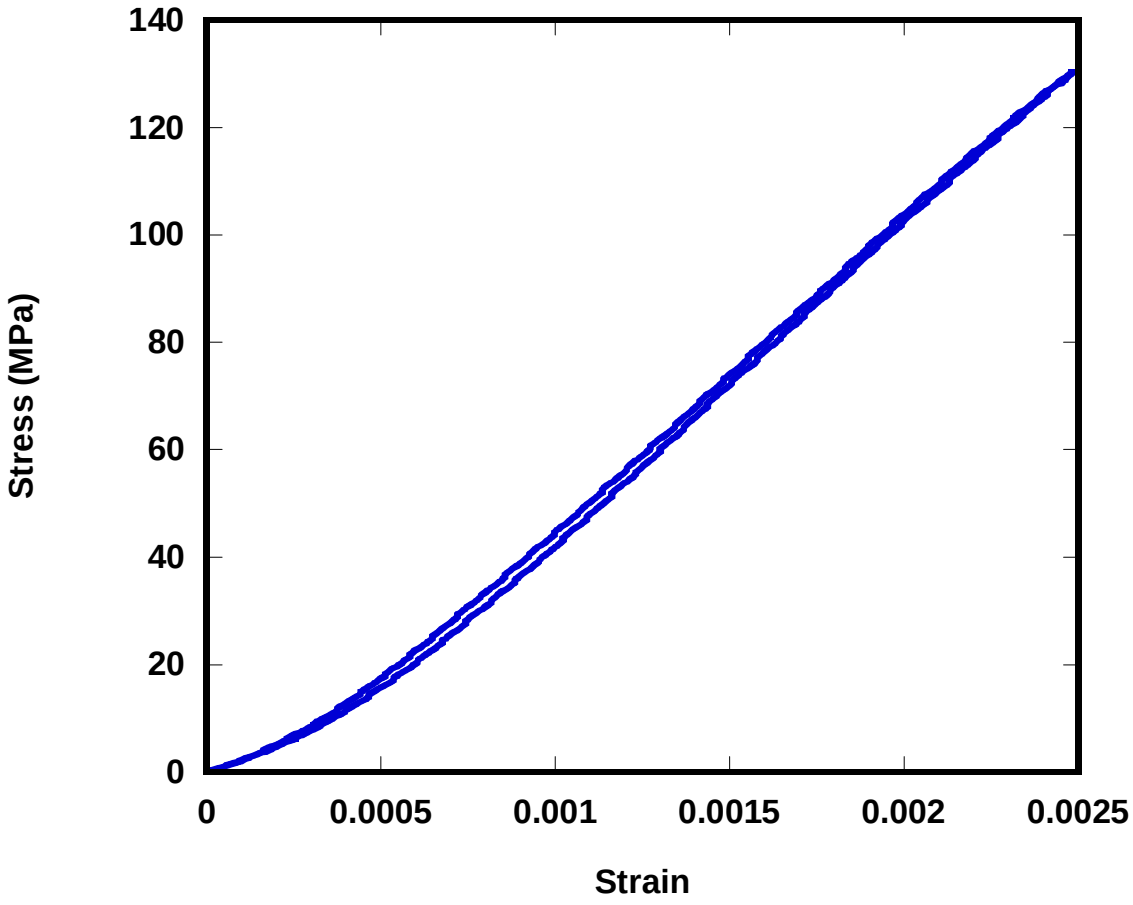

Figure 6.9: Stress-strain response of superelastic NiTi tested at room temperature.

The sample gauge length was 20 mm

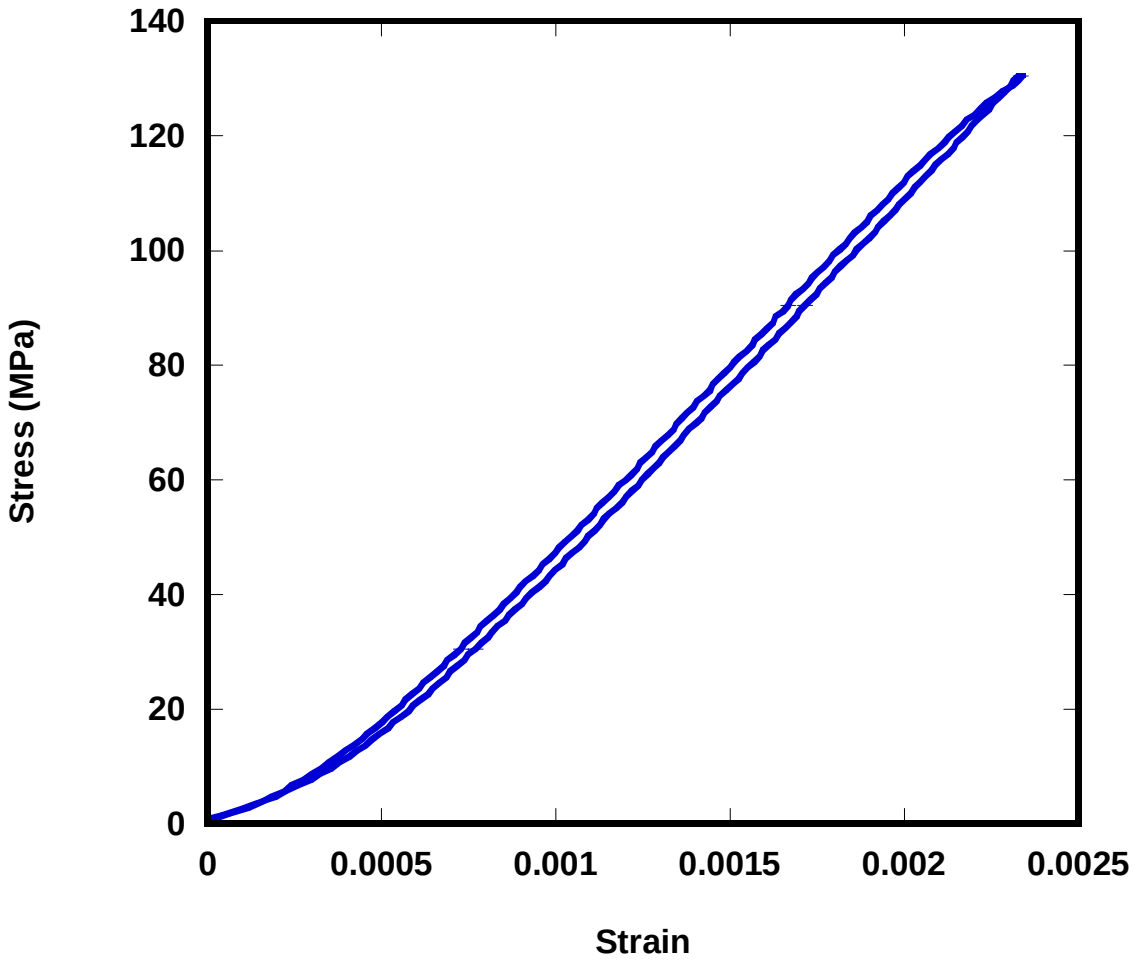

Figure 6.10: Stress-strain response of superelastic NiTi tested at room temperature.

The sample gauge length was 25 mm

The superelastic NiTi wire sample was also tested in L-control mode (displacement control mode) at 4 μm/min to higher loads at -150 °C to see the response of the instrument and the response is shown in Figure 6.11.

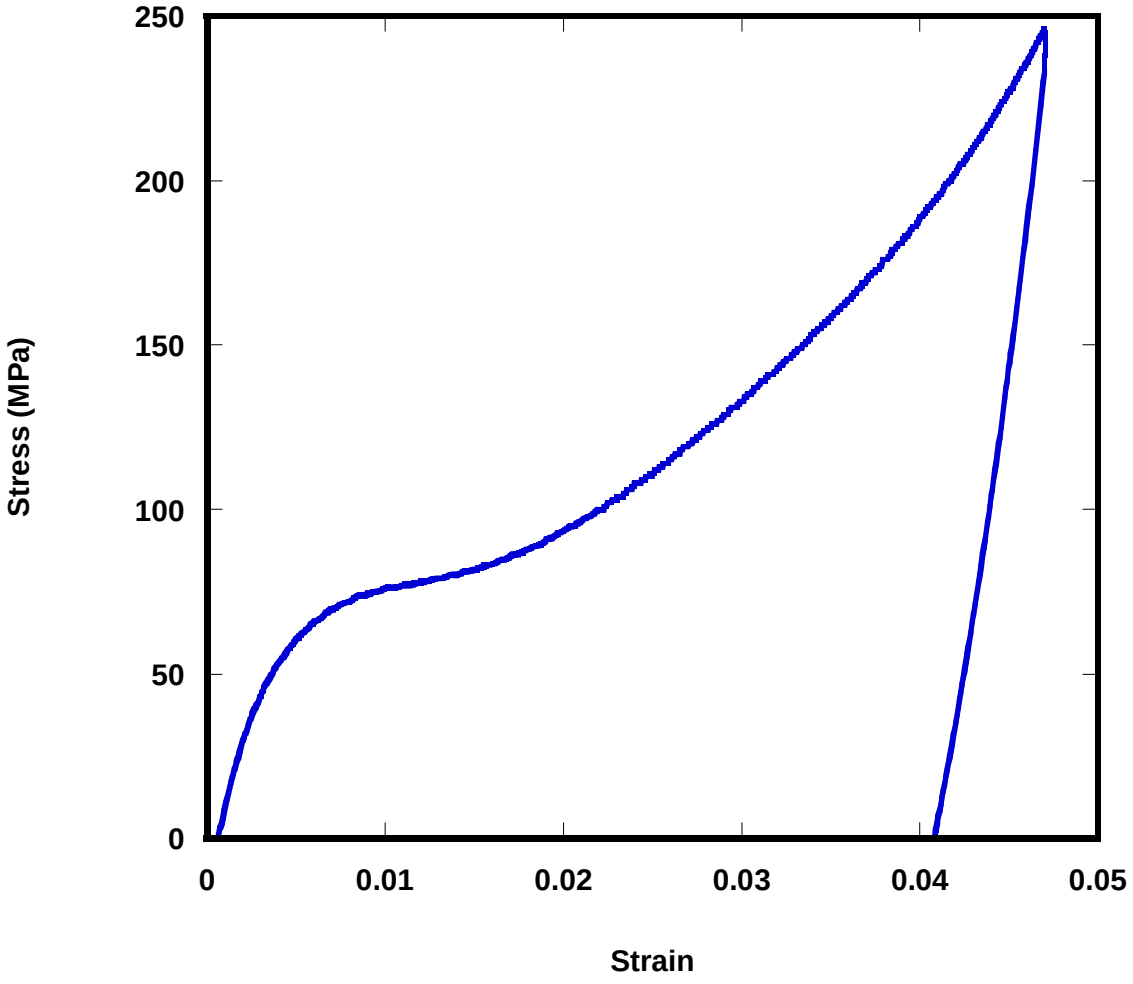

Figure 6.11: Superelastic NiTi wire tested at -150 °C in L-control mode

At -150 °C the superelastic NiTi is expected to be in the martensitic phase and the modulus determined in the elastic region of the graph is 14 GPa which is comparable to the value

reported for martensite in the literature which is around 20 GPa [Rajagopalan *et al.* 2005]. It can be concluded that the instrument (DMA) was commissioned successfully for mechanical testing of metals at different conditions.

6.3.1.2 PMMA Testing

A PMMA sample of dimension 1.46 mm X 9.87 mm X 20 mm was used as a standard and was tested in dynamic mode to verify the calibration of the DMA.

Figure 6.12 shows the determined modulus of the PMMA sample which was found to be 4.3 GPa. This was within the error limits of the instrument.

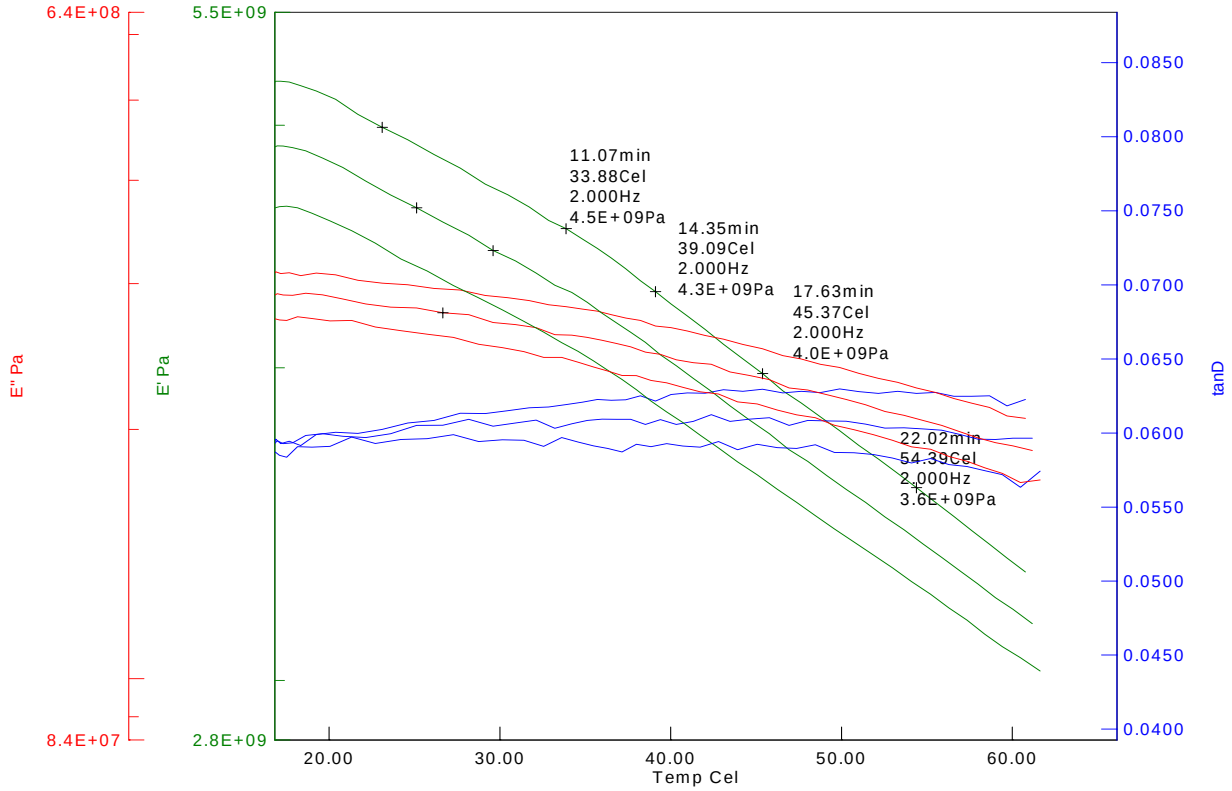

Figure 6.12: PMMA sample tested in dynamic mode

From the above results obtained in sections 6.3.1.1 and 6.3.1.2 it was concluded that the DMA was successfully commissioned for conducting further mechanical testing.

6.3.2 NiTiFe Testing

Thin wires of the alloy of various dimensions were cut by EDM and were tested in the DMA after providing various heat treatments to the samples and the following results were obtained. All the samples tested are designated as mentioned in section 6.1 and the procedure followed in getting the stress vs. strain responses is similar to that outlined in section 3.3.

6.3.2.1 As Received

Thin wires of dimension 0.07 mm x 0.1 mm x 25 mm were cut by EDM from the as received material of the billet and were tested at 10 MPa/min at room temperature and at -100 °C. The temperatures were selected in such a way that at room temperature the sample is completely in the austenite phase and at -100 °C the sample is completely in the R-phase from the DSC curves in Figure 6.1 (refer table 6.1 for transformation characteristics). The stress strain responses from these tests are given in Figures 6.13 and 6.14 respectively. At room temperature the sample failed at 225 MPa and the modulus in the linear region was determined to be 30 GPa. The failure of the sample at that low stress may be attributed to the presence of defects since the sample was in the as received condition. At -100 °C, the sample failed at 210 MPa and the modulus found in the linear region was 14 GPa and the reason for the modulus being low can be attributed to the twinning in the R-phase at low temperatures or stress-induced transformation to martensite and subsequent twinning.

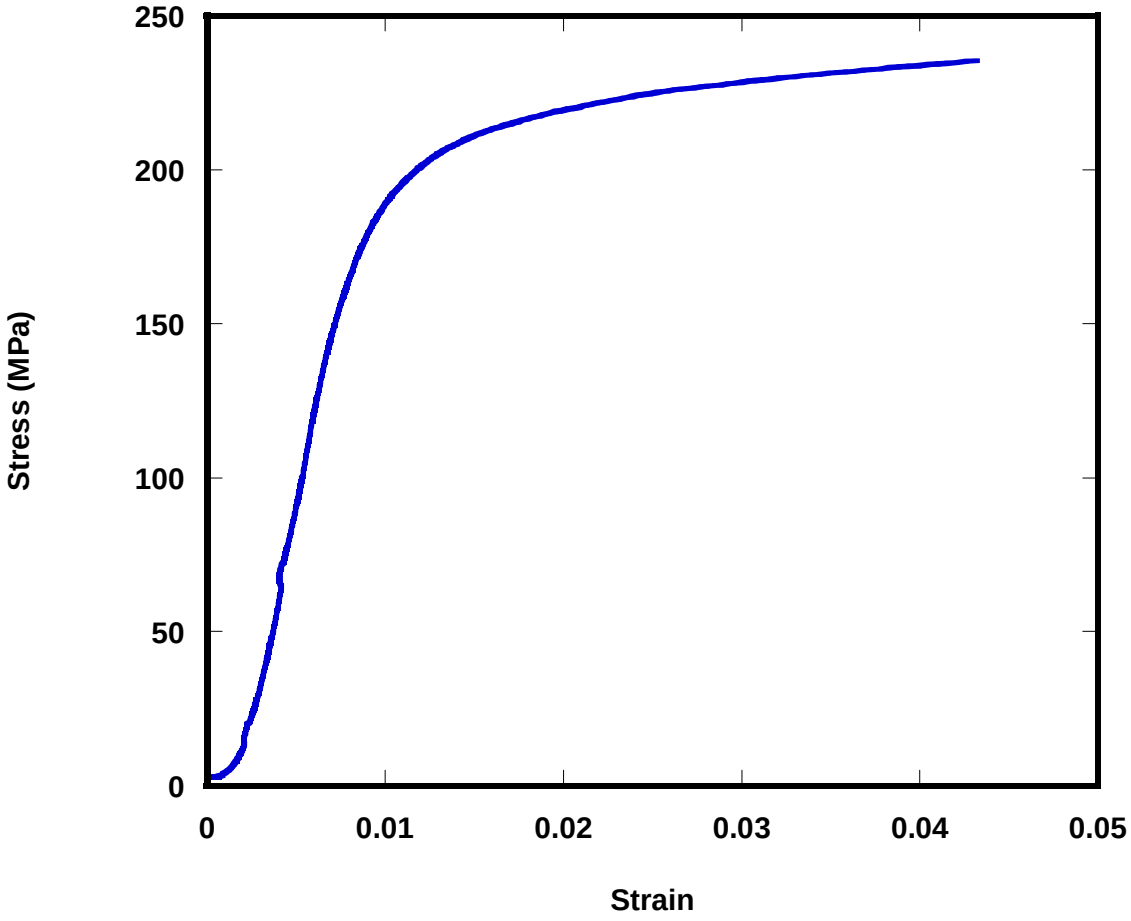

Figure 6.13: Stress-strain response of the as received NiTiFe sample tested at room temperature

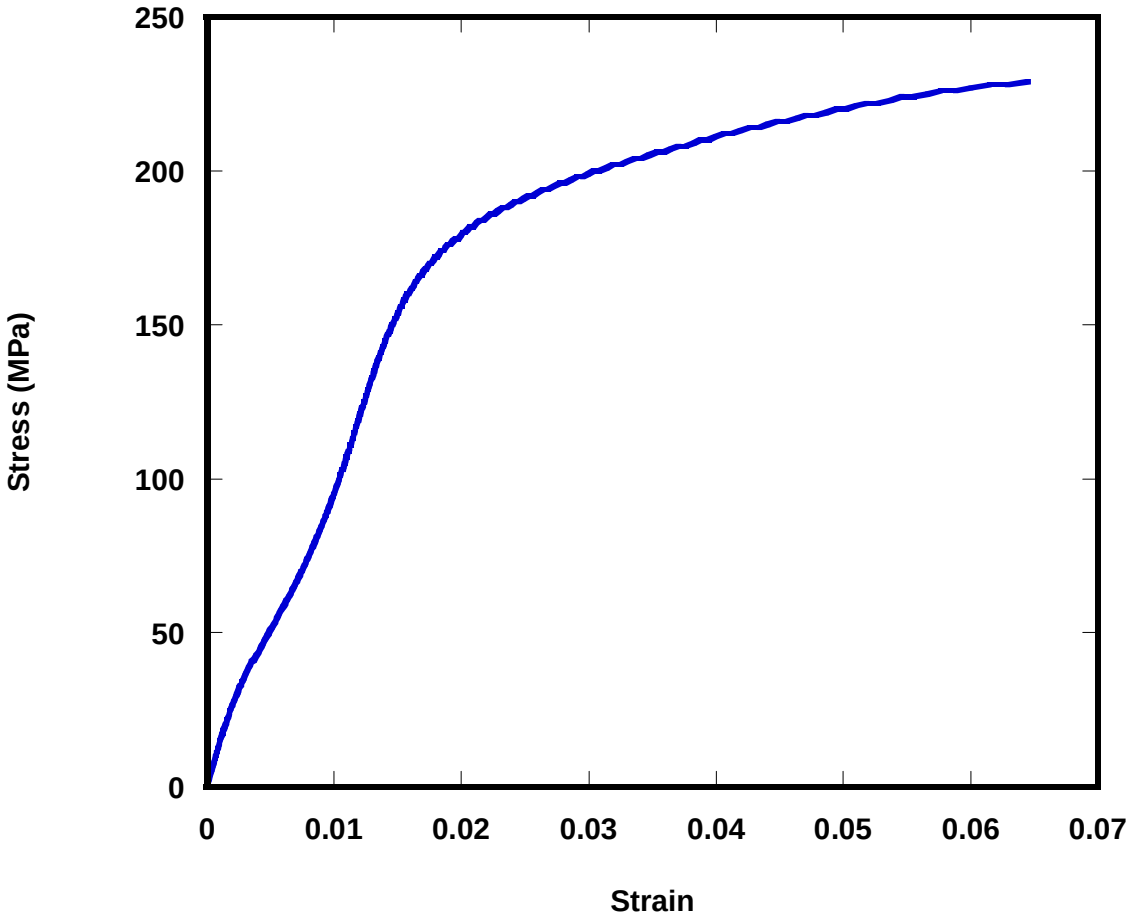

Figure 6.14: Stress-strain response of as received NiTiFe sample tested at -100 °C

Following these experiments the samples that were solutionized for 1 hr at 850 °C and vacuum cooled were tested in the DMA to observe the effect of solutionizing.

6.3.2.2 Testing at Lower Loads

NiTiFe samples (thin wires) measuring 0.1 mm x 0.1 mm x 40 mm were cut by EDM and solutionized at 850 °C for 1 hr and vacuum cooled using the vacuum quench facility described in section 4.1. These samples were tested upto 75 MPa at the rate of 10 MPa/min at different temperatures to determine the mechanical properties in the elastic region.

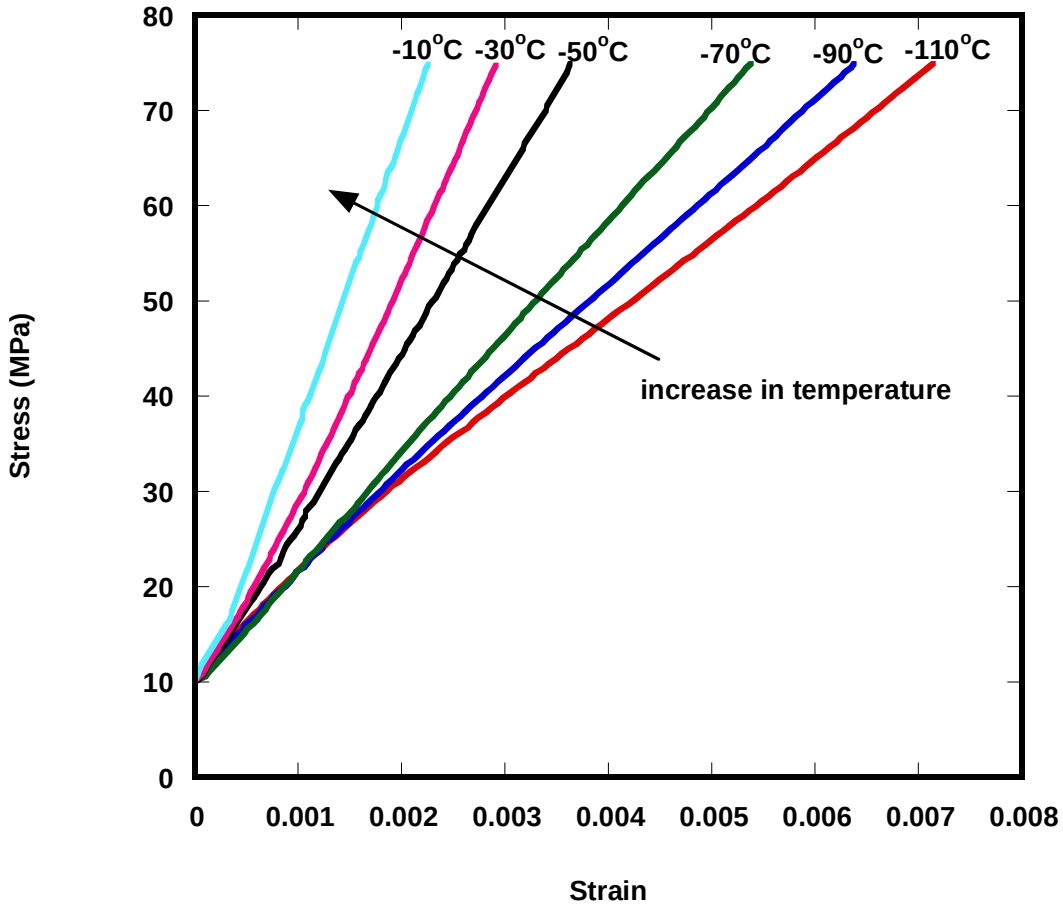

Figure 6.15: Stress-strain response of a NiTiFe sample (solutionized at 850 °C for 1 hr and vacuum cooled) as a function of temperature (low temperatures)

Figure 6.15 shows the curves in which the loading portions of the stress-strain responses at low temperatures are plotted. It was observed that the data obtained was in two different sets. One set corresponds to the sample being completely austenitic and the other corresponds to the sample being in the R-phase completely during the initial stage of the experiment. It was observed that the modulus decreased as the temperature decreased and the value obtained for austenite was comparatively lower than the reported value of 70 GPa [Vaidyanathan *et al.* 1999]. The change in elastic modulus was attributed to small amounts of twinning and stress induced transformations at lower loads at very low temperatures. In case of testing at -10 °C,-30 °C,-50 °C where the sample was expected to be in the austenitic phase in the initial condition (refer DSC values in section 6.1.1), stress induced R-phase formation, twinning in the R-phase followed by stress induced martensite and twinning in martensite could be the reasons for the lower modulus. But in case of temperatures of -70 °C,-90 °C,-110 °C where the initial phase was the R-phase (refer section 6.1.1 for DSC values), twinning in the R-phase, stress induced martensite and the twinning in martensitic phase could be the reasons for lowering the modulus.

Figure 6.16 shows the curves in which the loading portions of the stress-strain curve above room temperature are plotted. Similar to the previous case, the elastic modulus was found to be increasing with temperature and the values were found to be low when compared to the reported value of austenite which is around 70 GPa [Vaidyanathan *et al.* 1999]. Again, stress induced R-phase or martensite transformation and twinning in the R-phase or martensitic phase were assumed to be the reasons for observing the low modulus for austenite (since the initial phase at all the temperatures was austenite). However, there were two temperature regions one between room temperature to 150 °C and the other between 200 °C to 350 °C. The later region of temperatures which was separated in the stress-strain graph from the first region could be

explained based on M_d (martensite desist temperature) in such a way that the later region must have surpassed the M_d temperature above which inducing martensite through stress becomes difficult. The low modulus could be as a result of stabilized martensite (as opposed to stress induced) [Rathod et al. 2006].

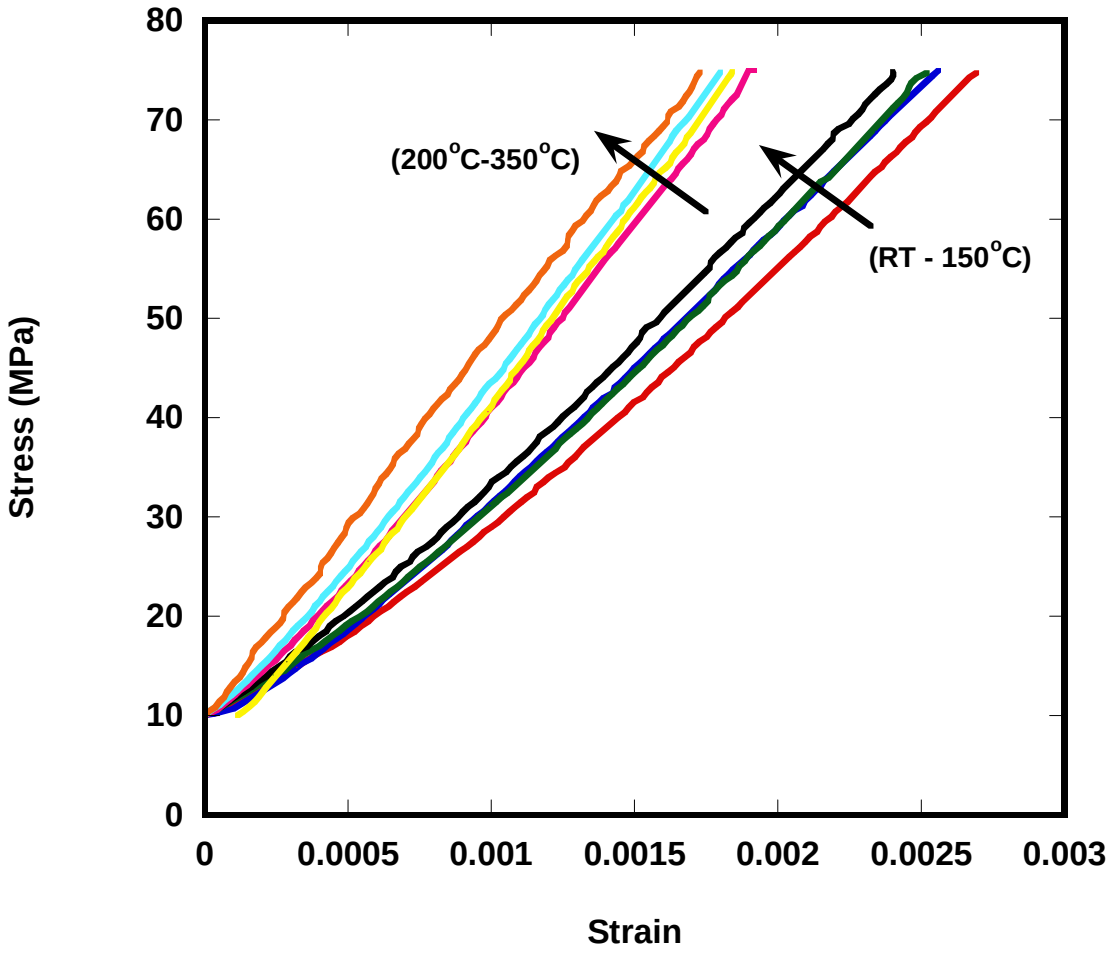

Figure 6.16: Stress-strain response of a NiTiFe sample (solutionized at 850 °C for 1 hr and vacuum cooled) as a function of temperature (high temperatures)

The values of modulus obtained from both the graphs (Figures 6.15 and 6.16) are listed in tables 6.4 and 6.5 respectively.

Table 6.4: Elastic modulus values (low temperatures)

Temperature (°C)	Young's Modulus (GPa)
-110	8.6
-90	9.9
-70	12.1
-50	18.2
-30	23.4
-10	27.0

Table 6.5: Elastic modulus values (high temperatures)

Temperature (°C)	Young's Modulus (GPa)
RT	25.8
50	27.6
100	27.8
150	28.5
200	36.3
250	38.4
300	38.0

6.3.2.3 Twinning at Low Loads

Testing at lower temperatures with low loads exhibited twinning in the material which was evident from the unrecoverable strain after the loading and unloading portions of the sample. However, at low loads it is also possible that slight amount of stress induced martensite is formed which does not transform back on unloading.

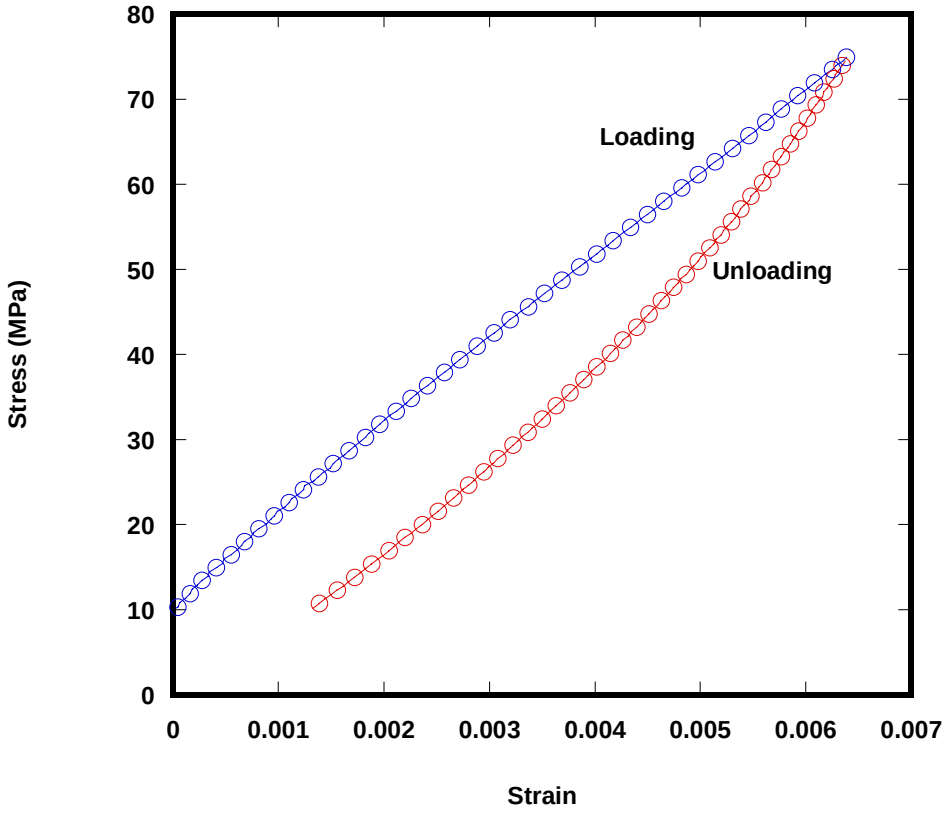

Figure 6.17: Complete load-unload response of a NiTiFe sample tested at -90 °C

Figures 6.17 and 6.18 show the stress-strain response of a NiTiFe sample tested at -90 °C and -110 °C respectively.

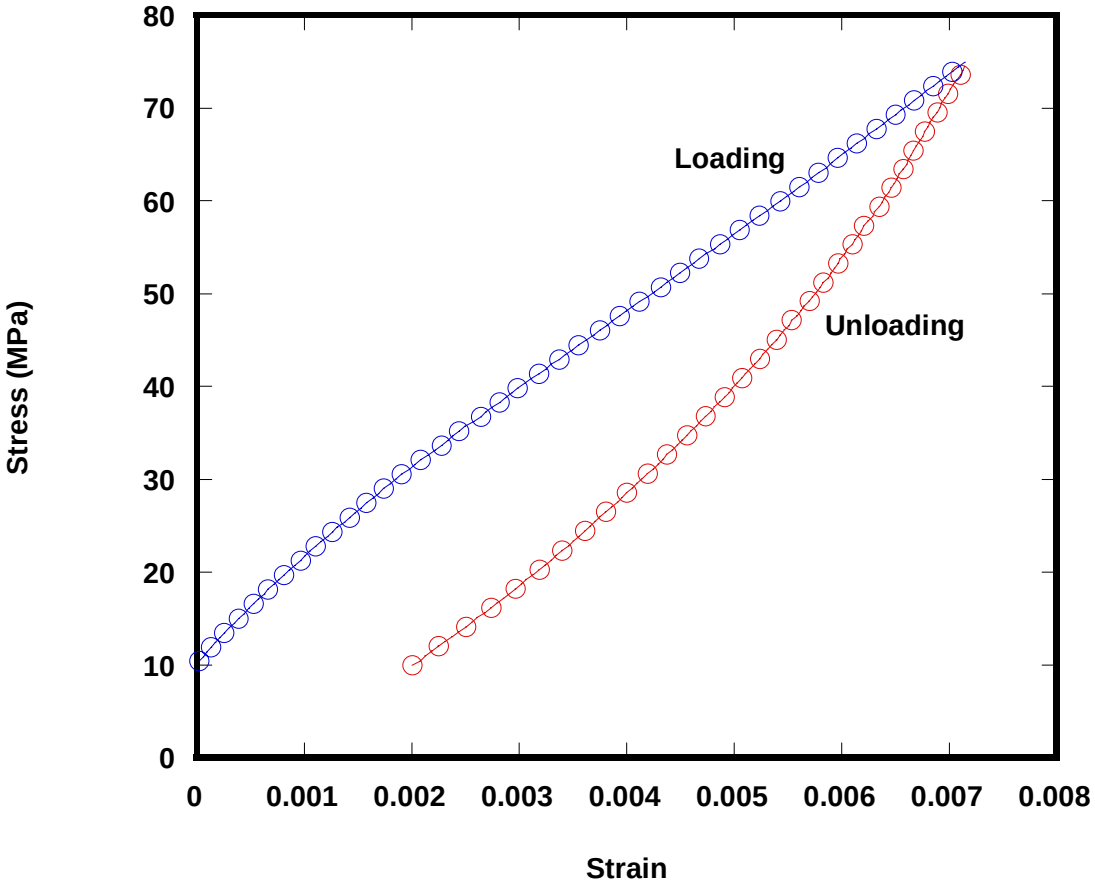

Figure 6.18: Complete load-unload response of a NiTiFe sample tested at -110 °C

6.3.2.4 Testing to High Loads

NiTiFe samples (thin wires) were cut from the billet which was solutionized at 850 °C for 1 hr and vacuum cooled. The dimensions of the samples are 0.1 mm X 0.1mm X 25 mm and these were tested at higher loads at various temperatures and were cycled at each temperature till 160 MPa at the rate of 10 MPa/min to examine the deformation behavior in the R-phase and austenite.

6.3.2.4.1 Cycling at Low Temperatures

Figures 6.19-6.23 show the stress-strain graphs at various temperatures with multiple cycles.

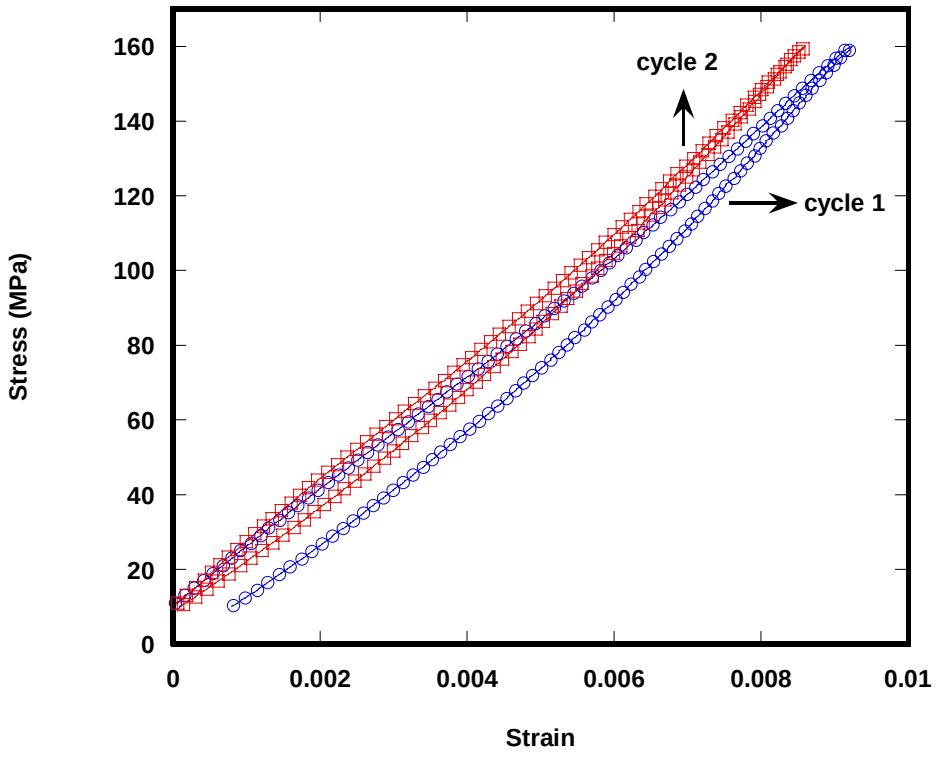

Figure 6.19: Cycling of NiTiFe sample tested at -70 °C

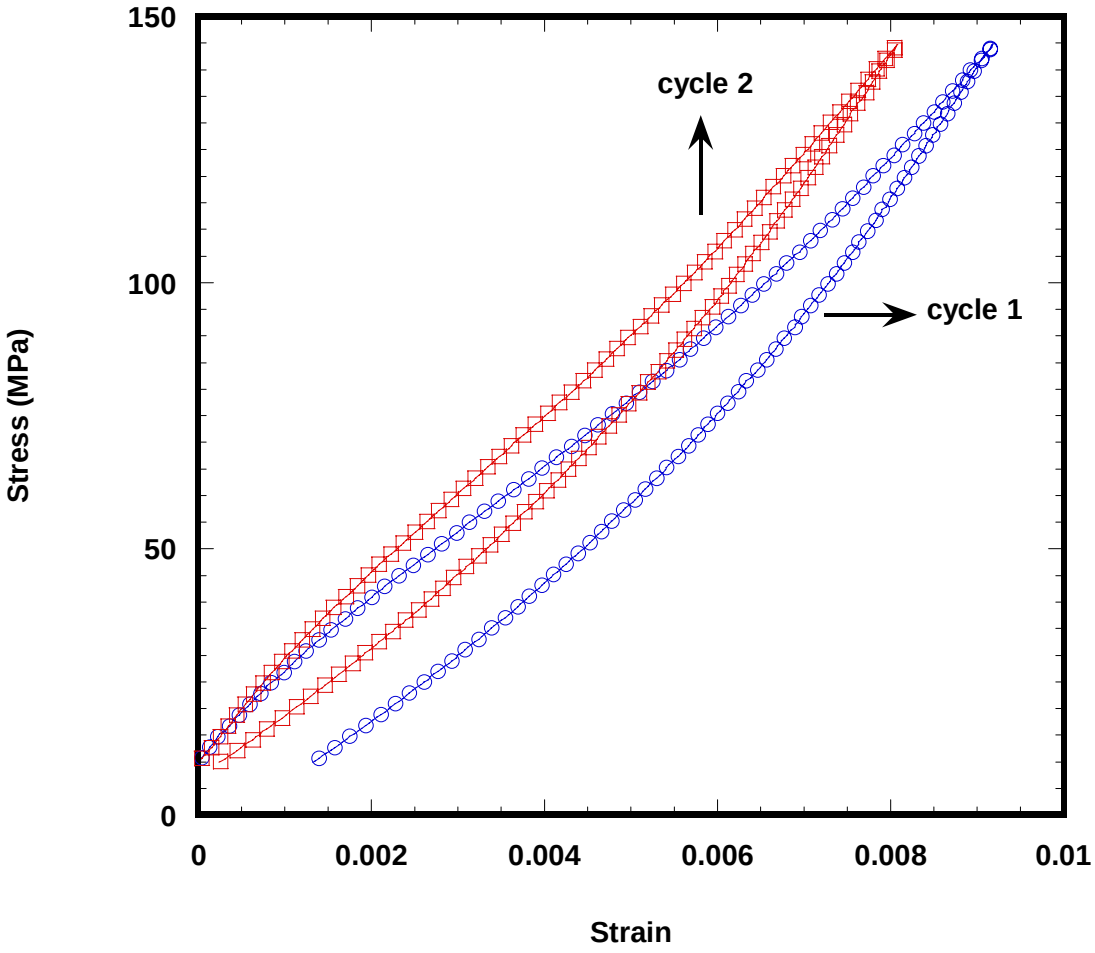

Figure 6.20: Cycling of NiTiFe sample tested at -90 °C

(solutionized at 850 °C for 1 hr and vacuum cooled)

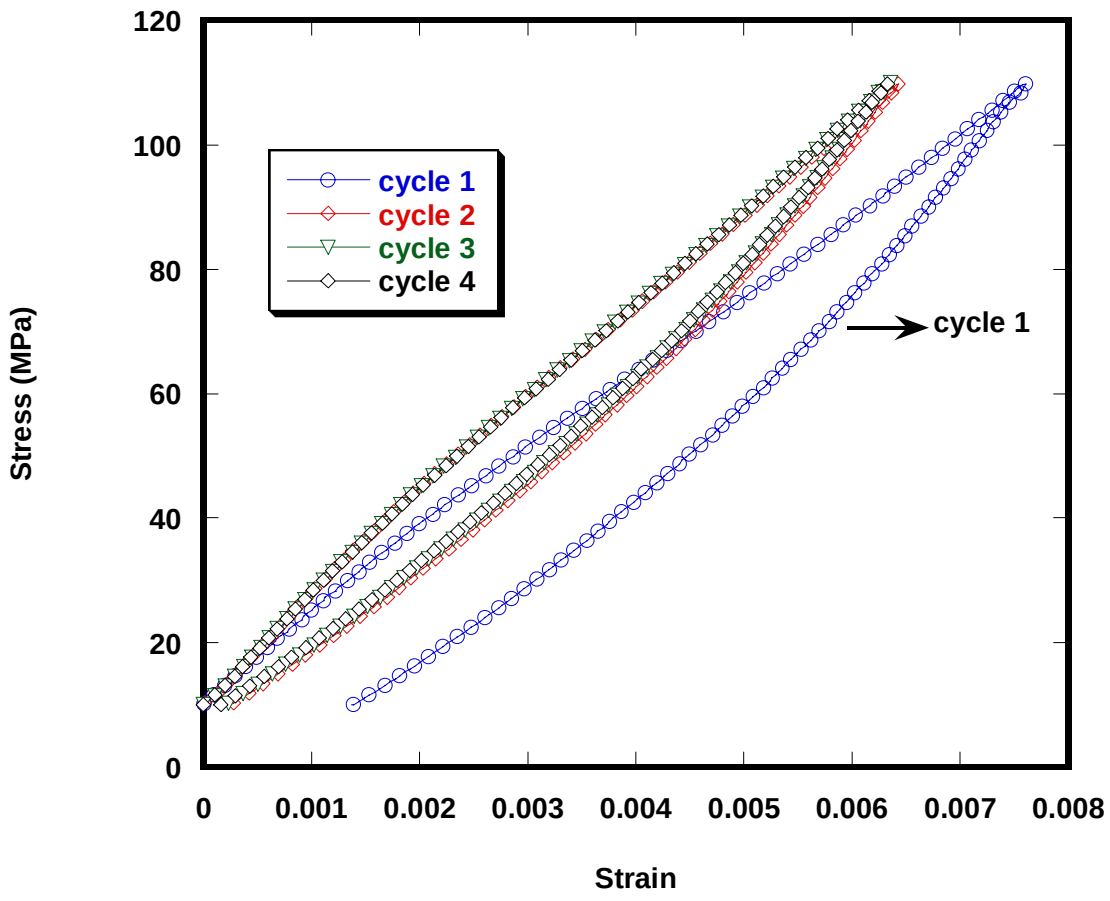

Figure 6.21: Cycling of NiTiFe sample tested at -100 °C

(solutionized at 850 °C for 1 hr and vacuum cooled)

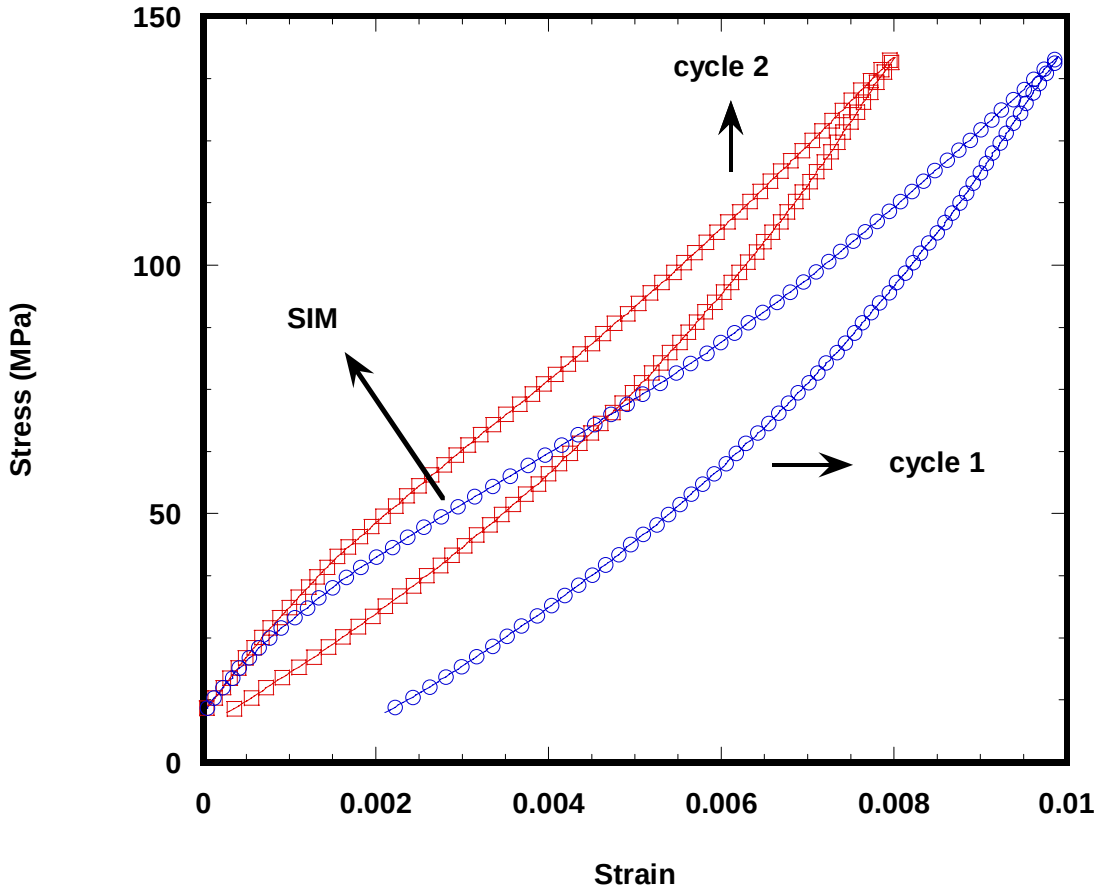

Figure 6.22: Cycling of NiTiFe sample tested at -110 °C

(solutionized at 850 °C for 1 hr and vacuum cooled)

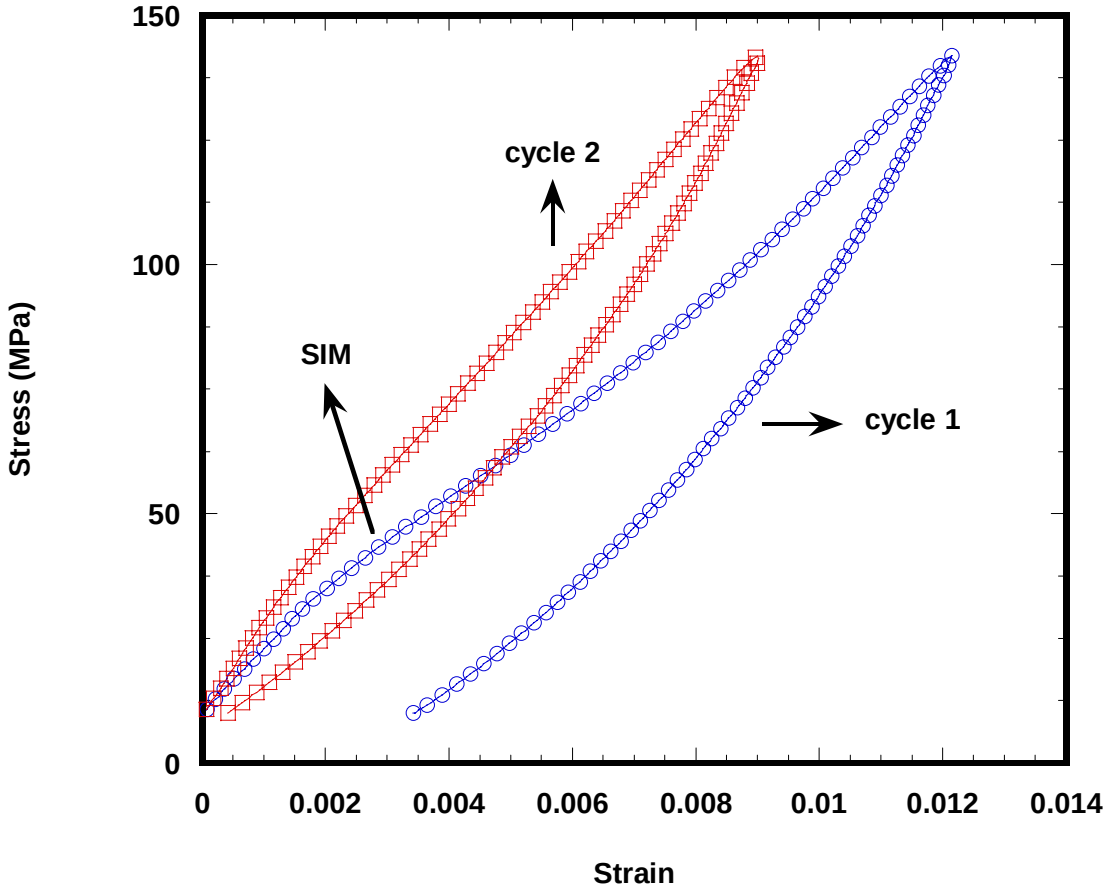

Figure 6.23: Cycling of NiTiFe sample tested at -130 °C

(solutionized at 850 °C for 1 hr and vacuum cooled)

It was observed that the unrecoverable strain increased during the first cycle as the temperature decreased. The unrecoverable strain is attributed to twinning in the R-phase and the stabilized martensite which is present after the first cycle in the completely unloaded condition [Rathod *et al.* 2006].

However, from the second cycle, the entire martensite which is induced by stress from the R-phase reverts back with the removal of stress forming a complete loop. The amount of unrecoverable strain with temperature is listed below in Table 6.6.

Table 6.6: Amount of unrecoverable strains at different temperatures

Temperature (°C)	-70	-90	-100	-110	-130
Unrecoverable strain in the first cycle (%)	0.08	0.13	0.14	0.22	0.34

6.3.2.4.2 Cycling at High Temperatures

NiTiFe samples (thin wires) were cut by EDM from the billet (solutionized at 850 °C for 1 hr and vacuum cooled) with dimensions of 0.1 mm x 0.1 mm x 25 mm and were cycled at higher temperatures to higher loads at the rate of 10 MPa/min. The temperatures selected were in the region where the initial phase is austenite (refer DSC values from section 6.1.1). Figures 6.24 – 6.26 show the cycling at room temperature, 70 °C and 90 °C respectively. It was observed that the unrecoverable strain in these cases were very less showing that the R-phase and martensite formation through stress was difficult at higher temperatures.

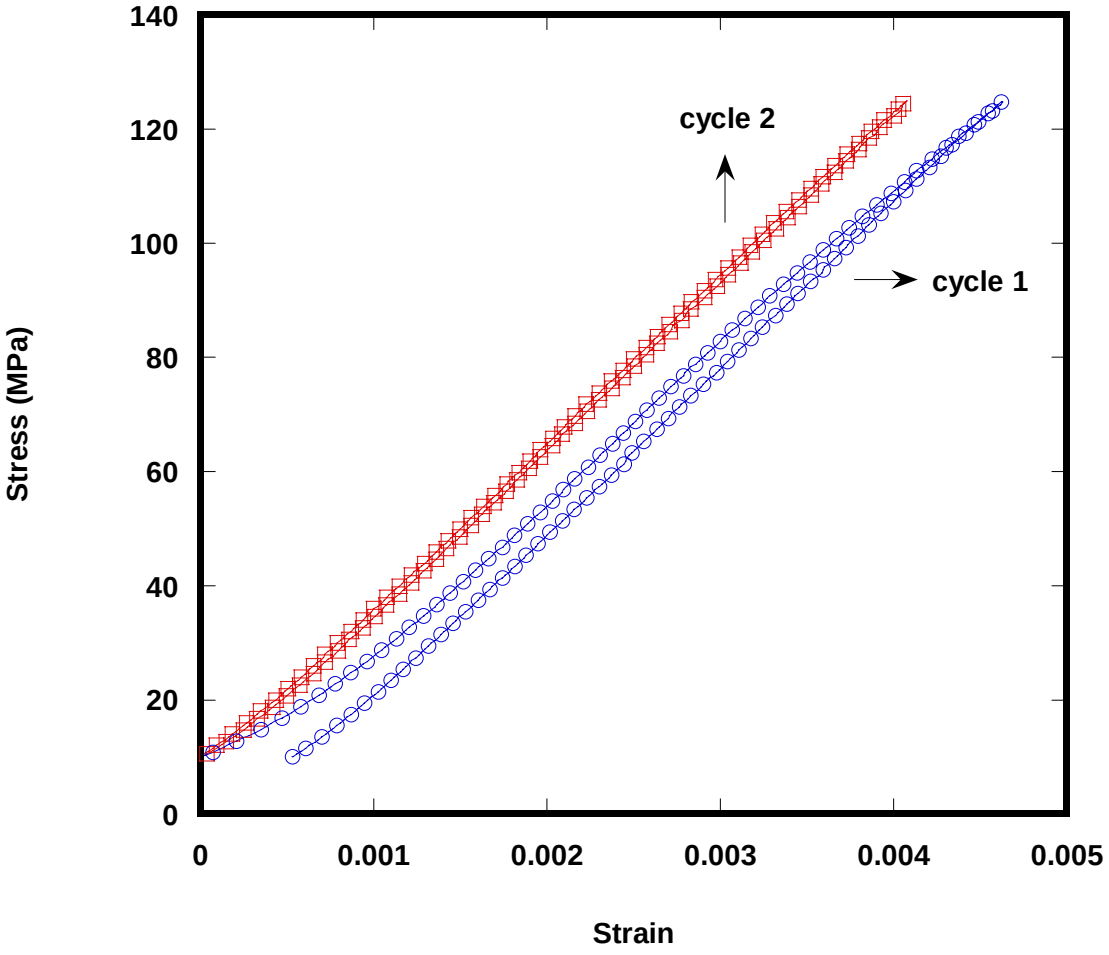

Figure 6.24: Cycling of NiTiFe sample tested at room temperature

(solutionized at 850 °C for 1 hr and vacuum cooled)

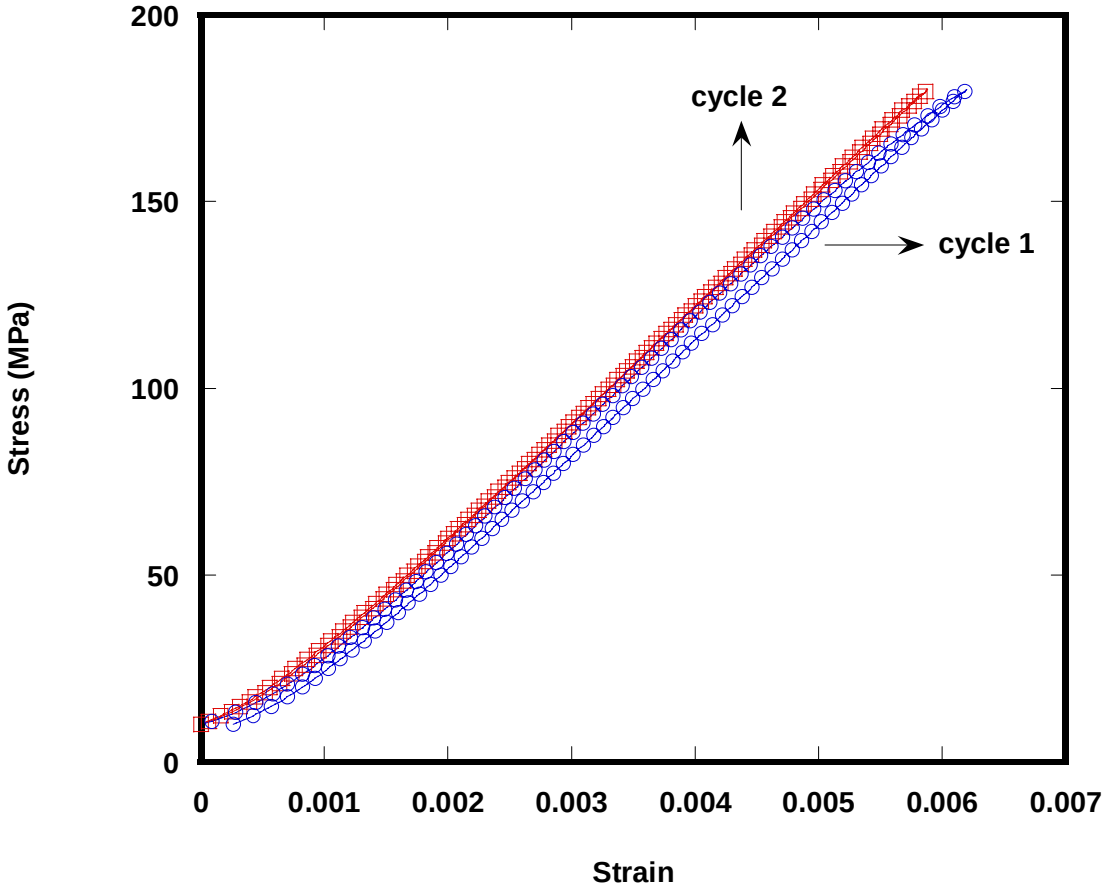

Figure 6.25: Cycling of NiTiFe sample tested at 70 °C

(solutionized at 850 °C for 1 hr and vacuum cooled)

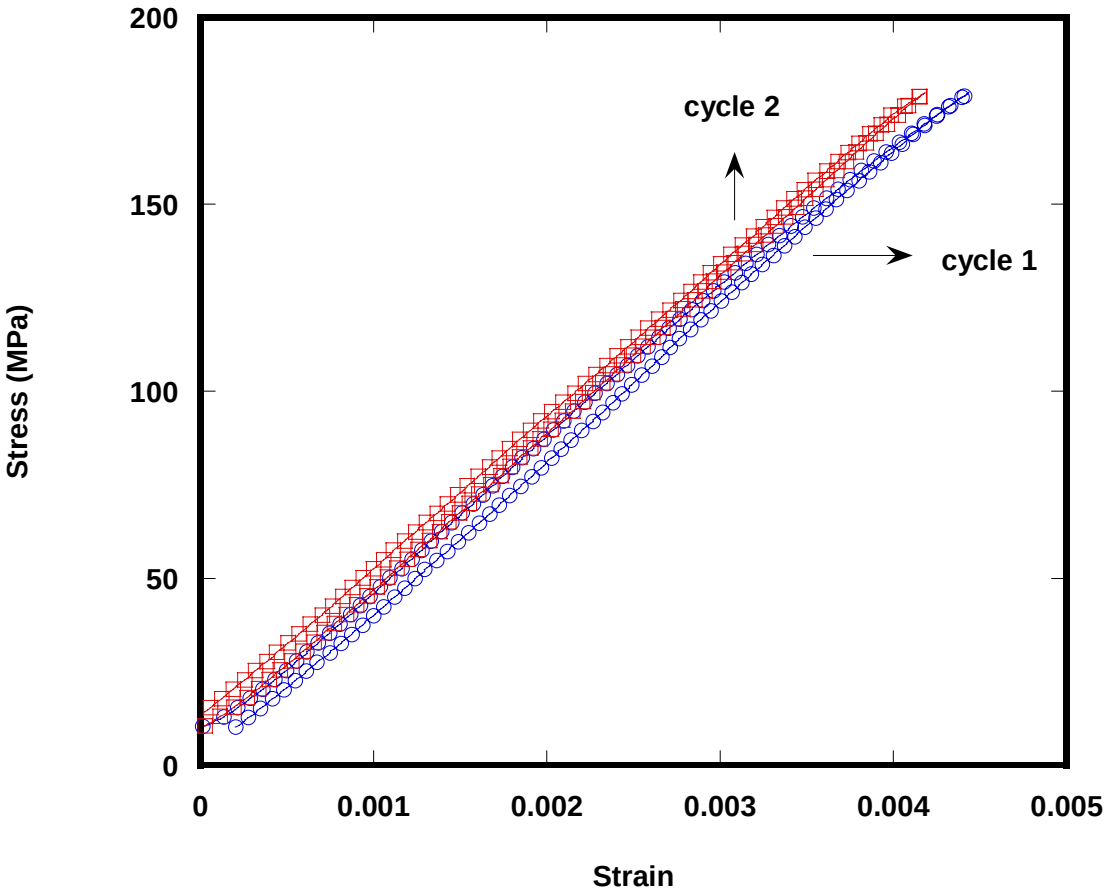

Figure 6.26: Cycling of NiTiFe tested at 90 °C

(solutionized at 850 °C for 1 hr and vacuum cooled)

6.3.2.5 Equivalence of Stress and Temperature

The stress at which stress induced R-phase forms varies linearly with temperature, and the relationship between the stress and temperature is given by the Clausius-Clapeyron equation. This equation in terms of the phase transformation is given below where ΔH and ΔV are material parameters.

$$\frac{d\sigma}{dT} = \frac{\Delta H}{T\Delta V} \longrightarrow \frac{d\sigma}{dT} = \frac{\rho.\Delta H}{T.\Delta\varepsilon}$$

where

dσ/dT is the temperature coefficient of the critical stress for the transformation

Δε is the amount of strain due to the transformation

ρ is the density of the alloy

ΔH is the enthalpy of transformation

T is the temperature at which two phases are in chemical equilibrium

Figure 6.28 shows the loading portions of cycle-1 at different temperatures. It was observed that the stress at which the SIR was induced increases with temperature and the values at different temperatures are given in Table 6.7.

Table 6.7: Values of stress induced R-phase at various temperatures

Temperature (°C)	30	70	90
Stress at which SIR forms (MPa)	163.8	175.6	190.9

Figure 6.27 shows the plot that exhibits the linearity between the stress at which the R-phase is induced from austenite and the corresponding temperature. The linearity is expected from the Clausius-Clapeyron equation.

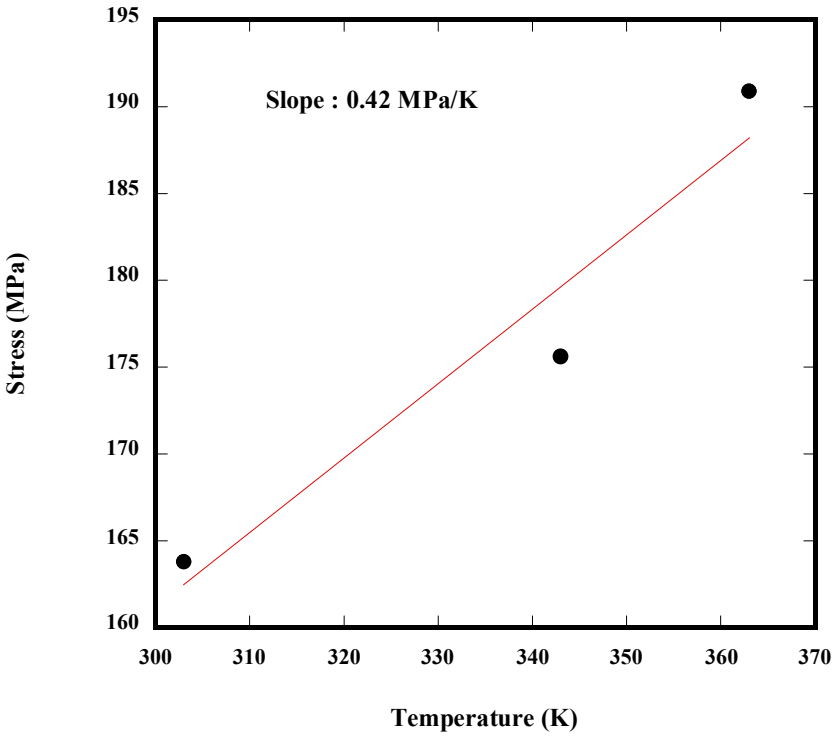

Figure 6.27: Stress at which R-phase is induced vs. temperature of a NiTiFe sample solutionized at 850 °C for 1 hr and vacuum cooled

To check if the behavior can be described by the Clausius-Clapeyron equation:

$T_o = ½ (R_s+A_f) = ½ (233.1 + 237.6) = 235.4$ K

$\Delta V = \Delta\varepsilon/ \rho$ where $\Delta\varepsilon$ = transformation strain during the transformation

ρ=density of the material

From the equation above

$$\frac{d\sigma}{dT} = \frac{\rho.\Delta H}{T.\Delta\varepsilon}$$

ΔH is obtained from the DSC graph of this particular sample

$\Delta\varepsilon$ is obtained by determining the amount of strain during the transformation (B2 to R)

$= \rho . \Delta H / \Delta\varepsilon . T_o = 6.45 \text{ X } 10\text{^}3 \text{ X } 2.99 / 0.002 \text{ X } 235.4 = 0.54$ MPa/K

This value is comparable to the slope of the graph obtained in Figure 6.27 (0.42 MPa/K) which shows the general agreement with the Clauisus-Clapeyron equation.

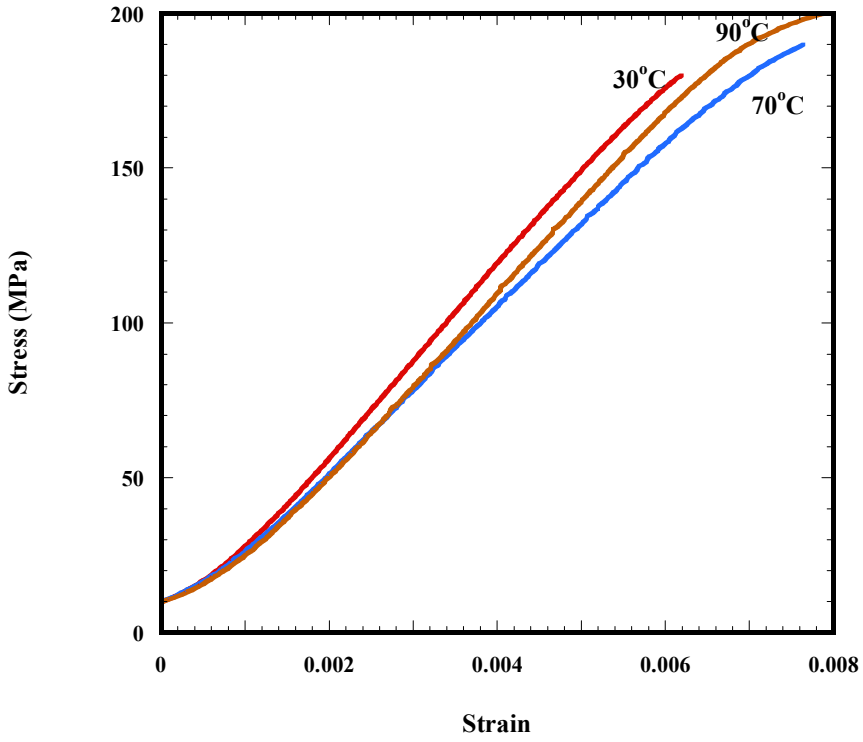

Figure 6.28: Overlaid first cycle graphs for NiTiFe sample tested at 30 °C, 70 °C and 90 °C

6.3.2.6 Effect of Heat treatment on Stress-Strain Response

Two NiTiFe samples of each type, one which was solutionized at 850 °C for 1 hr and vacuum cooled and the other which was solutionized at 850 °C for 24 hr and vacuum cooled (with dimension 0.1 mm x 0.1 mm x 40 mm) were tested in the DMA until failure.

Figure 6.29 shows the loading portions of the curves at room temperature. It was observed that the sample which was solutionized for 1 hr (denoted by red circles) failed at a lower stress compared to the sample which was solutionized for 24 hr (denoted by blue squares). Figure 6.30 shows the loading portions of the stress-strain graphs tested at -100 °C indicating similar behavior. This could be attributed to the annihilation of the defects present with additional solutionizing time. This entire phenomena with the solutionizing time can be explained based on the internal stresses which are larger in case of the sample which was solutionized for 1 hr. Due to the presence of more defects in this sample which results in more internal stresses, stress induced martensite and twinning can occur easily at lower stresses which deflates the modulus of the 1 hr solutionized sample as shown in Figure 6.24, tested at room temperature. However, in this case defects inhibit the accommodation of large amount of strains. At -100 °C formation of stress induced martensite and twinning of martensite is easier at low temperatures and it overcomes the defects present. As shown in Figure 6.30, the accommodation of strains in this case is more for the sample solutionized for 1 hr.

The macroscopic behavior is correlated with the microscopic behavior in the TEM (transmission electron microscopy) micrographs for both the samples. Samples for TEM were taken from a different end of the sample other than the failed end to avoid any defect

observation. The TEM images shown in Figures 6.31 and 6.32 indicate that the grain structure which was elongated before had become more equiaxed with the increase in solutionizing time.

Thus, the increase in mechanical strength with the solutionizing treatment which was observed in the DMA was correlated with the grain structure from the TEM micrographs.

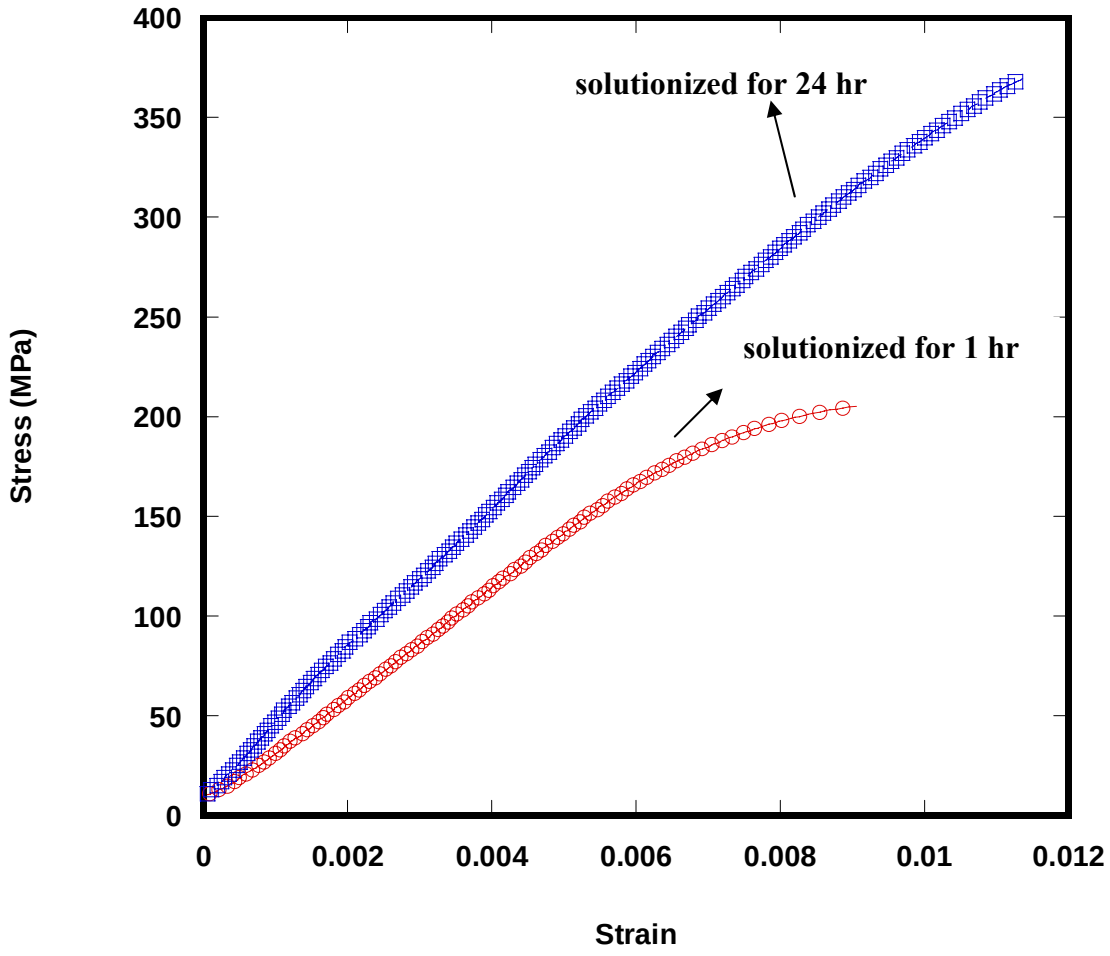

Figure 6.29: Stress-strain response of NiTiFe samples solutionized for 1 hr and 24 hr at 850 °C tested at room temperature

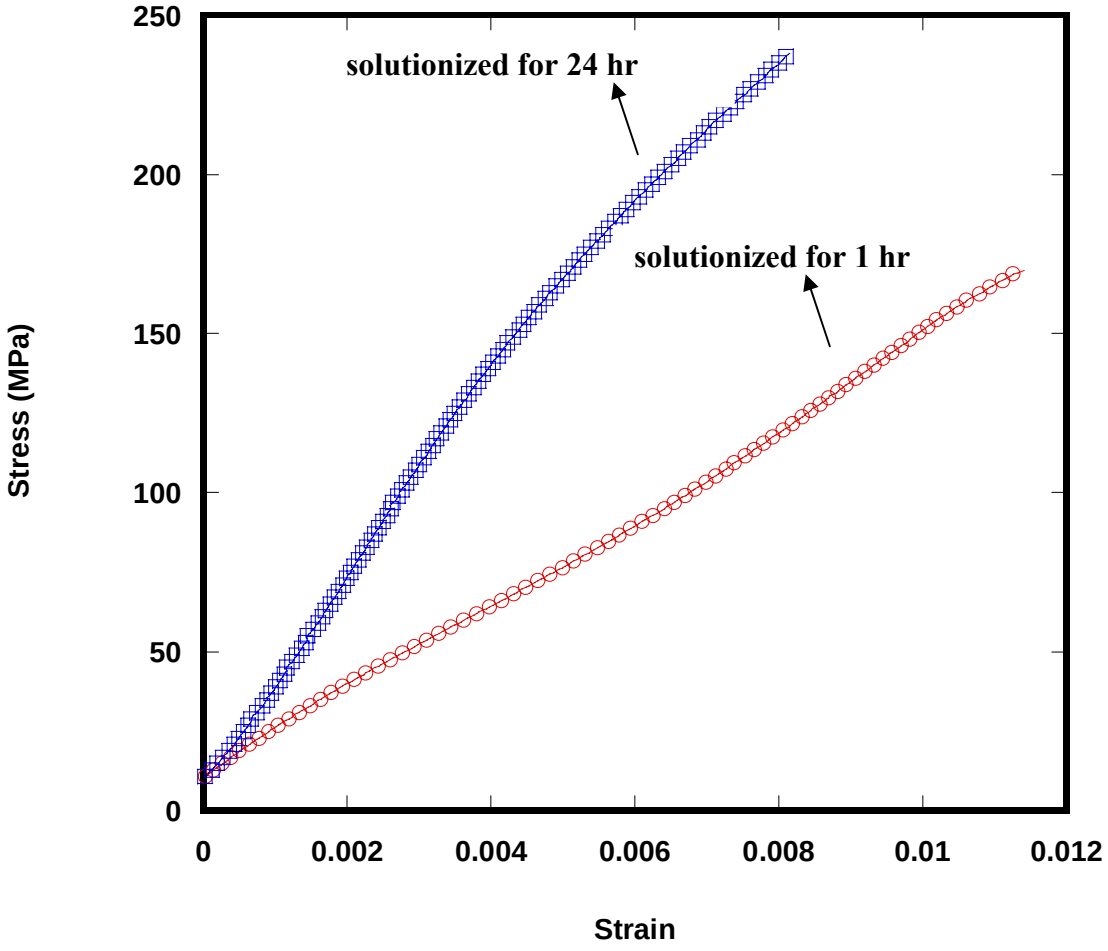

Figure 6.30: Stress-strain response of NiTiFe samples solutionized for 1 hr and 24 hr at 850 °C tested at -100 °C

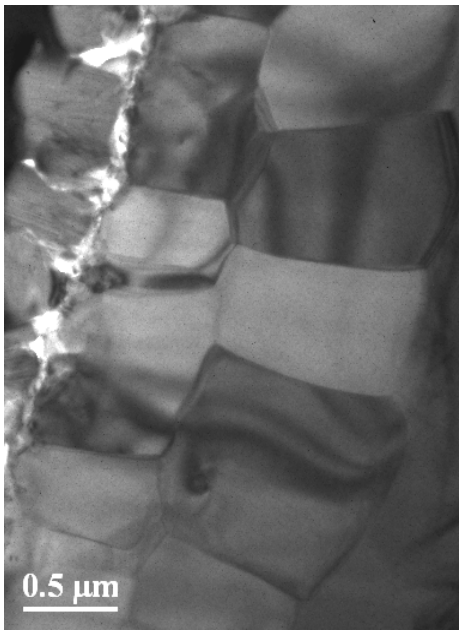

Figure 6.31: TEM micrograph of a NiTiFe sample solutionized at 850 °C for 24 hr

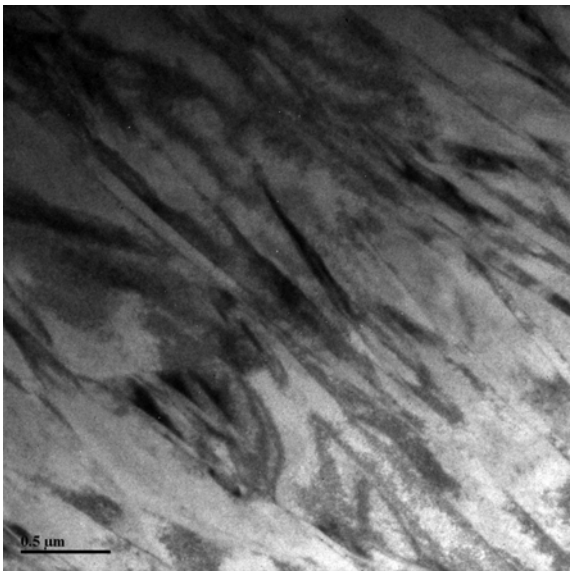

Figure 6.32: TEM micrograph of a NiTiFe sample solutionized at 850 °C for 1 hr

6.3.3 Constrained Recovery

As described in section 1.2.3 constrained recovery is the property of a shape memory alloy generating recovery stresses when impeded during heating from the martensite to the austenitic phase. In case of a NiTiFe alloy the constrained recovery involved the R-phase transformation. Initially a superelastic NiTi wire was tested in the DMA to check the feasibility of a constrained recovery experiment in the instrument.

6.3.3.1 NiTi Testing

A superelastic NiTi wire of diameter 0.17 mm was taken and cooled to -40 °C (to be completely in the martensite phase) and then loaded till 30 MPa with a loading rate of 5 MPa/min. Under a constant stress of 30 MPa it was heated to a temperature of 80 °C at 5 °C per min. As the temperature increased, strain recovery was observed demonstrating the constrained recovery. Figure 6.33 shows the strain vs. temperature curve of the NiTi wire which shows a strain recovery of 0.24 % when heated from -40 °C to 80 °C.

Thus, a constrained recovery experiment was conducted in the DMA and thus made sure that further experiments could be done on the NiTiFe alloy.

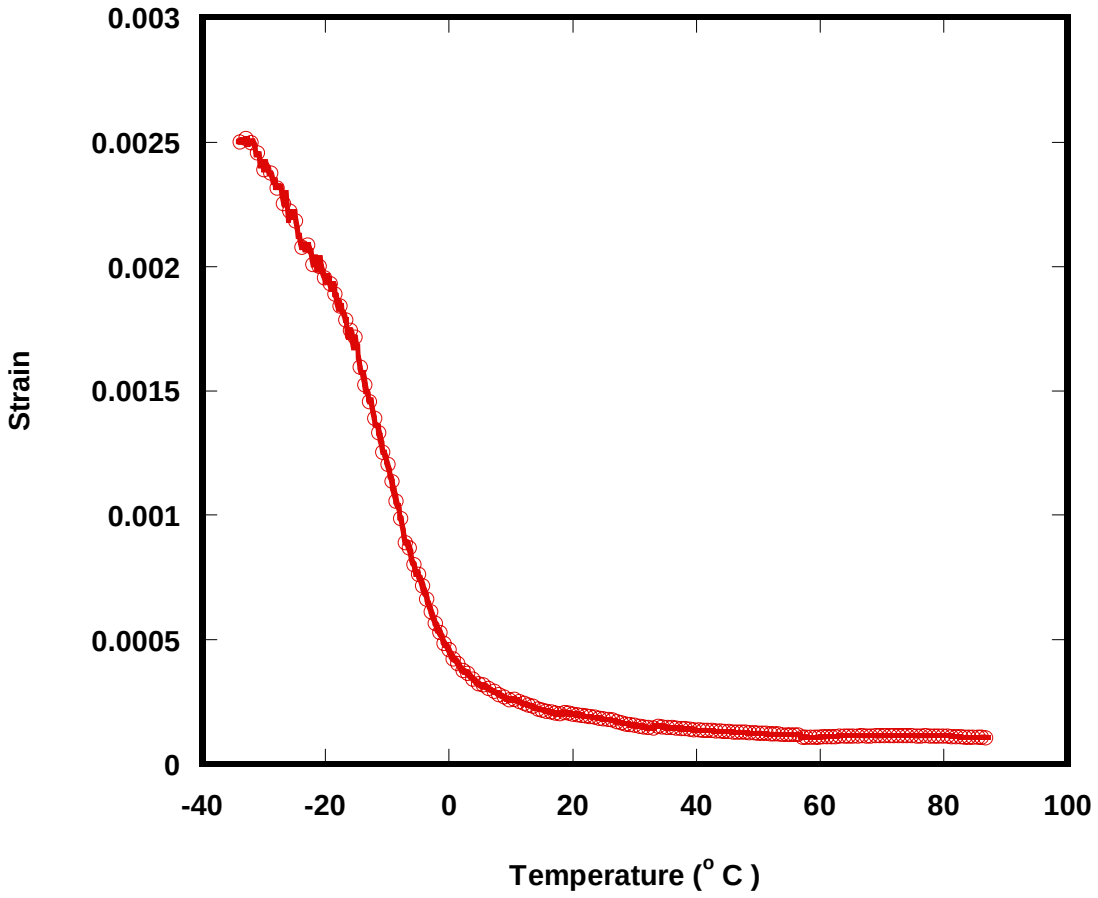

Figure 6.33: Strain vs. temperature of a superelastic NiTi wire under an external load of 30 MPa

6.3.3.2 NiTiFe Testing

Thin wires of dimension 0.1 mm X 0.1 mm X 40 mm were cut by EDM from the piece of billet (solutionized at 850 °C for 1 hr and vacuum cooled), and tested in the DMA for constrained recovery. Initially, two of these samples were cooled to -80 °C and -100 °C and then a stress of 30 MPa and 50 MPa was applied respectively at the rate of 5 MPa/min. Then at that constant stress, these samples were heated to room temperature at the rate of 5 °C /min. As seen in Figure 6.34 and 6.35 the strain was found to be increasing with the temperature, which was not expected.

To study this unusual behavior of NiTiFe at these temperatures, cycling with a constant stress to high and low temperatures had been conducted to determine if it was a machine artifact which is explained in the subsequent section.

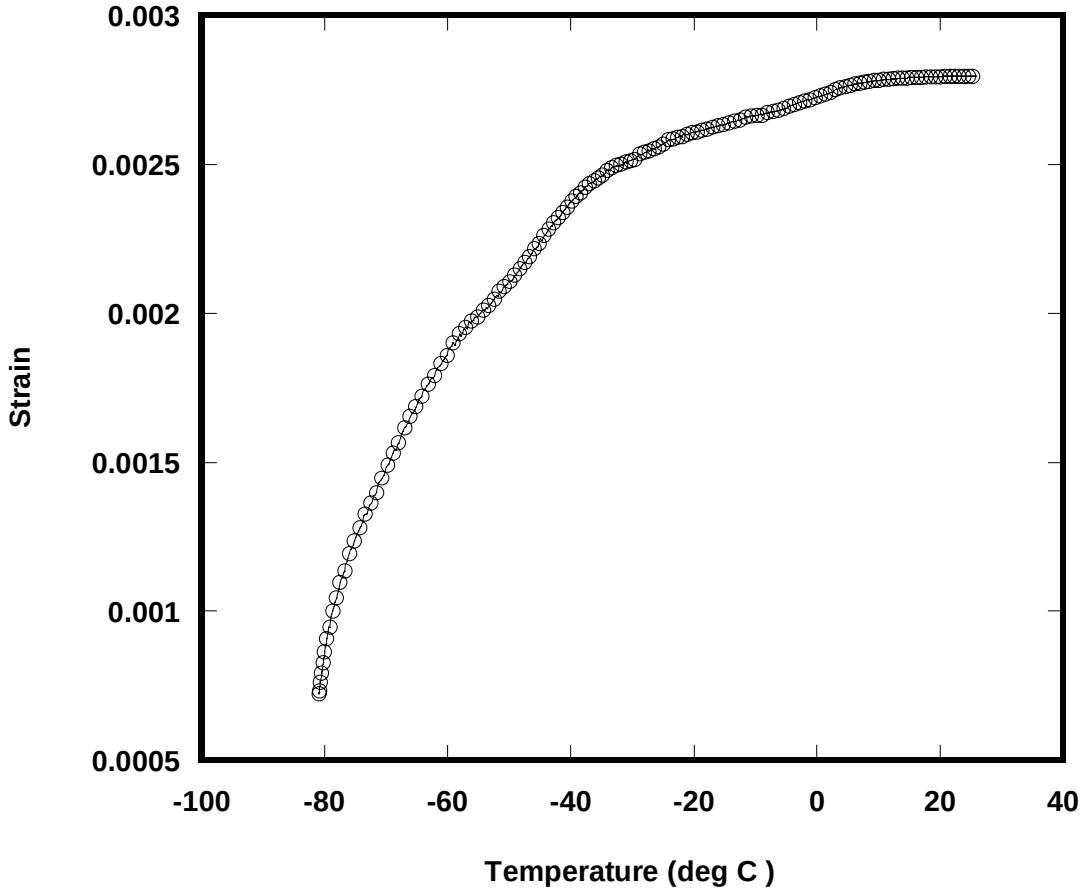

Figure 6.34: Strain vs. temperature of NiTiFe sample solutionized at 850 °C for 1 hr and vacuum cooled under an external load of 30 MPa

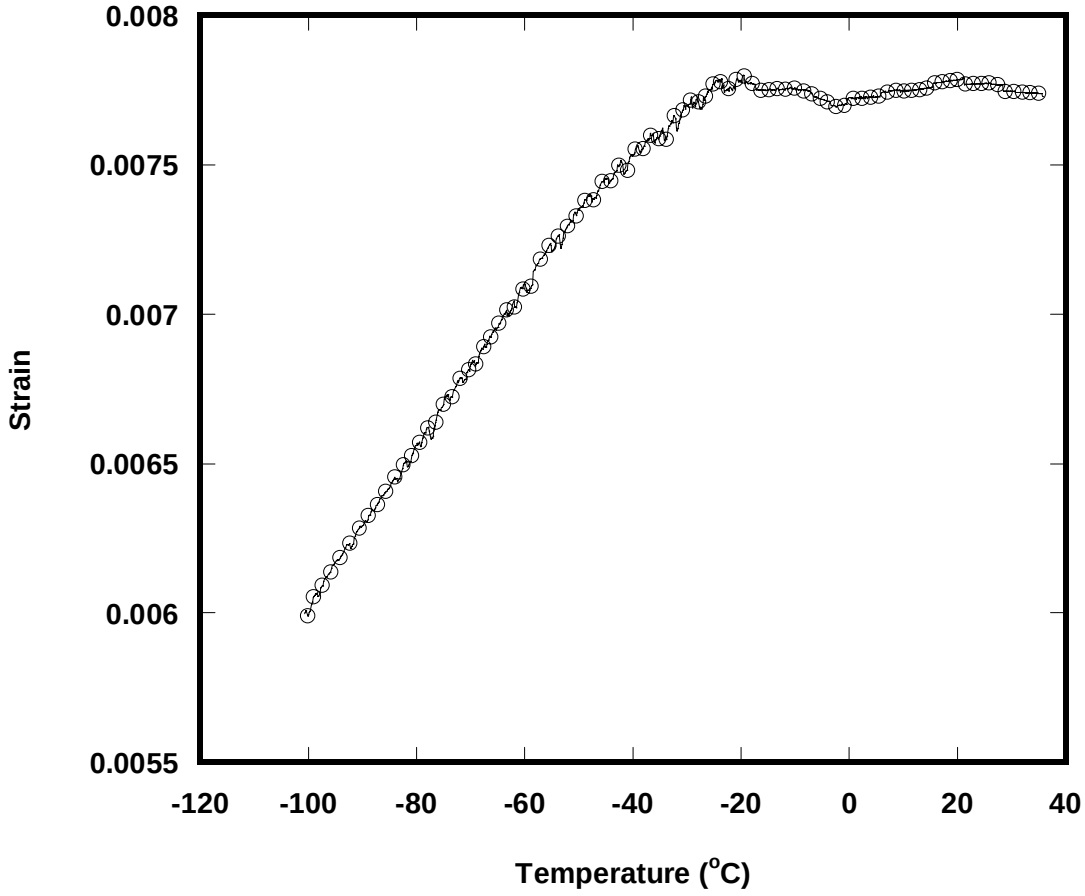

Figure 6.35: Strain vs. temperature of NiTiFe sample solutionized at 850 °C for 1 hr and vacuum cooled under an external load of 50 MPa

Cycling of NiTiFe

A NiTiFe sample (solutionized at 850 °C for 1 hr and vacuum cooled) was cooled and cycled between -65 °C and 150 °C for 9 cycles under a constant stress of 90 MPa. These temperatures were selected because at temperature of -65 °C the sample was in R-phase and at 150 °C it was in austenite phase (refer section 6.1.1 for DSC values). Figure 6.36 shows one of the cycles from which it was observed that though the heating and cooling rates were similar, the behavior of the sample differed in both these cases. The behavior of the sample could be because of the expansion and contraction during heating and cooling respectively.

A NiTiFe sample which was solutionized at 850 °C for 1 hr, when cycled between -75 °C and -45 °C at a constant stress of 100 MPa for 10 cycles to observe the effect of temperature in these cycling experiments. It was observed that in this range of temperature there was a little strain recovery during heating but was very little compared to the strain while loading. Figure 6.37 shows one cycle of the above mentioned experiment which exhibits strain recovery during heating.

To check the variation of this behavior at different temperatures a stainless steel wire was tested in the DMA to check if it was a machine artifact. The results obtained in that testing are outlined in the next section.

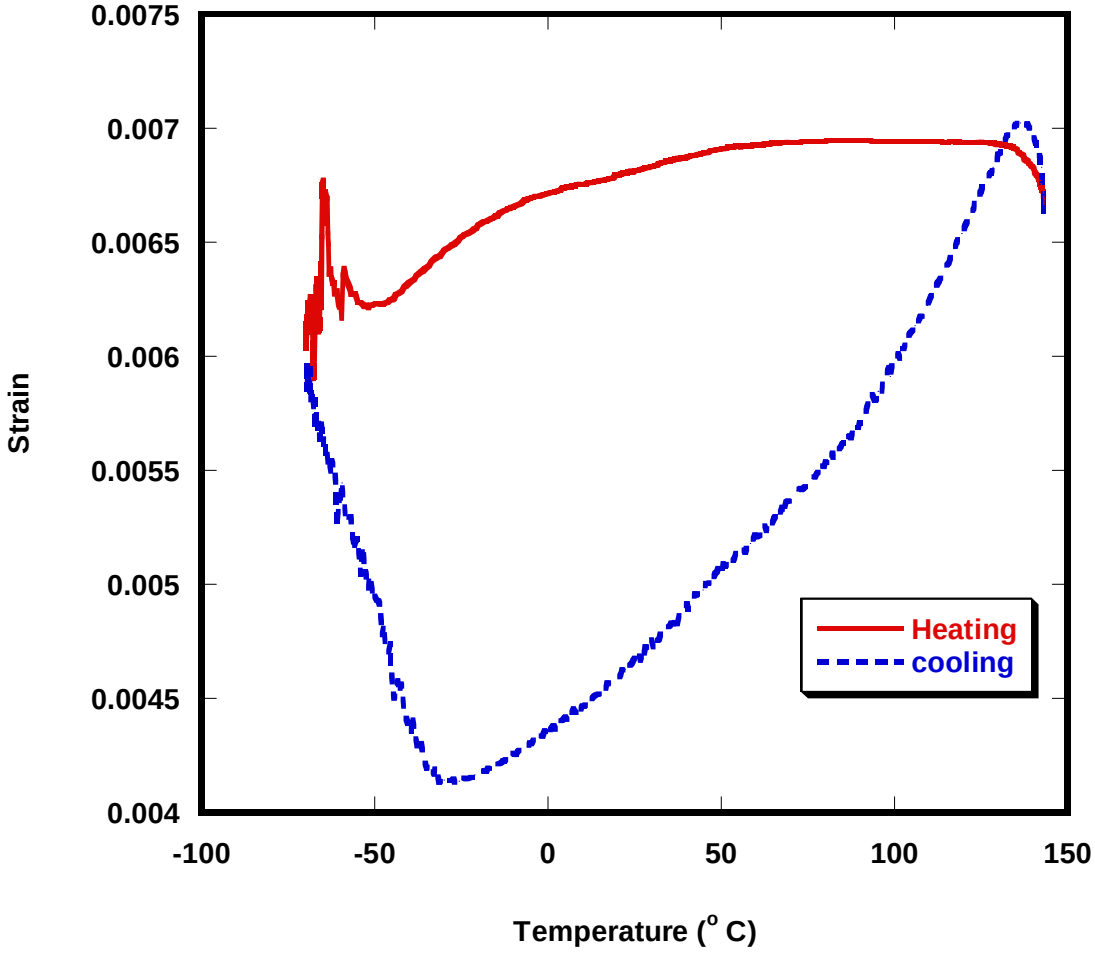

Figure 6.36: Strain vs. temperature curve of a NiTiFe sample cycled between -65 °C and 150 °C under a constant stress of 90 MPa.

(The sample was solutionized at 850 °C for 1 hr and vacuum cooled)

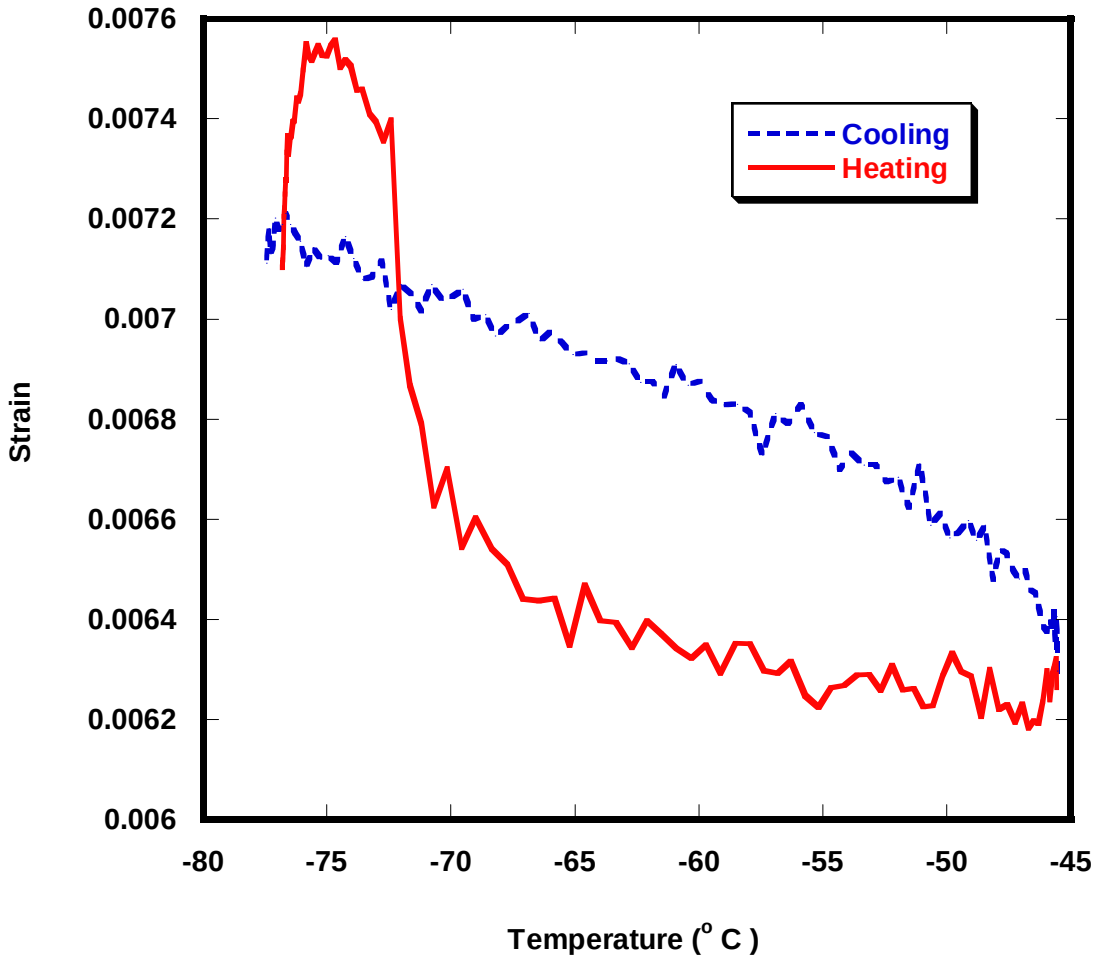

Figure 6.37: Strain vs. temperature curve of a NiTiFe sample cycled between -75 °C and -45 °C under a constant stress of 100 MPa.

(The sample was solutionized at 850 °C for 1 hr and vacuum cooled)

6.3.3.3 Stainless Steel Testing

A stainless steel wire of 0.127 mm diameter was tested in the DMA and a cycling experiment was conducted. The sample was cooled to -75 °C and a stress of 5 MPa was applied on it and cycled between -75 °C and 140 °C under that stress. It was observed that the strain decreased when the sample was cooled and it increased when the sample was heated. Calculation was done to check if this increase corresponded to the expansion and contraction of the sample in that temperature range due to coefficient of thermal expansion.

CTE of stainless steel 17.3 X 10^-6 / °C

$\Delta l = \alpha \, l \, \Delta T$

Δl = 17.3 X 10^-6 X 25 x 10^-3 X 291 = 1.06675 X 10^-4 m (which is close to 100 μm Δl from the graph).

As shown above the Δl which was obtained in the calculation correlated with the Δl obtained form the graph. So, from this it was confirmed that this behavior was due to the expansion and contraction of the sample.

Coefficient of thermal expansion is plotted along with the heating curve and the cooling curve as shown in strain vs. temperature curve in Figure 6.38. It was observed that, the cooling curve (denoted by the blue curve) matched with the coefficient of thermal expansion (denoted by the green curve) by having similar slopes. However, the heating curve (denoted by the red curve) did not coincide with the CTE curve indicating a difference in behavior during heating and cooling. Thus, this was concluded as a machine artifact and it has to be subtracted for further experimentation in the DMA during the constrained recovery testing.

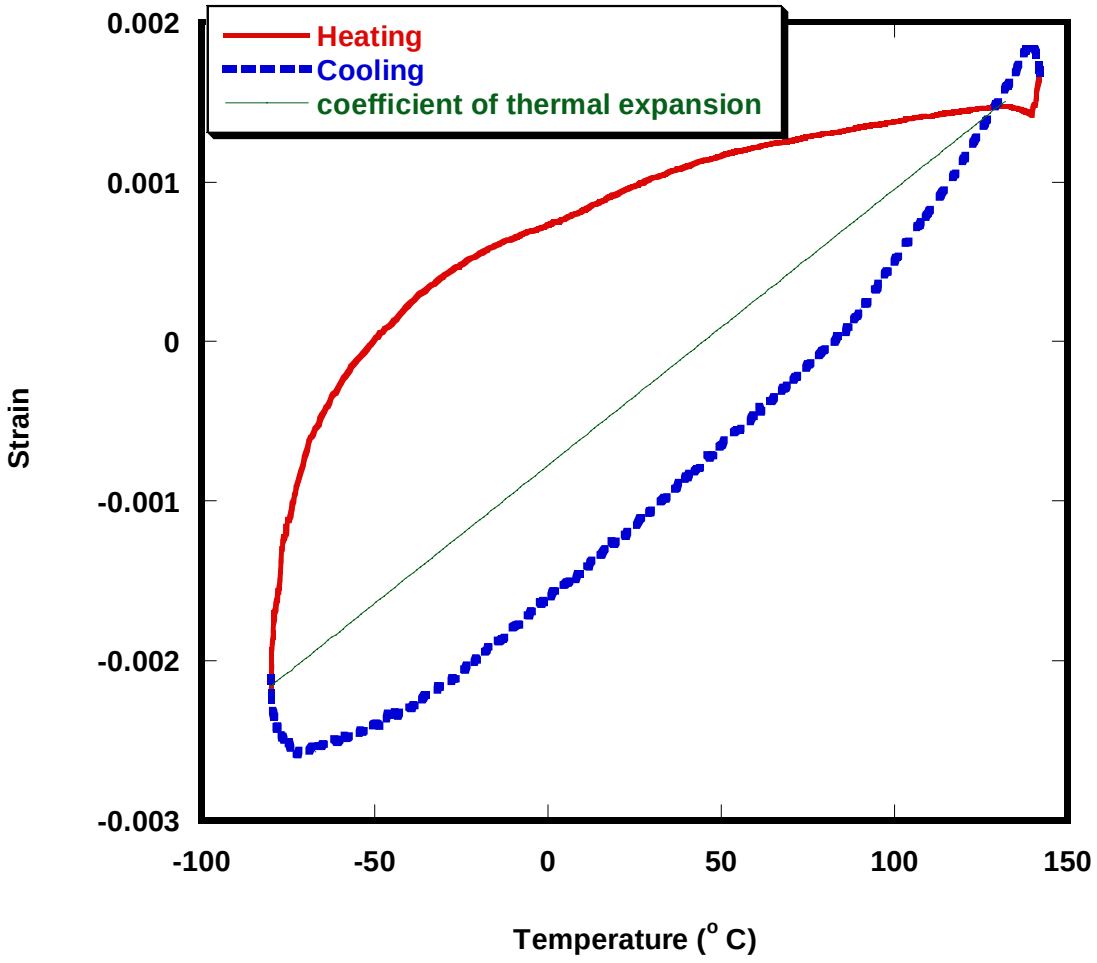

Figure 6.38: Strain vs. temperature of a stainless steel wire cycled between -75 °C and 140 °C

CHAPTER 7: CONCLUSIONS AND FUTURE WORK

7.1 Conclusions

NiTiFe shape memory alloys were selected for this study since the addition of Fe to the NiTi system introduces an intermediate trigonal R-phase and further suppresses the martensitic transformation. The R-phase transformation offers a favorable window for actuator operation since it exhibits low hysteresis (around 2 K) and good fatigue response. The effect of various thermo-mechanical treatments on the R-phase and the deformation behaviors of these alloys in the various phases were studied.

A dynamic mechanical analyzer (DMA) which was capable of mechanical characterization at different temperature and stress ranges was commissioned successfully as part of this work. Mechanical testing in the DMA was verified by testing a standard PMMA sample (poly-methyl methacrylate) in dynamic mode. To test the applicability of the instrument in static mode and for constrained recovery experiments, superelastic NiTi samples of different gauge lengths were tested at different loading rates. The results were consistent and the values obtained for the elastic moduli in both phases correlated with expected values. Thus, the successful commissioning of the instrument for further mechanical testing was established.

In addition to a dynamic mechanical analyzer, a differential scanning calorimeter and a liquid helium dilatometer which were capable of characterizing transformation temperatures at different temperature ranges were used. During the characterization process, the temperature range of the liquid helium dilatometer was enhanced by facilitating the instrument to test to

temperatures as low as 9 K (-264 °C). An encapsulation procedure for heat treating these samples at various temperatures under vacuum was established which will be of further use in the heat treatment of various alloys.

The mechanical characterization of $Ni_{46.8}Ti_{50}Fe_{3.2}$ alloy in the DMA was done at different combinations of stress and temperature cycles and the following observations were made:

1. The as received NiTiFe sample tested in the DMA at different temperature ranges failed at lower stresses than expected, indicating the presence of defects in the as received condition.
2. Testing NiTiFe at low temperatures in the elastic region exhibited small amounts of twinning and stress induced transformations which lowered the modulus from expected values. Similarly, testing NiTiFe above room temperature exhibited both stress induced transformation followed by twinning that deflated the modulus. The modulus was found to increase as the temperature increased.
3. Cycling NiTiFe at higher loads at low temperatures showed incomplete stress-strain loops which were attributed to twinning and stabilization of martensite during the first cycle. However, during later cycles it was observed the martensite reverted back to the R-phase forming a complete loop.
4. The stress at which the R-phase was induced at various temperatures varied linearly with temperature and was consistent with the Clausius-Clapeyron equation. The stress-temperature equivalence was determined to be 0.52 MPa/°C.
5. Two samples subjected to two different solutionizing times were tested until failure at two different temperatures. The results were consistent with the decrease in defect density with increasing solutionizing time. The results were also substantiated with

microscopy observations in the TEM where equiaxed grains were observed with increasing solutionizing time. The accommodation of strains at room temperature and low temperatures was explained on the basis of the internal stresses present in the material which assist in formation of stress induced martensite and twinning (in certain cases) in the material.

6. Constrained recovery experiments were also conducted with various loads at different temperature ranges but significant recovery was not observed. The issues related to these were studied by testing stainless steel wire samples and the recommendations in improving the testing procedures were outlined.

Various thermo-mechanical treatments were employed to study the effect on the transformation temperatures and the following observations were made based on the DSC and dilatometry results.

1. There was no martensite transformation observed in this $Ni_{46.8}Ti_{50}Fe_{3.2}$ alloy till 9 K with any of the heat treatments given.
2. The R-phase transformation temperatures did not change with any of the heat treatments and this result was correlated by both the DSC and dilatometry analyses. $Ni_{46.8}Ti_{50}Fe_{3.2}$ being a titanium rich alloy, in which the formation of precipitates are considerably lower, the aging treatments done on this alloy did not show any effect on the change in transformation temperatures. The small changes in transformation temperatures observed are well within the error limits of the instruments. These results were substantiated from the microscopy observations which showed lack of precipitates in the alloy.
3. The cold rolling and annealing treatments which were employed on this alloy showed better results from an actuator application point of view, narrowing the range over which

the R-phase transformation occurs. Increase in the annealing temperatures of the material enhanced the R-phase transformation. It was observed that an optimum number of dislocations or external defects were necessary inside the material that did not inhibit the R-phase transformation while assisting in the nucleation of the R-phase. However, large numbers of dislocations were undesired because they would inhibit the transformation of R-phase from austenite.

4. Annealing at higher temperatures favored the R-phase transformation but increasing the annealing temperature above the recrystallization temperature was not desirable for the transformation.

Thus, the deformation behaviors in various phases of this alloy were studied and the transformation characteristics were analyzed which provided information on this alloy for its further utilization in applications such as cryogenic thermal conduction switches, actuators, self-healing gaskets etc.

7.2 Future Work

The grains were oriented longitudinally in the billet selected, but the samples which were taken for various thermo-mechanical treatments were transversely cut from the billet. Due to this, the yield strength of this material observed was low which was evident from the mechanical characterization. The samples for further thermo-mechanical testing should be taken in the longitudinal direction. This is expected to result in higher yield stresses as well as larger recoverable strains for constrained recovery experiments. The dimensions of the thin wires which were tested in the DMA can also be increased since these wires easily fracture during

testing with low amount of stresses due to the defects present in the material. Furthermore, aging treatments can be tried on Ni-rich alloys since they allow the formation of precipitates which in turn can increase the mechanical strength of these materials.

REFERENCES

1. Allafi, J. K., X. Ren, G. Eggler., (2002). "The mechanism of multistage martensitic transformations in aged Ni-rich NiTi Shape Memory Alloys" Acta Materialia **50**(4): 793-803.

2. Allafi, J. K., Wolfgang W. Schmahl, D. M. Toebbens., (2006). "Space group and crystal structure of the R-phase in binary NiTi shape memory alloys" Acta Materialia **54**: 3171–3175.

3. Beyer, J. (1995). "Recent advances in the martensitic transformations of TiNi Alloys" Journal de Physique IV **5**(C2): 433-442.

4. Bozzolo, G., R. D. Noebe, H. O. Mosca., (2005). "Site preference of ternary alloying additions to NiTi: Fe, Pt, Pd, Au, Al, Cu, Zr, and Hf" Journal of Alloys and Compounds **389**(1-2): 80-94.

5. Buehler, W. J. and Wang F. E., (1967). "A summary of recent research on the nitinol alloys and their potential application in ocean engineering", Ocean Eng.I, pp.105-120.

6. Busch, J.D., M. H. Berkson, A. D. Johnson, (1991). "TiNi/GaAs thin film structures for gate metallizations" MRS Symp. Proc. **230** (91).

7. Canales, A., F. Morales., (1995). "Electric transport-properties of the B2 to R-phase-transition in TiNiFe alloy" Journal de Physique IV **5**(C2): 99-103.

8. Castleman, L. S., Motzkin, S., M. Alicandri, F. P. Bonawit., (1976). "Biocompatibility of nitinol alloy as an implant material." Journal of Biomedical Materials Research **10**(5): 695-731.

9. Chrobak, D., D. Stroz, H. Morawiec., (2003). "Effect of early stages of precipitation and recovery on the multi-step transformation in deformed and annealed near-equiatomic NiTi alloy" Scripta Materialia **48**(5): 571-576.

10. Chrobak, D. and D. Stroz (2005). "Two-stage R phase transformation in a cold-rolled and annealed Ti-50.6 at% Ni alloy" Scripta Materialia **52**(8): 757-760.

11. Clayton, P. (1993). "Tribological behavior of a titanium nickel-alloy" Wear **162**: 202-210.

12. Cross, W.B., A.H. Kariotis and F.J. Stimler, September (1969), "A new thermoelastic model for analysis of shape memory alloy hybrid composites" NASA CR-1433.

13. Cutright, D. E., S. N. Bhaskar, B. Perez, R. M. Johnson, G. S. M. Cowan., (1973). "Tissue reaction to nitinol wire alloy" Oral Surgery Oral Medicine Oral Pathology Oral Radiology and Endodontics **35**(4): 578-584.

14. Enami, K., T. Yoshida, S. Nenno, (1987). "Pre-martensitic and martensitic transformation in TiPd-Fe alloys" Proc. ICOMAT-**86**, 103 pp.

15. Fragnito, M. and S. Vetrella (2002). "A space release/deployment system actuated by shape memory wires" Acta Astronautica **51**(11): 761-770.

16. FukamiUshiro, K. L., D. Mari, D. C. Dunand., (1996). "NiTi and NiTi-TiC composites 2. Compressive mechanical properties" Metallurgical and Materials Transactions A-Physical Metallurgy and Materials Science **27**(1): 183-191.

17. Fukuda, T., A. Deguchi, T. Kakeshita, T. Saburi., (1997). "Stress induced R -> B2 transformation and pseudoelasticity associated with twinning in a Ti-Ni alloy including aligned particles of Ti_3Ni_4" Materials Transactions JIM **38**(12): 1057-1062.

18. Fukuda, T., T. Saburi, K. Doi, S. Nenno., (1992). "Nucleation and self-accommodation of the R-Phase in Ti-Ni alloys" Materials Transactions JIM **33**(3): 271-277.

19. Funakubo H (1987) in Shape Memory Alloys. Gordon and Breach Science Publishers, New York.

20. Grummon, D.S., T.J. Pence, (1997). "Simulation of cyclic displacement by counterpoised shape memory elements" MRS Symp. Proc. **459**:331.

21. Hara, T., T. Ohba, K. Otsuka, M.Nishida.,. (1997). "Phase transformation and crystal structures of Ti_2Ni_3 precipitates in Ti-Ni alloys" Materials Transactions JIM **38**(4): 277-284.

22. Hosoda, H., S. Hanada, K. Inoue, T. Fukui, J. Mishima, T. Suzuki., (1998). "Martensite transformation temperatures and mechanical properties of ternary NiTi alloys with offstoichiometric compositions" Intermetallics **6**(4): 291-301.

23. Hwang, C. M., M. Meichle, M. B. Salamon, C. M. Wayman., (1983). "Transformation behavior of a $Ti_{50}Ni_{47}Fe_3$ alloy. 2. Subsequent premartensitic behavior and the commensurate phase" Philosophical Magazine a-Physics of Condensed Matter Structure Defects and Mechanical Properties **47**(1): 31-62.

24. Hwang, C. M., M. B. Salamon, C. M. Wayman., (1982). "Transformation behavior of a $Ti_{50}Ni_{47}Fe_3$alloy 2. Martensitic-transformation" Journal de Physique **43**(NC-4): 237-242.

25. Kato, H., T. Koyari, M. Tokizane, S. Miura., (1994). "Stress-strain behavior and shape-memory effect in powder-metallurgy TiNi Alloys" Acta Metallurgica et Materialia **42**(4): 1351-1358.

26. Kim, H. Y., Y. Ikehara, J. I. Kim, H. Hosoda, S. Miyazaki., (2006). "Martensitic transformation, shape memory effect and superelasticity of Ti-Nb binary alloys" Acta Materialia **54**(9): 2419-2429.

27. Kim, H. Y., H. Satoru, J. I. Kim, H. Hosoda, S. Miyazaki., (2004). "Mechanical properties and shape memory behavior of Ti-Nb alloys" Materials Transactions **45**(7): 2443-2448.

28. Krishnan V. B., Thesis, "Design, fabrication and testing of a shape memory alloy based cryogenic thermal conduction switch", University of Central Florida, 2003.

29. Leo, P. H., T. W. Shield, O. P. Bruno (1993). "Transient heat-transfer effects on the pseudoelastic behavior of shape-memory wires" Acta Metallurgica et Materialia **41**(8): 2477-2485.

30. Lemanski, J., Thesis, "Cryogenic shape memory alloy actuators for spaceport technologies: materials characterization and prototype testing", University of Central Florida, 2005.

31. Lin, H. C., S. K. Wu, Y. C. Chang., (1995). "Damping characteristics of $Ti_{50}Ni_{49.5}Fe_{0.5}$ and $Ti_{50}Ni_{40}Cu_{10}$ ternary shape-memory alloys" Metallurgical and Materials Transactions a-Physical Metallurgy and Materials Science **26**(4): 851-858.

32. Lin, H. C., S. K. Wu, M. T. Yeh., (1993). "Damping characteristics of TiNi shape-memory alloys" Metallurgical Transactions A-Physical Metallurgy and Materials Science **24**(10): 2189-2194.

33. Matsumoto, M., and Honma, T., (1976). "New aspects of martensitic transformations", First Japan Institute of Metals International Symposium on Martensite, Kobe, Japan, p.199.

34. Melton, K. N. "Chapter 10: General Applications of SMAs and Smart Materials" in *Shape Memory Materials*, edited by K. Otsuka and C.M. Wayman, Cambridge University Press, 1998, pp. 220-239.

35. Miller, D. A. and D. C. Lagoudas (2001). "Influence of cold work and heat treatment on the shape memory effect and plastic strain development of NiTi" Materials Science and Engineering A-Structural Materials Properties Microstructure and Processing **308**(1-2): 161-175.

36. Miyazaki, S., Y. Ohmi, K. Otsuka, Y. Suzuki., (1982). "Characteristics of deformation and transformation pseudoelasticity in Ti-Ni Alloys" Journal de Physique **43**(NC-4): 255-260.

37. Miyazaki, S. and K. Otsuka (1984). "Mechanical-behavior associated with the premartensitic rhombohedral-phase transition in a $Ti_{50}Ni_{47}Fe_3$ alloy" Philosophical Magazine A-Physics of Condensed Matter Structure Defects and Mechanical Properties **50**(3): 393-408.

38. Miyazaki, S. and K. Otsuka (1986). "Deformation and transition behavior associated with the R-Phase in Ti-Ni Alloys" Metallurgical Transactions A-Physical Metallurgy and Materials Science **17**(1): 53-63.

39. Miyazaki, S. and C. M. Wayman (1988). "The R-Phase transition and associated shape memory mechanism in Ti-Ni Single-Crystals" Acta Metallurgica **36**(1): 181-192.

40. Moberly, W. J., J. L. Proft, T. W. Duerig, R. Sinclair., (1990). "Deformation, twinning and thermo-mechanical strengthening of $Ti_{50}Ni_{47}Fe_3$" Acta Metallurgica et Materialia **38**(12): 2601-2612.

41. Nakata, Y., T. Tadaki, K. Shimizu., (1991). "Composition dependence of the atom location of the 3rd Element in Ti-Ni-X shape memory alloys" Materials Transactions JIM **32**(12): 1120-1127.

42. Ohura, Y., (1984). "Shape memory alloys for medical applications" Jpn. Orthod. Soc. 4371.

43. Otsuka, K. and X. Ren (2005). "Physical metallurgy of Ti-Ni-based shape memory alloys" Progress in Materials Science **50**(5): 511-678.

44. Proft., J .L. and T.M. Duerig in Engineering Aspects of Shape Memory Alloy, ed T.W. Duerig, K. N. Melton, D. Stockel and C. M. Wayman, Butterworth-Heinemann (1990 pp 115-129.

45. Rajagopalan, S., A. L. Little, M. A. M. Bourke, R. Vaidyanathan., (2005). "Elastic modulus of shape-memory NiTi from in situ neutron diffraction during macroscopic loading, instrumented Indentation, and extensometry" Applied Physics Letters **86**(8).

46. Rathod, C. R., B. Clausen, M. A. M. Bourke, R. Vaidyanathan., (2006). "Neutron diffraction investigation of hysteresis reduction and increase in linearity in the stress-strain response of superelastic NiTi." Applied Physics Letters **88**(20).

47. Richman, R. H., A. S. Rao, D. E. Hodgson., (1992). "Cavitation Erosion of 2 NiTi Alloys" Wear **157**(2): 401-407.

48. Rozner, A. G. and Wasilews.R.J. (1966). "Tensile Properties of NiAl and NiTi" Journal of the Institute of Metals **94**(5): 169-&.

49. Saburi T., (1998). "Chapter 3: Ti-Ni Shape Memory Alloys" in *Shape Memory Materials*, edited by K. Otsuka and C.M. Wayman, Cambridge University Press, pp.49-96.

50. Sachdeva, R. and S. Miyazaki (1989). "Shape memory NiTi alloys-applications in dentistry" Proc. MRS Int'l Mtg on Adv Mats., 9:605.

51. Salamon, M. B., M. E. Meichle, C. M. Wayman., (1985). "Premartensitic phases of $Ti_{50}Ni_{47}Fe_3$" Physical Review B **31**(11): 7306-7315.

52. Sandrock, G. D., A. J. Perkins, R. F. Heheman., (1971). "Premartensitic instability in near-equiatomic TiNi" Metallurgical Transactions **2**(10): 2769-&.

53. Simon, M., R. Kaplow, E. Salzman, D. Freiman., (1977). "Vena-cava filter using thermal shape memory alloy - experimental aspects" Radiology **125**(1): 89-94.

54. Singh J. D., Master's Thesis, "Commissioning a controlled atmosphere arc melting facility and subsequent fabrication of low transformation temperature SMAs", University of Central Florida 2004.

55. Sitepu H. (2003). "Order parameter evaluation for the B2 to R phase transition in a NiTi shape memory alloy" Textures Microstruct. 35:185.

56. Vaidyanathan, R., M. A. M. Bourke, D. C. Dunand., (1999). "Phase fraction, texture and strain evolution in superelastic NiTi and NiTi-TiC composites investigated by neutron diffraction" Acta Materialia **47**(12): 3353-3366.

57. Walker, J. A., K. J. Gabriel, M.Mehregany., (1990). "Thin-film processing of TiNi shape memory alloy" Sensors and Actuators A-Physical **21**(1-3): 243-246.

58. Wang, F. E., W. J. Buehler, S. J. Pickart., (1965). "Crystal structure and a unique martensitic transition of TiNi" Journal of Applied Physics **36**(10): 3232-&.

59. Wang, J. J., T. Omori, Y. Situo, R. Kainuma, K. Ishida., (2005). "Two-way shape memory effect induced by cold-rolling in Ti-Ni and Ti-Ni-Fe alloys" Scripta Materialia **52**(4): 311-316.

60. Warlimon.H, L. Delaey, R. V. Krishnan, H. Tas., (1974). "Thermoelasticity, pseudoelasticity and memory effects associated with martensitic transformations 3. Thermodynamics and Kinetics" Journal of Materials Science **9**(9): 1545-1555.

61. Wu, S. K. and C. M. Wayman (1987). "Martensitic transformations and the shape memory effect in $Ti_{50}Ni_{10}Au_{40}$ and $Ti_{50}Au_{50}$ Alloys" Metallography **20**(3): 359-376.

62. Xu, H. B., C. B. Jiang, S. K. Gong, G. Feng., (2000). "Martensitic transformation of the $Ti_{50}Ni_{48}Fe_2$ alloy deformed at different temperatures" Materials Science and Engineering A-Structural Materials Properties Microstructure and Processing **281**(1-2): 234-238.

63. Zhang, C., P. E. Thoma, R. H. Zee (1997). "The effect of Hafnium content and cycling under an applied axial stress on the creep and martensite train of NiTi based shape memory alloy wires" Mat.Res.Soc.Symp.Proc. Vol.259, 281-286.